© Copyright 2023

Yuhang Yang

Electrochemical Oxidation of Pharmaceuticals in Human Urine

Yuhang Yang

A dissertation

submitted in partial fulfillment of the

requirements for the degree of

Doctor of Philosophy

University of Washington

2023

Reading Committee:

Hugh W. Hillhouse, Chair

Guozhong Cao

David Bergsman

Program Authorized to Offer Degree:

Materials Science and Engineering

University of Washington

Abstract

Electrochemical Oxidation of Pharmaceuticals in Human Urine

Yuhang Yang

Chair of the Supervisory Committee:
Hugh W. Hillhouse, Rehnberg Chair Professor
Chemical Engineering

Electrochemical oxidation of fresh human urine is a promising method to prevent pharmaceuticals from being discharged into the environment. Urine comprises only a small (~1%) volumetric fraction of municipal wastewater, but represents a dominant source of pharmaceuticals, many of which may pass through conventional wastewater treatment and pose risks to aquatic ecosystems. Point-source treatment of source-separated urine presents a unique opportunity to degrade pharmaceuticals before dilution with wastewater, and electrochemical advanced oxidation processes are one increasingly investigated option. However, they often lead to the formation of oxidation byproducts including chlorate, perchlorate, haloacetic acids, trihalomethane, etc. The work presented in this dissertation is broadly focused on developing

safe and effective electrochemical methods for the treatment in fresh human urine to mitigate the pharmaceutical contamination in the environment.

First, I demonstrate that the electrogenerated hydroxyl radicals (•OH) enables the selective oxidation of pharmaceutical during the electrolysis of fresh human urine, while •OH is quenched by HCO_3^- in hydrolyzed urine leading to a slower pharmaceutical degradation rate during the electrolysis of hydrolyzed urine. Additionally, I show that urea at the concentration present in fresh urine suppresses the oxidation pathways of Cl^- to ClO_3^- and ClO_4^-. Taken all together, it is advantageous to employ the electrochemical advanced oxidation processes in fresh human urine rather than the hydrolyzed urine.

Next, I focus on understanding the underlying chemistry and fundamental kinetics of pharmaceutical oxidation during electrolysis of fresh human urine. I use the selective radical quenchers to study the significance of individual oxidants for the oxidation of pharmaceutical in electrolyte only containing chloride ions. I show that electro-generated dissolved Cl_2 adjacent to the anode surface could contribute the pharmaceutical degradation which has been overlooked by the scientific community. Furthermore, I demonstrate that organic urine constituents (urea, creatinine, and uric acid) quench the dissolved oxidants leading to a mass-transfer limited reaction, while the inorganic urine constituents could quench chemisorbed oxidants resulting in a mixed kinetically and mass-transfer controlled reaction. Moreover, increasing the mass transfer rates and anode potential is essential for achieving faster pharmaceutical oxidation.

Finally, I design and develop an alternating scheme of oxidation and reduction using interdigitated working electrodes (IWEs) for the oxidation of pharmaceuticals while minimizing the formation of chlorinated byproducts. The alternating scheme is achieved by using (1) a *convention method* where a bipotentiostat applies a constant anodic potential to one side of the

IWE and a cathodic potential to the other side of the IWE while a stir bar directly on top of the planar IWEs moves fluid across the IWE (with separate counter and reference electrodes in the cell) and (2) an *alternating current method* where at any given time one side of the IWE is the working electrode and the other side is the counter electrode but over time the WE and CE are alternated by the potentiostat at a rate of up to 100 Hz. I demonstrate that the generation of chlorate, chloroacetic acids and chloroform is significantly suppressed for both methods above. However, the rates of pharmaceutical degradation are substantially enhanced for the alternating scheme achieved by convection method, while their rates decrease largely using alternating current method.

Collectively, the work included in this dissertation demonstrates considerable progress toward understanding the kinetics of electrochemical oxidation of pharmaceuticals in human urine and developing the safe and effective processes that could be implemented at the source of generation, with focus on the rapid pharmaceutical degradation and minimum generation of toxic byproducts.

TABLE OF CONTENTS

List of Figures xi

List of Tables xviii

Chapter 1. Introduction 23

1.1 Emerging Concern of Pharmaceutical Pollutants 23

1.2 Electrochemical Advanced Oxidation Processes (EAOPs) 25

1.3 The Complexity of Human Urine Matrixes 28

1.4 Advantages of Decentralized Treatment of Urine 30

1.5 Toxic Byproducts Formation 31

1.6 Outlines 33

Chapter 2. Materials and Methods 35

2.1 Chemicals and Solutions 35

2.2 Electrochemical Cell and Electrodes 36

2.3 Experimental Methods 39

2.3.1 Cyclic Voltammetry of Anode Reactions 39

2.3.2 Galvanostatic Oxidation of Pharmaceuticals in Urine 41

2.3.3 Galvanostatic Oxidation of Urine without Pharmaceuticals 42

2.3.4 Potentiostatic Oxidation of Urine by Alternating Scheme of Oxidation and Reduction 42

2.3.5 Mass-transfer Limiting Pseudo-first-order Rate Constants 43

2.4 Analytical Methods 45

2.4.1 Ion Chromatography 45

2.4.2 High Performance Liquid Chromatography 45
2.4.3 Gas Chromatography (GC) 46
2.4.4 Determination of free chlorine (FC – primarily the sum of HOCl + OCl^-, and to a lesser extent Cl_2 and/or Cl_2O), total chlorine (TC – the sum of FC + inorganic and organic chloramines), and ClO_2 during electrolysis 47
2.5 Theoretical Simulation and Calculation 49
2.5.1 Mass-transfer rates and kinetic rates under steady state assumption 49
2.5.2 The Stagnant Layer Thickness and Local pH at Electrode Surface 51
Chapter 3. Selective oxidation of pharmaceuticals and suppressions of perchlorate formation during electorlysis of fresh human urine 53
3.1 Abstract 54
3.2 Understanding the Reaction Network during Electrolysis of Fresh or Hydrolyzed Urine 55
3.3 Reactive Chlorine Species Scavenging by Urea 61
3.4 Pseudo-First-Order Kinetics and Mass Transfer 63
3.5 Electrolysis of Model Pharmaceutical Compounds in Various Urine Matrixes 66
3.5.1 Galvanostatic oxidation in fresh-urine matrixes 66
3.5.2 Differences between Synthetic Fresh, Hydrolyzed, and Hydrolyzed-Aged Urine Matrixes 68
3.6 Generation of Oxidation Byproducts 71
3.6.1 Inhibition of Oxychloride Formation Increases with Increased Urea or NH_4^+/NH_3. 72
3.6.2 Mechanism of Inhibition of Oxychloride Formation 74
3.7 Conclusions 78

Chapter 4. Electrochemical Oxidation of Pharmaceuticals in Synthetic Fresh Human Urine: Using Selective Radical Quenchers to Reveal the Dominant Degradation Pathways and the Scavenging Effects of Individual Urine Constituents 79

4.1 Abstract 80

4.2 Using Selective Radical Quenchers to Reveal the Dominant Degradation Pathways .. 81

4.3 Mass Transfer Limiting Pseudo-First-Order Rate Constants 82

4.4 Electrochemical Oxidation Pathways of Pharmaceuticals in Chloride only Solution .. 83

4.4.1 Rate of Degradation Due to Direct Electron Transfer (DET) 85

4.4.2 Rate of Degradation Due to $\bullet OH_{diss}$ 86

4.4.3 Rate of Degradation Due to Adsorbed •OH and Chemisorbed Oxygen (IrO_{2+1}) 87

4.4.4 Rate of Degradation Due to IrO_3-Cl, Dissolved $Cl^{\bullet}/Cl_2^{\bullet-}$, and Free Chlorine (FC) with IrO_2 87

4.4.5 Rate of Degradation Due to $Cl^{\bullet}_{ads}$, Dissolved $Cl_2^{\bullet-}$ and Free Chlorine (FC) with BDD 89

4.5 The Scavenging Effect of Organic Urine Constituents on Pharmaceutical Degradation 93

4.5.1 Urea 93

4.5.2 Creatinine 95

4.5.3 Uric Acid 96

4.6 The Effect of Inorganic Urine Constituents on Pharmaceutical Degradation 97

4.6.1 SO_4^{2-} 97

4.6.2 $H_2PO_4^-$ 97

4.6.3 Citrate ions 98

4.7 Electrolysis of Pharmaceutical in Full Synthetic Fresh Urine Matrixes (FUM) 99
4.8 Strategies of Faster Pharmaceutical Degradation by Active and Inactive Anodes..... 101
4.8.1 Increasing Mass Transfer Rates 101
4.8.2 Increasing Current Densities 102
4.8.3 Increasing the Concentration of Chloride Ions 103
4.9 Conclusions 104
4.10 Supplementary Information 105
Chapter 5. Enhancing Rates of Pharmaceutical Degradation and Suppression of Chlorinated Byproducts Formation by Alternating Scheme of Oxidation and Reduction during Electrolysis of Fresh Human Urine 107
5.1 Abstract 108
5.2 Introduction 110
5.3 The reactions during electrolysis of fresh human urine in the presence of alternating scheme of oxidation and reduction 112
5.4 The effect of cathode potentials and mass transport conditions on the application of alternating scheme in synthetic fresh urine matrixes (FUM) 113
5.4.1 Rates of Pharmaceutical Degradation in FUM due to Various Cathode Potentials 114
5.4.2 Rates of Pharmaceutical Degradation in FUM due to Mass Transfer Rates 119
5.4.3 Generation of Chlorinated Byproducts 119
5.5 The effect of synthetic hydrolyzed aged urine matrixes (HUM) for the application of alternating scheme. 122
5.5.1 Rates of Pharmaceutical Degradation in HUM 122
5.5.2 Generation of Chlorinated Byproducts: 124

5.6 The effect of AC electrolysis during electrolysis of FUM 127
5.6.1 Rates of Pharmaceutical Degradation in Synthetic Fresh Urine Matrixes (FUM) . 128
5.6.2 Generation of Chlorinated Byproducts 129
5.7 Conclusions 131
5.8 Supplementary Figures 132
Chapter 6. Conclusions and future outlook 133
Bibliography 137

LIST OF FIGURES

Figure 2.1 **Schematic overviews of electrochemical cell configurations used in this work.** (a) The undivided setup for oxidation experiments. (b) The divided cell setup for oxidation experiments. 37

Figure 2.2 (a) **Photograph of the electrochemical cell depicted in Figure 2.1** (b,c,d) **Schematics for the dimensions of the electrochemical cell** 38

Figure 2.3 **Linear sweep voltammetry (LSV) of equimolar $[Fe(CN)_6]^{3-}$/ $[Fe(CN)_6]^{4-}$ in K_2CO_3 supporting electrolyte on boron-doped diamond (BDD) electrode** at a stir rate of 600 rpm (Re = 2977) and a stir rate of 1000 rpm (*Re* = 11050). The grouped lines represent the triplicate experiments to determine the uncertainty of measurements. 45

Figure 2.4 **Possible concentration gradients of pharmaceuticals in the stagnant layer** (assuming constant bulk concentration). Gradient A: oxidation that is kinetically limited by the heterogeneous reactions at the anode surface (i.e., via direct anodic oxidation and surface bound oxidants). Gradient B: the oxidation is mass-transfer-limited and the concentration is zero at the anode surface but increases in solution. Gradient C: the oxidation is mass-transfer-limited, but in addition to heterogeneous reactions, oxidants generated at the anode desorb, diffuse outward, and react homogeneously with the pharmaceutical to drive the concentration to zero some distance away from the surface. Gradient D: the oxidation is mass-transfer-limited with a larger homogeneous reaction enhancement than gradient C. 50

Figure 2.5 **(a) pH gradient as a function of the distance from anode surface by Fick's first law. (b) FC speciation at various pH.** The simulated speciation was calculated based on acid dissociation constant of HOCl ($K_{a,\,HOCl} = 10^{-7.5}$ mol/L), equilibrium constants of Cl_2 and Cl_2O with HOCl ($K_{H,\,Cl2} = 4.35 \times 10^{-4}$ (mol/L)^2; $K_{H,\,Cl2O} = 8.74 \times 10^{-3}$ (mol/L)$^{-1}$), concentration of Cl^- ($[Cl^-]$ = 100 mM), and pH. 53

Figure 3.1 **Schematic illustration of reaction network during the electrolysis of human urine** 55

Figure 3.2 **Relative rate constants for important reactions during the electrolysis of pharmaceuticals in urine matrixes (with CP as an example pharmaceutical in an undivided cell setup).** Divided cell architectures will block r_{21} and subsequent reactions. The color coding indicates the relative range of large to small rate constants. The black arrows represent the transport of species. Furthermore, $^{\bullet}OH$, $Cl^{\bullet}$ and $Cl_2^{\bullet-}$ depicted at the anode surface may also desorb and diffuse outward through a relatively stagnant near-anode region. Likewise, Cl^-, urea, and the pharmaceuticals diffuse from bulk solution toward the anode as they are consumed at the anode or in the near-anode stagnant region. See chapter 3.5 for discussion of the importance of mass transport in galvanostatic experiments. Reactions, their rate constants and their origins are included in Table 3.1..... 59

Figure 3.3 **CVs in 100 mM $NaClO_4$, 100 mM NaCl, and 100 mM NaCl + 250 mM urea on (a) BDD and (b) IrO_2 anodes. (c) Concentration of cyclophosphamide (CP) during the electrolysis in simplified synthetic fresh urine matrixes** with a starting CP concentration of 1.9 mM. Inset: The chemical structure of CP. **(d) Concentration of sulfamethoxazole (SMX) during oxidation in simplified synthetic fresh urine matrixes** with a starting SMX concentration of 0.39 mM. Inset: The chemical structure of SMX. **(e) Observed pseudo-first-order rate constants for pharmaceutical degradation. (f) Observed pseudo-first-order rate constants for SMX degradation in simplified synthetic fresh urine, full synthetic fresh urine, and authentic fresh human urine with undivided electrochemical cell setup.** The error bars represent standard deviations about the means from triplicate experiments. 62

Figure 3.4 **(a) Extracted pseudo-first-order rate constants for the galvanostatic (10 mA/cm^2) degradation of cyclophosphamide as a function of different stirring conditions using a BDD electrode in an undivided cell.** (inset) Reynolds number was calculated using the linear velocity of the tip of the stir bar (u), the length of the stir bar (L), and the kinematic viscosity of water (v). **(b) A plot of the extracted pseudo-first-order rate constant vs. $Re^{1/2}$** is roughly linear, which is commensurate with the mass transfer correlation for a rotating disk electrode.[133] 65

Figure 3.5 **The pseudo-first-order pharmaceutical degradation rate constant is a critical factor in the design of electrochemical devices.** Modeled degradation profiles for various

pseudo-first-order rate constants suggest that a rate constant of >0.01 min^{-1} is required in a practical device. This would correspond to a decrease in pharmaceutical concentration by 3 orders of magnitude in a 12-hour period, which is a reasonable residence time for a practical at-home situation. Normalized rate constants take into account the current density, surface area, and solution volume. In this model, current density, surface area, and solution volume were respectively set as 10 mA/cm^2, 8.56 cm^2, and 40 mL to match the experimental parameters of this study. 65

Figure 3.6 **(a) Observed and geometry-normalized pseudo-first-order rate constants for pharmaceutical degradation on BDD** with undivided cell setup in: (1) simplified urine matrixes (250 mM urea and 100 mM Cl^-, pH 6.15); (2) synthetic full fresh urine matrixes (250 mM urea, 100 mM NaCl, 16 mM Na_2SO_4, 24 mM NaH_2PO_4, 13 mM creatinine, 3 mM uric acid**,** pH 5.87); (3) hydrolyzed, un-aged urine matrixes (100 mM Cl^-, 500 mM NH_4^+ and 250 mM HCO_3^-, pH 9.35); (4) hydrolyzed, aged urine matrixes adapted from Udert et al. [66] (100 mM Cl^-, 140 mM NH_4^+ and 250 mM HCO_3^-, pH 9.02); and (5) hydrolyzed, aged urine matrixes adapted from Hoffmann et al. (100 mM Cl^-, 33 mM NH_4^+ and 250 mM HCO_3^-, pH 8.88). The dotted line represents the mass-transfer limiting rate of pharmaceutical degradation obtained from Figure 3.4**.** The electrolytes (40 mL) were stirred at 500 rpm. The applied current density was 10 mA/cm^2. The error bars represent standard deviations about the means from triplicate experiments. **(b) Possible concentration gradients of pharmaceuticals in the stagnant layer** (assuming constant bulk concentration). 69

Figure 3.7 **Evolution of inorganic oxidation byproducts showing concentrations of (a) ClO_4^-, (b) ClO_3^-, (c) NO_3^-, and (d) NO_2^- during electrolysis at 10 mA/cm^2 on BDD and IrO_2 anodes in the undivided and divided setups.** Results are from oxidation of full synthetic fresh urine matrixes amended with 1.9 mM CP and 0.39 mM SMX. The error bars represent standard deviations from triplicate experiments. 72

Figure 3.8 **OBPs formation in galvanostatic electrolysis experiments undertaken over extended times compared to experiments from which the Figure 3 data were obtained. Concentrations of generated (a) ClO_3^- and (b) ClO_4^- were measured for various matrixes treated using a BDD anode in the undivided setup.** For the matrixes containing

NH_4^+/NH_3, the pH was 9–10. For the matrixes containing only Cl^- and/or urea, the pH was 6–7. Galvanostatic treatments were performed for 90 mins at a current density of 93 mA/cm^2 for a final charge passed of 30 A·hr/L. The dashed lines indicate concentrations 100x higher than suggested drinking water limits for each oxychloride species (see accompanying discussion in the main text). 74

Figure 3.9 **Concentration profiles of various chlorine species during electrolysis on the BDD anode in four different matrixes.** Starting from a baseline solution 100 mM Cl^-, 33 mM NH_4^+, 250 mM HCO_3^-, the four solutions were: (a) baseline solution at pH 6.75. (b) baseline solution at pH 8.88; (c) baseline solution with high ammonium (500 mM NH_4^+) at pH 9.35; (d) Full synthetic fresh urine matrix (no ammonium and bicarbonate but with urea, creatine, uric acid, etc.) at pH 5.87). The current densities were 93.3 mA/cm^2; the stir rate was 500 rpm. FC and ClO_2 were not measurable in any of the four matrixes investigated. FC measurements via DPD were verified by ABTS in matrixes (a) and (b). The measurement of total chlorine via DPD was checked by ABTS in matrix (a). Potential interference of H_2O_2 with the measurements of TC was investigated by pretreating diluted samples with catalase to decompose any H_2O_2 that may have been present. The absence of any effect from catalase treatment indicates that H_2O_2 was not present at concentrations sufficient to interfere with TC measurements. Error bars represent standard deviation about the means from triplicate experiments. 76

Figure 4.1 **(a) Scheme of relative rate constants for reactions of selective quenchers (AA and t-BuOH) with radicals.** The black arrows represent the transport of species. The color coding indicates the relative range of large to small rate constants. **Free chlorine (FC) production on (b) BDD and (c) Ti/IrO_2 anodes in a 100 mM chloride electrolyte in the presence of quenchers.** Error bar represents the standard deviation from triplicate measurements. 81

Figure 4.2. **Pseudo-first-order electrolysis rates of target pharmaceuticals on (a) BDD anodes and (b) IrO_2 anodes.** Error bars represent standard deviations from triplicate measurements. As shown in Table 4.1, the electrolysis rates of pharmaceuticals shown in green column consist of the contribution of DET, dissolved and adsorbed $^{\bullet}OH$ and $Cl^{\bullet}/Cl_2^{\bullet-}$ and FC; the orange columns indicate the contribution of DET only; the red columns

represent the electrolysis rates from DET, dissolved and adsorbed •OH; the pink columns indicate the electrolysis rates from DET and adsorbed •OH; and the blue columns reveal the electrolysis of pharmaceuticals via DET and adsorbed •OH and Cl•/$Cl_2^{\bullet-}$..... 85

Figure 4.3 **Observed and normalized pseudo-first order rate constants during electrolysis of CP, CBZ, SMX, and IBP with the addition of individual constituent from synthetic urine matrixes with (a) & (c) BDD and (b) & (d) IrO_2.** The black horizontal line of observed rate constants represents mass-transfer limiting rates, including the measured standard deviation k_m. 94

Figure 4.4 **Target pharmaceuticals removal during electrolysis in FUM matrixes on (a) BDD electrode; (b) Ti/IrO_2 electrode. (c) Observed and geometry normalized pseudo-first order rate constants of target pharmaceutical electrolysis in FUM on BDD and Ti/IrO_2.** The black horizontal line represents the measured mass-transfer limiting rate constants with uncertainties. Error bars represent the standard deviation of replicate experiments. 100

Figure 4.5 **Electrolysis rates of test pharmaceuticals in FUM investigated in this work with different stir rates by (a) BDD and (b) IrO_2. Electrolysis rates of four pharmaceuticals in FUM under a stir rate of 600 rpm (*Re* = 2977) with various applied current densities and initial Cl^- concentration by (c) BDD and (d) IrO_2.** 103

Figure 5.1 **(a) Schematics for the dimensions of the Ti/IrO_2 interdigitated working electrodes (IWEs) attached on a 40 x 100 mm clean soda-lime glass substrate. (b) Photograph of the Ti/IrO_2 IWEs fabricated.**..... 108

Figure 5.2 **(a) Schematic view of planar IWEs using Ti/IrO_2; (b) the detailed schematic view of one pair of the anode and cathode in IWEs, (c) side view of (b) as well as the relative rate constants for reactions that have been reported or speculated during the electrolysis of pharmaceuticals in urine matrixes (with CP as an example pharmaceutical)**. The compounds in the dash rectangles are the CBPs generated during the oxidation of human urine. 113

Figure 5.3 **(a) The observed pseudo-first order rate constants (k_{obs}) and normalized k_{obs} of the pharmaceutical degradation** obtained with the potential of 2.5 V (*vs.* Ag/AgCl) applied to working electrode 1 (WE1) and (1) open circuit, (2) 2.5 V, (3) 0 V, (4) -1 V, (5) -

2 V, and (6) -3 V (*vs.* Ag/AgCl) applied to working electrode 2 (WE2). **The generation of (a) ClO_3^-, (b) $CHCl_3$, and (c) total chlorine in the chlorinated acetic acid** (− total count of chlorine in MCAA, DCAA, and TCAA) in full synthetic fresh urine matrixes (FUM) at stir rates of 600 (*Re* = 2977) or 1000 rpm (*Re* = 11050)..... 115

Figure 5.4 **(a) Free chlorine speciation as a function of the distance away from the cathode.** The simulated speciation was calculated based on acid dissociation constant of HOCl ($K_{a, HOCl} = 10^{-7.5}$ mol/L), equilibrium constants of Cl_2 and Cl_2O with HOCl ($K_{H, Cl2} = 4.35 \times 10^{-4}$ $(mol/L)^2$; $K_{H, Cl2O} = 8.74 \times 10^{-3}$ $(mol/L)^{-1}$), concentration of Cl^- ($[Cl^-] = 100$ mM), and pH. **(b) Cyclic voltammograms (CVs)** in (1) N_2 saturated 100 mM $NaClO_4$, (2) O_2 saturated 100 mM $NaClO_4$, and (3) 10 mM NaOCl in N_2 saturated 100 mM $NaClO_4$; **(c) Free chlorine (FC) production on Ti/IrO_2 IWEs** in a 100 mM chloride electrolyte (1) without the alternating scheme at the stirring rate of 600 rpm (□) and 1000 rpm (◁), (2) with the application of alternating scheme at the stirring rate of 600 rpm (▽) and 1000 rpm (▷), and (3) AC electrolysis with alternating frequencies of 1 Hz (×) and 100 Hz (∗) at the stirring rate of 600 rpm..... 117

Figure 5.5 **Cyclic voltammograms (CVs) of the N_2 saturated 100 mM $NaClO_4$ with the addition of 20 ppm of (a) CP, (b) CBZ, (c) SMX, and (d) IBP.** The scan started from 0 V to -1.5 V and then swept to 1.5 V and finally returned to 0 V at a scan rate of 100 mV/s. The direct cathodic reduction peaks were observed in CVs of 20 ppm CBZ and SMX in 100 mM $NaClO_4$ electrolyte, consistent with our hypothesis that the direct cathodic reduction could contribute to the degradation of CBZ and SMX with the application of alternating scheme. 118

Figure 5.6 **(a) The observed pseudo-first order rate constants (k_{obs}) and normalized k_{obs} of the pharmaceutical degradation** obtained with the applied potential of 2.5 V (*vs.* Ag/AgCl) at working electrode 1 (WE1) and (1) open circuit, and (2) -2V (*vs.* Ag/AgCl) applied to working electrode 2 (WE2). **The generation of (b) ClO_3^-, (c) $CHCl_3$, and (d) total chlorine in the chlorinated acetic acid** (− total count of chlorine in MCAA, DCAA, and TCAA) in synthetic hydrolyzed aged urine matrixes (HUM) under stirring rates of 600 (*Re* = 2977) or 1000 rpm (*Re* = 11050)..... 124

Figure 5.7 **Voltages applied to the electrode in the AC electrolysis with the frequency of (a) 1 and (b) 100 Hz.** 127

Figure 5.8 **The electrolysis of pharmaceutical in FUM was conducted at a stirring rate of 600 rpm (*Re* = 2977)**. (a) The electrolysis rates of pharmaceuticals, and the generation of (b) ClO_3^-, (c) TCM ($CHCl_3$), and (d) total chlorine in chlorinated acetic acids for the alternating scheme and AC electrolysis with alternating frequencies of 1 and 100 Hz at the amplitude of 2.5V and -2V (Figure 5.7). 129

Figure 5.9. **The measured concentrations of (a) monochloroacetic acid (MCAA), (b) dichloroacetic acid (DCAA), and trichloroacetic acid (TCAA) during the electrolysis in FUM and HUM with or without the application of alternating scheme and AC electrolysis.**..... 133

LIST OF TABLES

Table 1.1 Reaction Equations 27
Table 1.2 Comparison of relative advantages of degrading pharmaceuticals in urine before dilution with other domestic wastewater.[68,69] 31
Table 2.1 Proposed Composition of Full Synthetic Urine Matrixes..... 36
Table 3.1 Reactions in Scheme 1 57
Table 3.2 Significant Electrochemical Reactions during Oxidation..... 62
Table 4.1 Constituents of Pseudo-first-order Rate Constants due to Different Electrolytes84
Table 4.2. Contribution to Pharmaceutical Oxidation in 100 mM Cl^- with BDD and IrO_2 Electrodes. The contribution to pharmaceutical degradation from $Cl_2^{\bullet-}$ and FC with BDD cannot be distinguished due to the quenching effect of t-BuOH on both oxidants. . 86
Table 4.3 Molecular Structures of Investigated Pharmaceuticals and Their Reactivities towards Oxidants and Radicals..... 91
Table 4.4 Geometry-normalized Pseudo-first-order True Kinetic Rate Constants (k') Obtained from k_{obs} at *Re* =11050 in Figure 5a, b, given by the equation $kobs = 11k' + 1km$ (Chapter 2.5). 102
Table 4.5 Pseudo-first-order Rate Constants of Pharmaceutical Removal during Electrolysis on BDD used for the electrolytes in Figure 4.2a..... 105
Table 4.6 Pseudo-first-order Rate Constants of Pharmaceutical Removal during Electrolysis on Ti/IrO_2 used for the electrolytes in Figure 4.2b. 105
Table 4.7 Pseudo-first-order Rate Constants of Pharmaceutical Removal during Electrolysis on BDD used for the electrolytes in Figure 4.3a and Figure 4.3c..... 106
Table 4.8 Pseudo-first-order Rate Constants of Pharmaceutical Removal during Electrolysis on IrO_2 used for the electrolytes in Figure 4.3b and Figure 4.3d..... 106
Table 4.9 Pseudo-first-order Rate Constants of Pharmaceutical Removal during Electrolysis with BDD used for the electrolytes in Figure 4.5a, c..... 106
Table 4.10 Pseudo-first-order Rate Constants of Pharmaceutical Removal during Electrolysis with IrO_2 used for the electrolytes in Figure 4.5b, d..... 107

Table 5.1 The normalized yield of CBPs after 2hr electrolysis in FUM with or without the alternating scheme. 122
Table 5.2 The normalized yield of CBPs after 2 hr electrolysis in HUM with or without the alternating scheme. 127
Table 5.3 The normalized yield of CBPs after 2hr AC electrolysis in FUM and electrolysis with alternating scheme. 130

ACKNOWLEDGEMENTS

I have been fortunate to have an incredible support network, both professionally and personally, that has enabled the completion of this work. I would like to acknowledge some notable individuals who have supported me through my PhD.

First of all, I would like to acknowledge my advisor, Dr. Hugh Hillhouse. Thank you for challenging me and holding my work to a high standard. Your guidance has indeed enabled me to become a thoughtful scientist. Thank you for giving me flexibility in my PhD and for always encouraging efficient and effective scientific debate. I especially appreciate your natural curiosity and interest in scientific breakthroughs, and your contagious enthusiasm of education and scientific research can truly lead to positive societal change.

I would like to acknowledge my other committee members. Dr. Guozhong Cao, thank you for your kindness and encouragement through the years as we crossed paths in my every single exam. Dr. David Bergsman, thank you for serving as my reading committee and defense committee and for being interested in my research. Dr. Brandi Cossairt, thank you for serving as GSR on the committee and for being curious and interested in my research work.

I also greatly thank Prof. Michael C. Dodd (University of Washington, Department of Civil and Environmental Engineering) for the advice on chlorine and radical chemistry. I thank Kameron Harmon (University of Washington, Department of Chemical Engineering) for helping fabricate the electrochemical cell based on my design at my early stage of the project. I thank Prof. Ed Kolodziej (University of Washington-Tacoma) for helpful scientific discussions. I thank

Prof. Ilwhan Oh (Kumoh National Institute of Technology, Korea) for useful discussions. I thank Dr. Martin Sadilek (University of Washington, Department of Chemistry) for training and helpful discussion on HPLC-UV-MS. I also thank J. Sean Yeung (University of Washington, Department of Civil and Environmental Engineering) for training and helpful discussion on IC. Additionally, I thank Jesse Yu (University of Washington, Department of Pharmaceutics) for helpful discussions about elimination routes for pharmaceuticals. Furthermore, I would like to thank Benjamin Hornburg (University of Washington, Department of Chemical Engineering) for constantly supporting me to realize my design from a mere paper into practical parts with such a short turnaround time.

I would also like to thank my colleagues from Hilhouse research group. Dr. Felix Eickemeyer, thank you for all your help and support to familiarize me about lab when I first join the group. Dr. James A. Clark, thank you for working closely with me on the experimental setup from scratch as well as my first manuscript, especially how to design good experiments and conduct research with excellence. Dr. Ryan Stoddard, thank you for being a good and successful model for me to follow your trajectory to success. Dr. Wiley Dunlap-Shohl, thank you for your helpful discussion on both science and life. Nathanael R. Ramos, thank you for such helpful for the early stage of my research. I would not be able to finish the 2nd manuscript without your help and support. I also want to thank Dr. Timothy Siegler, Yuhuan Meng, and Preetham P Sunkari for being supportive about my work and asking insightful questions during my presentations.

DEDICATION

This dissertation is dedicated to my wife Sicong Sun and my daughter Mia L. Yang. Sicong, thank you for being extremely supportive of the long journey of my Ph.D. study and sacrifice your own career to support me to complete my Ph.D. Mia, thank you for coming to the world during the pandemic and choosing to be my daughter. I'm grateful to spend the joyful time with you and watch you grow. You're always my powerhouse when I am tired or feeling down. Love you three thousand, Yuhang.

Chapter 1. INTRODUCTION

1.1 EMERGING CONCERN OF PHARMACEUTICAL POLLUTANTS

Yearly pharmaceutical spending in the United States is $1,376 per capita in 2019, and 45.7% of Americans take at least one prescription drug per month.[1] A large portion of these drugs are excreted unchanged or as active metabolites via human urine and feces and join municipal wastewater streams.[2-4] Most of these compounds are not removed or sufficiently deactivated in wastewater treatment facilities (WWTFs). These pharmaceuticals eventually end up being discharged into the environment, threatening aquatic ecosystems,[5] and returning to human drinking water supplies.[6] Numerous studies have reported the detection of pharmaceuticals in drinking water [6], groundwater[7], surface water,[8] and wastewater [9] from ng/L to μg/L concentrations.

In one recent study, Meador et al.[7] has quantified 150 compounds of emerging concern in estuaries fed by rivers with waste water treatment plants in Washington State's Puget Sound. They found 81 of these 150 compounds in the WWTP effluent, 25 in the estuary water, and 42 in the tissue of whole-body juvenile Chinook salmon and Pacific staghorn sculpin in the estuary. The higher number of compounds found in the fish tissue than in the estuary water highlights the effect of bioaccumulation. A couple of the pharmaceuticals detected in fish tissue at high concentration were fluoxetine (antidepressant sold as Prozac found at 5 ng/g of salmon) and metformin (metabolic regulator for type-2 diabetes found at 28 ng/g of sculpin). Like many pharmaceuticals, fluoxetine is not completely metabolized in the body, and 11% is excreted unchanged as fluoxetine, while 7% is excreted as a biologically active metabolite

norfluoxetine.[10] In contrast, metformin is excreted 100% unchanged. Both compounds are excreted in humans primarily via urine, 80% and 90%, respectively.

The environmental problem is big and growing due to the proliferation of new pharmaceuticals, and it is both scientifically and economically challenging to treat large volumes of WWTP effluent polluted with dilute concentrations of 1000+ different chemical compounds. Currently, there is a dangerous absence of legislative or regulatory statues that could help address the problem. While the U.S. FDA does require an environmental assessment for new pharmaceutical approval, it is only required if the estimated environmental concentration of the drug is above 1 μg/L at the point of entry.[11] Despite that the vast majority of drugs do not exceed this, they have serious impact on fish and ecosystems at concentrations a thousand times less. This is a serious enough problem today, but there are dozens of new unique pharmaceutical compounds approved by the FDA each year, with 48 "new molecular entities" approved in total in 2019.[12] Furthermore, the COVID-19 pandemic significantly increases the consumption of non-steroidal anti-inflammatory drugs (specially ibuprofen) and is predicted to last for several years.[13] Consequently, this is a growing environmental problem with long term impact on aquatic ecosystems, species biodiversity, and human health. Therefore, the extensive occurrence of pharmaceuticals in aquatic environments and potable water demands efficient treatment of these micro-pollutants at the source.[14]

The removal of pharmaceuticals can be achieved by implementing physical or chemical treatment technologies such as advanced oxidation, filtration coupled with reverse osmosis,[15] sorption on activated carbons, etc.[16] However, without stricter regulation from government agencies (e.g., the Environmental Protection Agency in the U.S), WWTFs rarely install these advanced treatments. Therefore, treatment of pharmaceuticals at the source is particularly

important to reduce pharmaceutical discharge into aquatic environments and from entering the potable water supply.[14]

One of the dominant routes for human elimination of pharmaceuticals is via urine,[17] and most excreted compounds retain key pharmacological properties of their parent compounds.[18] Urine comprises only ~1% by volume of a typical municipal wastewater, yet represents a dominant source of pharmaceutical loading to wastewater treatment facilities, where ~75% by mass of ingested pharmaceuticals are typically excreted in urine as parent compounds and/or active metabolites.[4,19] Such compounds are often incompletely removed during typical municipal wastewater treatment and have potential negative impacts such as threats to wildlife,[20] contribution to the development of antibiotic-resistant bacteria,[21] and returning to drinking water supplies.[22] As a result, urine diversion (the collection and treatment of urine prior to or in lieu of discharge into mixed waste streams) has been proposed as an alternative approach to mitigate their discharge to the environment.[23] As urine is also a dominant source of the nutrients in typical municipal wastewaters (~80% of nitrogen and ~55% phosphorus by mass[24]), urine diversion has been widely investigated as a potential means of removing and recovering nutrients from waste streams for use in the production of liquid or dry fertilizer products.[25,26] In such cases, pre- or post-treatment to eliminate or separate pharmaceuticals from the product streams are likely to be necessary to ensure protection of human and ecosystem health, as well as to improve end-user acceptance and adoption.

1.2 Electrochemical Advanced Oxidation Processes (EAOPs)

Various advanced oxidation processes (AOPs) for wastewater treatment have been widely developed in the degradation of organic micropollutants in wastewater stream including Fenton process,[27] photocatalysis,[28] UV/H_2O_2.[29] However, research regarding the pharmaceutical

degradation in fresh human urine is quite limited. Few studies focus on the impacts of the unique urine matrix on AOPs for the destruction of pharmaceuticals in human urine. A range of physiochemical and biological treatment strategies have been explored to achieve the aim of pharmaceutical elimination or separation from urine,[30-32] including a variety of conventional and advanced oxidation processes. These processes can degrade organic contaminants via oxidizing species ($^{\bullet}OH$, O_3, HOCl, $Cl^{\bullet}$, $Cl_2^{\bullet-}$ and etc.) through chemical, photochemical, or electrochemical means.[23] Strategies that employ the use of chemical reagents (e.g., ozone, Fenton's reagent, peroxides, persulfate, or other oxidants or catalysts)[30,33,34] are often unsuitable for distributed or in-home use due to safety concerns regarding the handling of oxidants, removal or disposal of wastes from the process, and high-cost.

In comparison, electrochemical treatments – including electrochemical advanced oxidation processes (EAOPs) – have the potential to enable point-source treatment of urine that is safe and easy to operate since they do not require the addition of oxidants or generate new waste streams, and have received increasing attention as preferred options for source-separated urine treatment.[35-38] Furthermore, the scalability of EAOPs devices may enable treatment directly at the point of urine generation (e.g., a small in-line device connected to a conventional urinal or in the liquid waste stream of a urine-diverting toilet) as shown below, rather than after collection and storage of urine, as has typically been investigated for oxidative treatment.[39] This could in turn present opportunities for exploiting differences in the chemistry of fresh versus stored, hydrolyzed urine.

Furthermore, EAOPs are non-selective and can oxidize most organic compounds in general.[40] The efficacy of electrochemical treatment is determined by electrode materials, electrolyte compositions, mass transport conditions, geometry of electrolytic cell and applied

current densities (or potential) due to the kinds and yields of oxidants during electrolysis. The hydroxyl radical (•OH) is one of the strongest electrochemically generated oxidants with a standard potential of 2.86 V (vs. SHE), but to use its oxidative power effectively, it needs to be weakly bound to the anode surface. Typically, electrodes with high over-potential required for the evolution of oxygen gas, known as "inactive" electrodes, tend to have weak-interaction with •OH.[41,42] Boron-doped diamond (BDD) is an example of this class of anodes and has very strong oxidizing power due to the formation of weak surface-bound hydroxyl radicals (Equation 1.1).[43]

Equation 1.1:

$$BDD + H_2O \rightarrow BDD(^{\bullet}OH)_{ads} + H^+ + e^-$$

In contrast, electrodes with low over-potential for O_2(g) evolution, known as "active" electrodes, have strong interactions with •OH (forming a higher oxide on the surface; Equation 1.2).

Equation 1.2:

$$IrO_2 + H_2O \rightarrow IrO_{2+1} + 2\ H^+ + 2\ e^-$$

In electrolyte only containing Cl^-, IrO_{2+1} oxidizes Cl^- to form chemisorbed chlorine (IrO_3-Cl) via direct electron transfer (Volmer-step),[44] and then undergoes Herovsky (Table 1.1, eq. 1) and/or Tafel steps (Table 1.1, eq. 2) to generate Cl_2 followed by a fast hydrolysis to form HOCl in solution. IrO_2 is often referred to as an "active" electrode while BDD is referred to as an "inactive" electrode. This jargon survives from research aimed at increasing the rate of chlorine gas evolution for industrial chlorine production.

Table 1.1 Reaction Equations

Equation Number	**Reactions**	**Rate Constants/Standard Reduction Potential**	**Reference**
1	IrO_3-Cl + $Cl^- \rightarrow Cl_2 + e^-$	Rapid	[45]
2	2 IrO_3-Cl $\rightarrow Cl_2$	Rapid	[46]
3	Cl_2 + CBZ $\rightarrow$ products	$k = 6.7 \times 10^4\ M^{-1}s^{-1}$	[47]
4	Cl_2O + CBZ $\rightarrow$ products	$k = 2.7 \times 10^4\ M^{-1}s^{-1}$	[47]

5	$SO_4^{2-} \rightarrow SO_4^{\bullet-} + e^-$	$E^0 = 2.43$ V	[48]
6	$HSO_4^- + {}^{\bullet}OH \rightarrow SO_4^{\bullet-} + H_2O$	$k = 4.7 \times 10^5$ $M^{-1}s^{-1}$	[49]
7	$H_2SO_4 + {}^{\bullet}OH \rightarrow SO_4^{\bullet-} + H_3O^+$	$k = 1.4 \times 10^7$ $M^{-1}s^{-1}$	[49]
8	$SO_4^{\bullet-} + SO_4^{\bullet-} \rightarrow S_2O_8^{2-}$	$k = 1.6 \times 10^8$ $M^{-1}s^{-1}$	[50]
9	$Cl^{\bullet} + SO_4^{2-} \rightarrow Cl^- + SO_4^{\bullet-}$	$k = 2.5 \times 10^8$ $M^{-1}s^{-1}$	[51]
10	$Cl^- + SO_4^{\bullet-} \rightarrow Cl^{\bullet} + SO_4^{2-}$	$k = 2.6 \times 10^8$ $M^{-1}s^{-1}$	[52]
11	${}^{\bullet}OH + H_2PO_4^- \rightarrow H_2PO_4^{\bullet} + OH^-$	$k = 2.0 \times 10^4$ $M^{-1}s^{-1}$	[53,54]
12	$H_2PO_4^{\bullet} + Cl^- \rightarrow Cl^{\bullet} + H_2PO_4^-$	$k = 2.2\times 10^6$ $M^{-1}s^{-1}$	[53,54]
13	${}^{\bullet}OH$ + citrate ion → citrate radical + OH^-	$k = 2.4 \times 10^8$ $M^{-1}s^{-1}$	[55]
14	$Cl_2^{\bullet-}$ + citrate ion → citrate Radical + 2 Cl^-	$k = 10^7$ $M^{-1}s^{-1}$	Assumed
15	HOCl + citrate → chloroform	$k = 5.5 \times 10^{-3}$ $M^{-1}s^{-1}$	[56]
16	Cl_2 + citrate → chloroform	Fast	Assumed

Many materials have been studied as effective electrodes for EAOPs, including BDD, DSA®, PbO_2, doped SnO_2. Of the electrodes that exhibit weakly bound hydroxyls, PbO_2 has not been widely considered for wastewater treatment due to concerns of corrosion and contamination of the wastewater with lead. Doped SnO_2 received a lot of attention due to its potential for low cost and environmental friendliness. While the predominantly SnO_2 surface yields weakly bound ${}^{\bullet}OH$ surface species and strong oxidizing power, doped SnO_2 anodes have been repeatedly shown to be not stable enough for extended usage, unless coated with an interlayer of IrO_2.[57,58] This led to a large number of research groups shifting their focus towards BDD electrodes over the last decade. However, the Achilles heel of BDD is prohibitively high cost preventing it being used in real application.

1.3 The Complexity of Human Urine Matrixes

Human urine is a complex matrix that is very different from wastewater (post-secondary treatment) and drinking water where EAOPs have been successfully applied.[50] Fresh urine (authentic and synthetic) has a high concentration of urea ~250 mM (pH 6).[59] By contrast, stored hydrolyzed authentic urine has a urea concentration of ~0 mM, ammonium concentration of 30-

120 mM, bicarbonate/carbonate concentration of 25-30 mM (pH 9).[60] This is due to the urease-driven hydrolysis of urea to form ammonium, bicarbonate, and hydroxide (Equation 1.3).

Equation 1.3:

$$(NH_2)_2CO + 3H_2O \xrightarrow{\text{urease}} 2NH_4^+ + HCO_3^- + OH^-$$

This reaction happens rapidly, so that urea is nearly completely hydrolyzed within 5 hours of storage in a pipe.[61] The concentration of ammonium decreases over time with elevation of pH and volatilization of ammonia. The concentrations of carbonate species decrease due to precipitation as $CaCO_3$ [62].

A number of studies have examined electrochemical treatment of synthetic and human-generated urine for various purposes.[36-38,63-66] Most studies of EAOPs for urine treatment have focused on their application to *stored hydrolyzed urine*. In contrast, this study focuses on the underlying chemistry relevant to the application of EAOPs for treatment of *fresh urine*. Two significant challenges facing this approach are (1) the relatively low concentrations of pharmaceuticals in comparison to urea (and other oxidant scavenging constituents of the urine matrix) and (2) the potential formation of oxidation byproducts (OBPs) that results from oxidation of halides.

While the high electrical conductivity of fresh urine (due primarily to chloride salts) is an advantage for EAOPs, the presence of high concentrations of urea (over two orders-of-magnitude greater than pharmaceutical concentrations) could be anticipated as a major hurdle to pharmaceutical oxidation; potentially forcing one to oxidize urea before achieving significant oxidation of the pharmaceuticals. Organic compounds (e.g., urea, creatinine, and uric acid) in fresh urine compete with pharmaceuticals for the electro-generated oxidants during electrolysis. This has some benefits for the electrolysis of fresh urine where urea scavenges the reactive chlorine species (but not $^{\bullet}OH$) and decreases the formation of chlorate and perchlorate.[67]

Additionally, SO_4^{2-}, $H_2PO_4^-$ and citrate ions have the potential to scavenge $^{\bullet}OH$ and/or $Cl^{\bullet}$ and generate new oxidants such as $SO_4^{\bullet-}$, $H_2PO_4^{\bullet}$ and citrate radicals. Despite some research focusing on the applicability of EAOPs for pharmaceutical destruction in full synthetic fresh urine matrixes (FUM),[35,67] few studies have been conducted to understand the effect of electrode materials and individual urine components on the kinetics and pathways of pharmaceutical degradation.

1.4 Advantages of Decentralized Treatment of Urine

Point-source electrolysis of pharmaceuticals in source-separated urine has multiple advantages compared with centralized treatment at a WWTF mixing with other wastewater streams (Table 1.2). These advantages are: (1) small treatment volumes, (2) high pharmaceutical concentration, (3) absence of non-urine derived background organics or other interfering compositions, and (4) high electrical conductivity. Average human urine production is approximately 1.3 L/(person·day), while average domestic wastewater discharge is two orders of magnitude higher at 148 L/(person·day).[68] The dilution of urine with other waste streams not only decreases the absolute concentration of pharmaceuticals, but also decreases their relative concentration compared to the total concentration of organics in the solution (due to mixing with feces, cooking oils, detergents, etc.). This domestic wastewater may be further diluted by other waste streams containing other organics (such as industrial wastewater, urban runoff, etc.) before reaching a WWTF. The daily per capita load of chemical oxygen demand (COD) to domestic wastewater from all sources (e.g., including feces, urine, greywater, etc.) is more than 6x higher than from urine alone. The ratio of the chemical oxygen demand of pharmaceuticals to the chemical oxygen demand of total matrixes (COD_{pharm}/COD_{total}) is correspondingly 3.8% for domestic wastewater compared to 24.2% for urine (Table 1.2). Furthermore, the typical

conductivity of fresh urine is two orders-of-magnitude higher than domestic wastewater. The combination of large treatment volumes and low conductivity for domestic wastewater streams would correspond to massive ohmic losses in the solution, making EAOPs as a "polishing" or tertiary wastewater treatment step more costly. By contrast, the estimated electricity cost is more reasonable, and supposed to be much less than $57.60 per person per year (Table 1.2) due to the selective oxidation of pharmaceuticals before significant oxidation of organic constituents of urine. Nevertheless, the cost of electrochemical devices should be minimized by the development of reactors and inexpensive anodes where our follow-up work will be focusing on.

Table 1.2 Comparison of relative advantages of degrading pharmaceuticals in urine before dilution with other domestic wastewater.[68,69]

Matrix	Wastewater Contribution [L/person/day][a]	Conductivity [mS/cm][a]	Daily Per Capita COD Load [mg O_2/ person/ day]	Matrix COD [mg/L]	Pharm COD [mg/L]	Pharm COD/ (Pharm COD +Matrix COD)	Required Charge Passed [A·hr][b]	Electricity Cost [$/person/ day][b]	Electricity Cost [$/person/ year][b]
Pharmaceuticals Only	--	--	2080	--	--	--	29.0	$0.022	$7.95
Urine (including pharmaceuticals)	1.3	160	15080	10000	1600	13.8%	210	$0.16	$57.60
Domestic Wastewater	148	1.8	106080	702.7	14.05	2.0%	1480	$1.11	$405

[a] Dilution with other wastewater increases the treatment volume and reduces the matrix conductivity by two orders of magnitude. Pharmaceuticals are at their highest absolute and relative concentration when they are in urine, before they are diluted by other domestic wastewater sources. [b] To estimate the electricity cost of electrochemically oxidizing all organics in the matrix, chemical oxygen demand (COD) was used. The assumptions for these calculations are an electricity cost of 0.15 $/kWhr, a pharmaceutical concentration of 10 mM, a COD of 5 mols O_2/mol pharmaceutical, a total applied voltage of 5 V, a Faradaic efficiency toward oxidant reaction with organics of 30%, and full mineralization of pharmaceuticals to CO_2, H_2O, etc.

1.5 TOXIC BYPRODUCTS FORMATION

The high Cl^- content of urine creates opportunity for electrogenerated reactive chlorine species, but it also creates the possibility of forming organic and inorganic chlorinated oxidation byproducts (OBPs) at the anode.[70] The OBPs formed during EAOPs, including chlorate,

perchlorate, haloacetic acids, etc. may themselves pose risks for human health and the environment.[50] Thus, it is important to develop novel EAOPs or improved approaches to existing EAOPs that enable high efficiency of pharmaceutical degradation while minimizing OBPs formation.

Many reports highlight large amounts of OBPs generated from EAOPs of urine. The halogenated OBPs are mostly chlorinated species; however, brominated and iodinated species may be present at much lower concentrations but with higher toxicity.[70] ClO_4^- is the most challenging to remediate due to its high stability. ClO_4^- has a large activation barrier for reduction to ClO_3^- of 120 kJ/mole,[71] which makes its reduction very sluggish. The slow kinetics of ClO_4^- reduction accentuate the need that EAOPs do not generate significant quantities of ClO_4^-, even if an OBP remediation step is applied after oxidation. Interestingly, the concentrations of OBPs reported in different studies for roughly equivalent oxidation treatments are vastly different. For example, some studies report large amounts (>10 mM) of ClO_4^- after 30 A·hr/L of treatment using a boron-doped diamond (BDD) electrode,[66,70,72] while a similar report measured ClO_4^- below the detection limit for the same normalized charge passed.[36] One critical aspect of these studies that may explain the inconsistencies is variation in the compositions of the urine matrixes, in particular with respect to variations in concentrations of urea versus NH_4^+/NH_3 and carbonate species in *fresh* versus *hydrolyzed* urine.

Although ClO_4^- is the most challenging to remediate among all OBPs due to its large activation barrier of reduction to ClO_3^-,[71] the generation of organic chlorinated by-products (CBPs) is strictly regulated by US EPA and have been measured during treatment of domestic wastewater,[73,74] latrine wastewater,[70,75] urine,[66] and surface water.[76] Jasper, et al. has reported the generation of 25 mM ClO_3^-, 60μM dichloroacetic acids (DCAA), 30 μM chloroform ($CHCl_3$)

and monochloroacetic acids (MCAA), and 20 μM trichloroacetic acid (TCAA) after 30 Ah/L charge passed in the authentic stored latrine wastewater using IrO_2 electrode.[70] Additionally, Wang and his coworkers have studied the formation and transformation of organic and inorganic CBPs during electrolysis of synthetic fresh urine using Ru-IrO_2 and BDD electrodes.[77] Thus, it is important to develop novel EAOPs or improved approaches to existing EAOPs that enable high efficiency of pharmaceutical degradation while minimizing the formation of organic and inorganic CBPs.

1.6 OUTLINES

This dissertation contributes to development of electrochemical advanced oxidation processes for the pharmaceutical degradation in human urine through three different thrusts: (1) thorough investigation of the advantages and disadvantages of employing electrolysis in fresh urine as compared to that in hydrolyzed urine, (2) fundamental study of the significance of individual oxidants for the oxidation of pharmaceuticals as well as the scavenging effect of urine constituents during electrolysis in fresh human urine, and (3) development of an alternating scheme of oxidation and reduction for selective oxidation of pharmaceuticals and minimum generation of chlorinated byproducts. The chapters of this dissertation are organized as follows:

Chapter 2 summarizes the materials and solutions in this dissertation as well as the electrochemistry methods, analytical techniques and fundamental simulation based on theoretical calculations. This chapter can be read as a reference for experimental details and supplementary information for the discussion of experimental results, including the theory and modeling of mass transfer conditions, and determination of the stagnant layer thickness and local pH at anode or cathode.

Chapter 3 presents work examining the pseudo-first order rates constants of pharmaceutical oxidation and the generation of oxychlorides in various synthetic fresh urine matrixes and synthetic hydrolyzed urine matrixes. This work was published in Water Research.[67] In this work, we show that the unusually slow rates of $^{\bullet}OH$ with urea provides a selectivity of $^{\bullet}OH$ towards pharmaceutical degradation. Additionally, we demonstrate that urea (or NH_4^+/NH_3 from hydrolyzed urea) at the concentrations present in fresh human urine can suppress the pathways of Cl^- oxidation to ClO_3^- and ClO_4^- during EAOPs. This work provides an important contribution to the scientific community focusing on the electrolysis of fresh urine to mitigate the release of pharmaceuticals and other contaminants into the environment.

Chapter 4 studies the dominant degradation pathways and the scavenging effects of individual urine constituents during the electrochemical oxidation of pharmaceuticals in synthetic fresh human urine. This work was also published in Water Research.[78] This work progresses the understanding of the underlying chemistry and kinetics of the pharmaceutical oxidation via various electro-generated oxidants during electrolysis in synthetic fresh urine matrixes. In addition, we investigate various methods to accelerate the oxidation of pharmaceuticals in synthetic fresh human urine matrixes. We show that increasing the mass transfer rates or increasing the applied potential could enhance the oxidation rates of pharmaceuticals in synthetic fresh human urine matrixes.

Chapter 5 develops an alternating scheme of oxidation and reduction using interdigitated working electrodes (IWEs) for the selective oxidation of pharmaceutical and minimum generation of chlorinated byproducts during the electrolysis of various urine matrixes. In this work, we demonstrate that the oxidation rates of pharmaceuticals are enhanced but the generation of chlorinated byproducts is suppressed when the alternating scheme of oxidation and

reduction is employed. This work provides proof of principle for the future work aimed at engineering a flow cell using interdigitated electrodes as working electrodes at high mass transfer rates for rapid pharmaceutical remediation in human urine at the source of generation.

Chapter 2. MATERIALS AND METHODS

2.1 CHEMICALS AND SOLUTIONS

Ultrapure water (>18.2 MΩ/cm resistance) was used for preparation of all standards and test solutions. Reagent grade (99% purity or higher) $(NH_2)_2CO$, NaCl, $NaHCO_3$, NH_4OH, NH_4Cl, HCl, $NaClO_3$, $NaClO_4$, $HgCl_2$, $Na_2S_2O_3$, Na_2SO_4, $NaNO_3$, $NaNO_2$, glycine, creatinine, uric acid, and urea obtained from Sigma-Aldrich were used for all standards and test solutions.

DPD free and total chlorine test kits were obtained from Sigma-Aldrich. NaOCl (Sigma-Aldrich; 13.5% available chlorine) stock solution was calibrated every month by iodometry. Catalase (Sigma-Aldrich) was vortexed and centrifuged to remove the supernatant, then reconstituted in phosphate buffer and centrifuged again, with the process repeated 5 times to remove thymol. Analytical reference standards of cyclophosphamide (CP), sulfamethoxazole (SMX), carbamazepine (CBZ) and ibuprofen (IBP) from Sigma-Aldrich were used. Simplified synthetic fresh urine matrixes consisted of an aqueous solution of 250 mM urea, 100 mM NaCl. Synthetic full fresh urine matrix solutions consisted of 250 mM urea, 100 mM NaCl, 16 mM Na_2SO_4, 24 mM NaH_2PO_4, 13 mM creatinine, 3 mM uric acid (Table 2.1). All prepared synthetic fresh urine matrixes were at pH 6. Synthetic hydrolyzed urine matrixes consisted of an aqueous solution of 250 mM $NaHCO_3$, 100 mM NH_4Cl, and 400 mM NH_4OH (i.e., $[NH_4^+]_{total}$ = 500 mM) at pH 9.35. Synthetic hydrolyzed aged urine matrixes were adapted from Udert et al.[66] and Hoffmann et al.,[70] and consisted of 250 mM $NaHCO_3$, 100 mM NaCl, and either 140 mM or 33

mM NH_4OH at pH 9.02 and 8.88, respectively. Authentic fresh urine was collected at 10 A.M. and blended from 6 people, 3 males and 3 females, with different ethnic backgrounds and diets. The blended urine was pH 6.3. Electrolysis of authentic fresh urine was started immediately after the addition of 0.39 mM SMX to 40 mL of the blended urine.

Table 2.1 Proposed Composition of Full Synthetic Urine Matrixes

Components	Molecular weight (g/mol)	Concentration (mM)
Urea	60.06	250
NaCl	58.44	100
Na_2SO_4	142.04	15
NaH_2PO_4	119.98	20
Na_3Citrate	258.06	3
Creatinine	131.13	13
Uric Acid	168.11	3
pH		6

2.2 Electrochemical Cell and Electrodes

As shown in Figure 2.1 and Figure 2.2, the cell was designed to accommodate a large planar working electrode with dimensions 40 mm x 80 mm, which is held in place between the bottom of the cell and a base plate. A seal is formed with a Kalrez gasket exposing a planar surface area of the working electrode of 8.56 cm^2. Planar anodes (BDD or IrO_2) were used for oxidation experiments. SAE 304 stainless steel tubes were used as the counter electrodes in all oxidation experiments. An Ag/AgCl (3 M NaCl) reference electrode (BASi, West Lafayette, IN, USA) was used in all experiments. In the “undivided cell” setup, the counter electrode was immersed in the same solution as the working electrode. In the “divided cell” setup, the counter electrode was placed inside a glass tube with a 12 mm O.D. porous frit at the bottom (4-8 μm pores, ACE Glass #7209 porosity E). For oxidation experiments, three counter electrodes in fritted glass

tubes were used in parallel to minimize resistance and potential drop due to ionic transport through the frits.

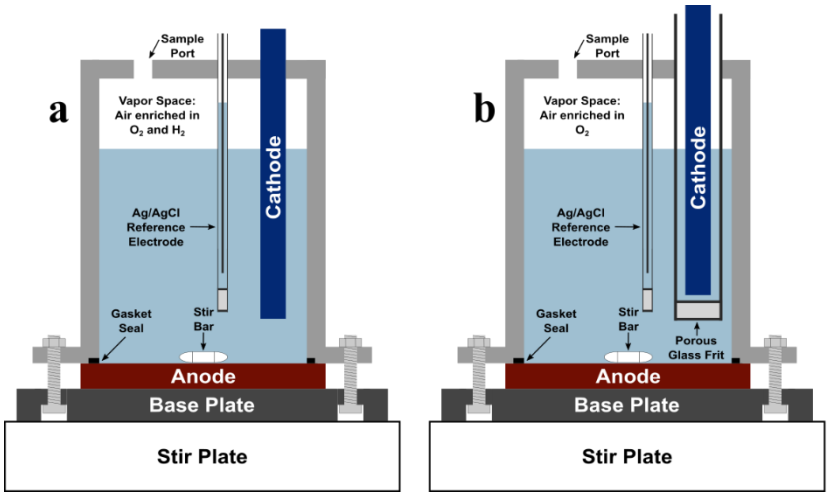

Figure 2.1 **Schematic overviews of electrochemical cell configurations used in this work.** (a) The undivided setup for oxidation experiments. (b) The divided cell setup for oxidation experiments.

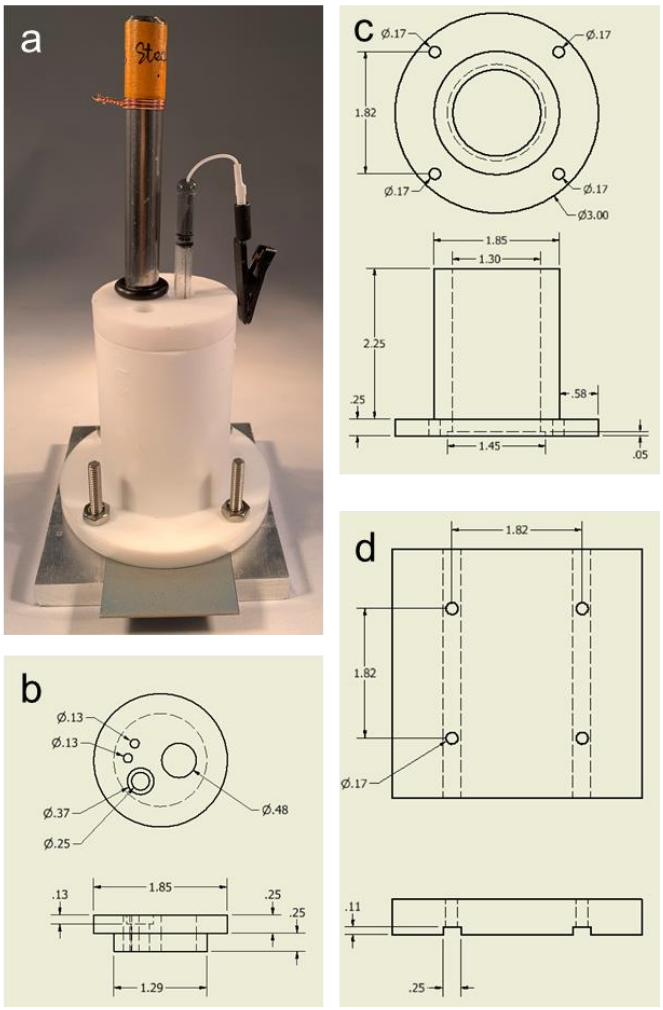

Figure 2.2 (a) **Photograph of the electrochemical cell depicted in Figure 2.1** (b,c,d) **Schematics for the dimensions of the electrochemical cell**

Planar boron-doped diamond (BDD) electrodes were purchased from Condias GmbH. Planar Ti/IrO_2 electrodes were prepared by thermal decomposition of a 250 mM H_2IrCl_6 precursor solution similar to a method described previously.[66] Ti sheet metal was first sandblasted and cleaned with 1 M oxalic acid for 1 hour at 95 °C. The precursor solution was spray-coated onto the Ti substrates on a hotplate held at 500 °C, and then the substrates were annealed at 500 °C for 1 hr after precursor deposition.

Ti/IrO_2 interdigitated working electrodes (IWEs) were designed and used as the working electrodes (see schematic drawing and pictures in Chapter 5). Planar Ti/IrO_2 IWEs were prepared by thermal decomposition of a 250 mM H_2IrCl_6 precursor solution similar to a method described above. Ti shim (0.127 mm thick) metal was first cut into the shape of the strips of IWEs, and then was sandblasted and cleaned with 1 M oxalic acid for 1 hour at 95 °C. The precursor solution was spray-coated onto the Ti substrates on a hotplate held at 500 °C, and then the substrates were annealed at 500 °C for 1 hr after precursor deposition. After cooling down the room temperature, the Ti/IrO_2 IWEs were epoxy-glued on a clean soda-lime glass substrate.

2.3 Experimental Methods

2.3.1 *Cyclic Voltammetry of Anode Reactions*

Each electrode (BDD and IrO_2) was sonicated in deionized water then pretreated in 40 mL 100 mM Na_2SO_4 for 5 minutes at 3.5 V or 2 V respectively. The electrochemical cell was then thoroughly rinsed with deionized water. The matrix of interest was then added to the cell and a single scan was initiated from 0 V to 3.5 V or 2.5 V respectively, and back to 0 V at a scan rate of 50 mV/s in the undivided cell setup. Nitrogen gas bubbled through the solution for two minutes prior to and blanketed during the cyclic voltammetry.

For the limiting current measurement in Chapter 2.3.5, the solution properties, D of $[Fe(CN)_6]^{3-}$, and v of electrolyte, were assumed from literature values (D = 0.76 x 10^{-9} m^2/s and v = 0.88 x 10^{-6} m^2/s) resulting in Sc ~ 1200.[79] The effective area of the working electrode was 8.56 cm^2 and the electrolyte volume was 40 mL for all experiments. K_2CO_3 was used as supporting electrolyte due to its long term stability during limiting current measurements,[80] large inert potential window,[81] and basicity for stabilizing solutions containing $[Fe(CN)_6]^{4-}$.[82] K_2CO_3 was

used at 100x the concentration of $K_3[Fe(CN)_6]$ and $K_4[Fe(CN)_6]$ to eliminate the effect of ionic migration in mass transfer of $[Fe(CN)_6]^{3-}$ and $[Fe(CN)_6]^{4-}$. The reduction of $[Fe(CN)_6]^{3-}$ was studied for the limiting current because the $[Fe(CN)_6]^{3-}/[Fe(CN)_6]^{4-}$ has well-known, facile, electrochemically reversible behavior.[79,83] An equimolar concentration of $[Fe(CN)_6]^{3-}$ and $[Fe(CN)_6]^{4-}$ was used to ensure the bulk concentration of $[Fe(CN)_6]^{3-}$ did not change appreciably during a limiting current measurement. A UV-Vis spectrometer (PerkinElmer LAMBDA 1050) was used to determine the exact bulk concentration of $[Fe(CN)_6]^{3-}$ from its characteristic absorbance at 420 nm. The other electrolyte components (K^+, CO_3^{2-}, $[Fe(CN)_6]^{4-}$) did not interfere with this absorbance measurement.

Prior to each set of experiments, the electrodes and electrochemical cell were sonicated in DI water for 10 min. All electrolytes were held at 20 °C (near ambient lab temperature) and purged with nitrogen gas to remove dissolved oxygen that may interfere with electrochemical measurements. Cyclic voltammetry (CV) was used to pretreat the working electrode (between 1.1 and -1.4 V vs. Ag/AgCl) in background electrolyte (500 mM K_2CO_3) at 100 mV/s. The electrochemical system (500 mM K_2CO_3, 5 mM $K_3[Fe(CN)_6]$, 5 mM $K_4[Fe(CN)_6]$) was characterized with CV (between -0.75 and 0.75 V vs. Ag/AgCl) at a scan rate of 100 mV/s.

Steady state linear sweep voltammetry (LSV) was used to obtain the limiting current given a stir rate and stir bar.[84] All LSVs were conducted in 500 mM K_2CO_3, 5 mM $K_3[Fe(CN)_6]$, 5 mM $K_4[Fe(CN)_6]$. After a steady flow pattern was attained at a given stir rate, an LSV was swept from open-circuit potential (~ 0.24 V vs. Ag/AgCl) to -0.5 V vs. Ag/AgCl at a scan rate of 5 mV/s. The plateau in current with increasing overpotential represents the mass-transfer limited reduction of $[Fe(CN)_6]^{3-}$ at the working electrode surface. All limiting current experiments were repeated to test for reproducibility.

2.3.2 *Galvanostatic Oxidation of Pharmaceuticals in Urine*

Electrochemical oxidations of pharmaceutical compounds were performed galvanostatically at a current density of 10 mA/cm^2 for 90 or120 min (reaching 4.2 A-h/L) while the solution was stirred at 600 rpm (*Re* = 2977) or 1000 rpm (*Re* = 11050) for experiments in Chapter 3 and Chapter 4.

In Chapter 3, the experiments were conducted in a supporting electrolyte with the major constituents of simplified synthetic fresh urine (– 100 mM NaCl and 250 mM urea, pH 6.15) or full synthetic fresh urine matrixes (Table 2.1) or synthetic hydrolyzed, aged urine matrixes (i.e., [NH_4^+/NH_3] = 33 or 140 or 500 mM, [HCO_3^-/CO_3^{2-}] = 250 mM and pH 9) and SMX or CP at a concentration of 0.39 mM or 1.92 mM, respectively. Based upon the suggested dosage from U.S. FDA [85,86] and percentage of excretion via urine,[87,88] SMX and CP will theoretically remain in human urine at concentrations of 0.975 mM and 1.92 mM, respectively. While the solubility of SMX is 610 mg/L (2.41 mM) at 37 °C,[89] dissolving this concentration of SMX at room temperature was difficult. Therefore, 100 mg/L SMX (0.39 mM) was used for electrolysis at room temperature.

In Chapter 4, electrolysis experiments were conducted in electrolyte containing a mixture of 20 mg/L each of CP (0.076 mM), CBZ (0.085 mM), SMX (0.079 mM), and IBP (0.097 mM) and 100 mM NaCl/$NaClO_4$ or the constituents of synthetic fresh urine at desired concentrations.[30,69,90] Based upon the suggested dosage from U.S. FDA and percentage of excretion via urine,[87,88,91,92] CBZ and IBP will theoretically remain in human urine at concentrations of 1.92 mM, 1.22 mM, 0.975 mM, and 3.95 mM, respectively. Since the solubility of IBP in water at 20 °C is 21 mg/L,[93] 20 mg/L of each pharmaceutical was selected to avoid the competition from the differences in pharmaceutical concentrations. 100 mM $NaClO_4$

was used as the supporting electrolyte to evaluate the importance of adsorbed and dissolved $^{\bullet}OH$. Allyl alcohol (AA; 500mM), or tert-butanol (t-BuOH; 500 mM) were used as selective quenchers to differentiate the importance of adsorbed radicals ($Cl^{\bullet}_{ads}$ and $^{\bullet}OH_{ads}$) and dissolved radicals ($Cl^{\bullet}$, $Cl_2^{\bullet-}$ and $^{\bullet}OH$) for pharmaceutical degradation, respectively.[94]

For all experiments above, aliquots were periodically collected, quenched with excess thiosulfate, and analyzed for target compounds and oxidation byproducts. The pseudo-first-order rate constants of pharmaceutical degradation were determined by fitting the pseudo-first-order kinetic models to the measured pharmaceutical concentrations during electrolysis.

2.3.3 *Galvanostatic Oxidation of Urine without Pharmaceuticals*

In Chapter 3, electrochemical oxidations were performed galvanostatically for the investigation of oxychloride generation during electrolysis of various urine matrixes. The electrolysis was conducted at a current density of 93 mA/cm^2 on BDD electrode for 90 min (reaching 30 Ah/L), stirred at 600 rpm. These experiments were conducted in the supporting electrolytes that simulated different urine matrixes (simplified vs full urine matrixes, fresh vs. hydrolyzed, ammonia loss vs. no ammonia loss). A control experiment was conducted in NaCl solution to yield maximal oxychloride generation as a reference.

2.3.4 *Potentiostatic Oxidation of Urine by Alternating Scheme of Oxidation and Reduction*

In Chapter 5, Electrolysis experiments were conducted in electrolyte similar to Chapter 3 and Chapter 4. Electrolytes (40 mL) were magnetically stirred at a rate of 600 rpm (*Re* = 2977) or 1000 rpm (*Re* = 11050) for all experiments. Ti/IrO_2 tubes were sued as the counter electrodes in all electrolysis experiments if not specified. All electrolysis experiments were conducted potentiostatically at 2.5 V (vs. Ag/AgCl) on one of the strips of the IrO_2 IWEs, and open circuit,

0, -1, -2, -3 V (vs. Ag/AgCl) on another strip of the IDEs for 120 min. The bi-potentiostatic experiments were performed with a Pine Instrument Company Model AFRDE5 Bi-Potentiostat. The currents were read and recorded by a NI myRIO-1900 analog-to-digital converter and a LabView program for all experiments. For the AC electrolysis, the potential was only applied to one specific strip of the IrO_2 IWEs. The AC electrolysis was achieved by employing a potential square-wave of 2.5 V and -2 V with an alternating frequency of 1 Hz or 100 Hz using Princeton Applied Research Potentiostat/Galvanostat Model 263A.

2.3.5 *Mass-transfer Limiting Pseudo-first-order Rate Constants*

The mass-transfer limiting pseudo-first-order rate constants (k_m) were calculated using the limiting current approach.[95] Linear sweep voltammetry (LSV) in magnetic stirring mode was performed in a 500 mM K_2CO_3 background electrolyte with concentrations of 5 mM $K_3[Fe(CN)_6]$ and 5 mM $K_4[Fe(CN)_6]$. The LSV scans swept from 0.4 V to -0.5 V (vs. Ag/AgCl) at 10 mV/s and the limiting current for the reduction of $[Fe(CN)_6]^{3-}$ was measured. Therefore, the mass transfer coefficient of species $[Fe(CN)_6]^{3-}$ ($k_{c,ferrocyanide}$) were determined by the equation $k_{c,ferrocyanide} = I_{lim}/(nFAC_b)$, where n is the number of electrons transferred, F is Faraday's constant, and C_b is the bulk concentration of the $[Fe(CN)_6]^{3-}$. $[Fe(CN)_6]^{3-}/[Fe(CN)_6]^{4-}$ was chosen due to its facile one electron transfer reaction at the electrode surface.

The limiting currents at a stir rate of 600 rpm (*Re* = 2977) and at a stir rate of 1000 rpm (*Re* = 11050) are -1.12 mA/cm^2 and -3.08 mA/cm^2 for a bulk concentration of ~5.8 mM $[Fe(CN)_6]^{3-}$ (Figure 2.3). Therefore, the $k_{c,ferrocyanide}$ were determined to be 0.117 cm/min ± 2.14% and 0.300 cm/min ± 5.90% at stir rates of 600 rpm and 1000 rpm, respectively. However, the k_c should be corrected for different solution viscosity (ν), and diffusion coefficients of species (D). Additionally, the k_c can be predicted from Sherwood number ($Sh = k_c L/D$) which is expressed as

a function of Reynolds number (*Re*) and Schmidt number (*Sc*). The Levich equation for a rotating disk electrode (RDE) predicts Sh to be proportional to the product $Re^{1/2}Sc^{1/3}$ with a proportionality constant.[79] The rotational system in this magnetically stirred geometry is similar to RDE. Therefore, we can derive the $k_{c,\ pharmaceutical}$ from $k_{c,\ ferrocyanide}$ by the same Sh due to the identical convective conditions (i.e., stir rate) and cell geometry (i.e., characteristic length and proportionality constant):

Equation 2.1:

$$\frac{k_{c,pharmaceutical}\nu_{water}^{1/6}}{D_{pharmaceutical}^{2/3}} = \frac{k_{c,ferrocyanide}\nu_{water}^{1/6}}{D_{ferrocyanide}^{2/3}}$$

The $D_{ferrocyanide}$ is determined to be 5.6 x 10^{-6} cm^2/s from the Randles-Sevcik equation.[79] Therefore, the $k_{c,pharmaceutical}$ are 0.130 cm/min and 0.335 cm/min at stir rates of 600 rpm and 1000 rpm, respectively (assuming $D_{pharmaceutical}$ = 6.6 x 10^{-6} cm^2/s). These rates were converted to the pseudo-first-order pharmaceutical degradation rates by $k_m = k_{c,\ pharmaceutical} \times (S.A.)/V$, where S.A. is the surface area of electrode, V is the volume of electrolyte, and S.A./V = 0.214 in this work. Therefore, the k_m are 0.028 min^{-1} ± 2.14% and 0.072 min^{-1} ± 5.90% for stir rates of 600 rpm and 1000 rpm, respectively.

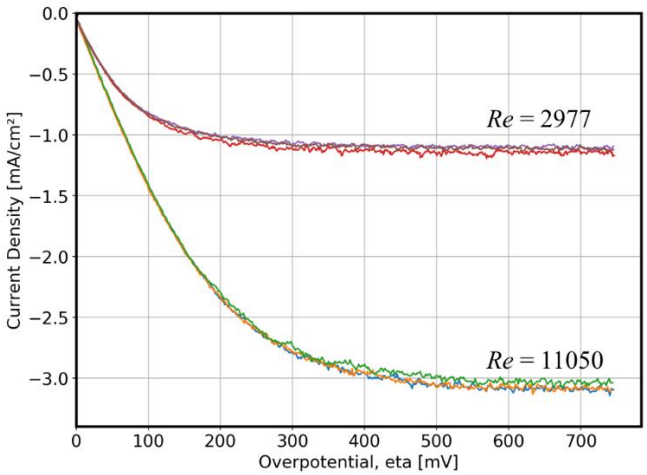

Figure 2.3 **Linear sweep voltammetry (LSV) of equimolar $[Fe(CN)_6]^{3-}$/ $[Fe(CN)_6]^{4-}$ in K_2CO_3 supporting electrolyte on boron-doped diamond (BDD) electrode** at a stir rate of 600 rpm (Re = 2977) and a stir rate of 1000 rpm (*Re* = 11050). The grouped lines represent the triplicate experiments to determine the uncertainty of measurements.

2.4 Analytical Methods

2.4.1 *Ion Chromatography*

Inorganic ions were measured by ion chromatography (IC), where 0.2 mL sample aliquots were mixed with 0.2 mL of 20 mM $Na_2S_2O_3$ (to quench oxidants and prevent column damage) and 0.6 mL of ultrapure water (HPLC grade) prior to analyses. In Chapter 3 and Chapter 4, IC chromatograms were obtained using a Dionex ICS-3000 with an AS19 column and a conductivity detector. The mobile phase consisted of 10 mM KOH ramped up to 58 mM KOH over 30 min, then held constant for 10 min, and returned over 0.5 min to initial conditions to establish separation between anions (Cl^-, NO_2^-, ClO_3^-, NO_3^-, SO_4^{2-}, $S_2O_3^{2-}$, and ClO_4^-).

For the experiments in Chapter 5, IC chromatograms of ClO_3^- were obtained using a Dionex ICS-1000 with an AS9 column (I.D. 4 mm), a suppressor, and a conductivity detector. The mobile phase consisted of 9 mM Na_2CO_3 (isocratic elution) and held constant at a flow rate of 1 mL/min for 17.5 min. The ClO_4^- was measured using an AS16 column with 50 mM KOH isocratic elution at a flow rate of 1 mL/min for 20 min. **ClO_4^- was not measured in any experimental setup in Chapter 5**.

2.4.2 *High Performance Liquid Chromatography*

For HPLC-UV-MS analyses of organic analytes, 0.02 mL and 0.2 mL aliquots were taken for CP and SMX oxidation experiments, respectively. These aliquots were mixed with 0.2 mL of 20 mM $Na_2S_2O_3$ and diluted with ultrapure water (HPLC grade) to a final volume of 1 mL. The

concentrations of target compounds were quantified by an HP Agilent 1100 high-performance liquid chromatography system coupled with a DAD UV detector and Bruker Esquire LC ion trap mass spectrometer. Test compounds were separated by an Agilent Zorbax SB-C18 column (2.1 x 100 mm; 3.5 μm), with elution at 0.2 mL min^{-1} using acetonitrile with 1% acetic acid (Eluent A) and water with 1% acetic acid and 5% acetonitrile (Eluent B). The following gradient was used: 0 min, 10% Eluent A; 9 min, 100% Eluent A; 14 min, 100% Eluent A; 16 min, 10% Eluent A. Column temperature was held at 30 ℃. SMX was detected by UV absorbance (280 nm) and CP was detected by positive electrospray ionization (ESI+) mass spectrometry in standard resolution mode with a capillary voltage of 3.5 kV and a source offset of -500 V. Desolvation temperature was 350 °C. Desolvation gas was 600 L/h. Scan time was 0.2 s in continuum mode.

2.4.3 *Gas Chromatography (GC)*

The concentration of monochloroacetic acid (MCAA), dichloroacetic acid (DCAA), trichloroacetic acid (TCAA) and chloroform ($CHCl_3$; TCM) were measured by an Agilent 5973 GC-MS using a HP-5ms column, and the sample preparation and GC methods were adapted from literature.[70,96,97] For HAAs (i.e., MCAA, DCAA and TCAA) analysis, samples (1 mL) were amended with 0.5 g Na_2SO_4 and extracted 0.5 mL supernatant using methyl tert-butyl ether (MTBE; 1 mL). HAAs were converted to their corresponding methyl esters by addition of 10% (v/v) H_2SO_4 in methanol (0.5 mL) at 50 ºC for 2 hr. After conversion, samples were cleaned with 10% (w/w) Na_2SO_4 in water (3 mL), and the organic phase was collected for GC-MS analysis. The method of GC-MS was followed exactly the same as Xie's technical note.[96] For TCM analysis, 1 mL sample aliquots were collected periodically and TCM was extracted using 0.25 mL pentane. The organic phase was collected using a glass transfer pipet for GC analysis. All GC samples were stored in a freezer (-10 ºC) until the chromatographic analysis. The GC method

for TCM analysis was adapted from Hoffmann et. al.[70] with small modifications: the oven was set at 30 ºC and held for 2 min, then ramped to 50 ºC for 2 min at a rate of 5 ºC/min, and then ramped to 185 ºC for 5 min at a rate of 25 ºC/min.

2.4.4 *Determination of free chlorine (FC – primarily the sum of HOCl + OCl^-, and to a lesser extent Cl_2 and/or Cl_2O), total chlorine (TC – the sum of FC + inorganic and organic chloramines), and ClO_2 during electrolysis*

For all chlorine species measurements, triplicate samples were periodically collected when electrolysis was employed in the undivided cell configuration on the BDD anode with 100 mA/cm^2 energy input under a stir rate of 500 rpm. FC, TC, and ClO_2 concentrations were determined via UV/Visible spectrophotometer based on absorbances at 535 nm (DPD method) or 410 nm (ABTS method), as described below.

FC was measured colorimetrically using *N*,*N*-diethyl-*p*-phenylenediamine (DPD) free chlorine test kits (Sigma-Aldrich) in accord with standard methods,[98] or (2,2-azino-bis(3-ethylbenzothiazoline)-6-sulfonic acid-diammonium salt (ABTS) (Sigma-Aldrich) as an alternative method for verification.[99]

For the DPD method, sample aliquots (0.2 mL) were amended with 0.1 mL $HgCl_2$ (11 mM; to sequester trace iodide), diluted in phosphate buffer (100 mM; pH 6) to a total volume of 10 mL, dosed with 1 spoon of Cl_2-1 powder (DPD method), vigorously shaken, and their UV-Vis absorbances then determined, in order to enable direct measurements of FC.

For the ABTS method, sample aliquots (0.1 mL) were first added to 1 mL phosphate buffer (100 mM; pH 8) to raise pH, and then pretreated with 0.05 mL $NaNO_2$ (0.1 M) for 5 min to quench HOCl and ClO_2. Then 1 mL ABTS (19 mM), 4 drops of Cl_2-2 reagent (KI), and phosphate buffer (100 mM; pH 6) were added to a total volume of 10 mL, samples were

vigorously shaken, and their UV-Vis absorbances were determined, yielding measurements of chloramine concentrations. FC concentrations were determined by subtracting the measured chloramine concentrations from measured TC concentrations for the same samples (*see below*).

TC was measured colorimetrically using DPD/KI reagent kits (Sigma-Aldrich) in accord with standard methods,[100] or ABTS as an alternative method for verification.[99] Sample aliquots (0.1 mL) were dosed with 4 drops of Cl_2-2 reagent (KI), diluted in phosphate buffer (100 mM; pH 6) to a total volume of 10 mL, then dosed with 1 spoon of Cl_2-1 powder or 1 mL ABTS (19 mM), and vigorously shaken prior to determination of their UV-Vis absorbance, in order to enable direct measurements of TC.

Additional measurements were undertaken to confirm the absence of H_2O_2, and in turn exclude the possibility of false-positive responses in TC measurements due to the presence of H_2O_2. Samples were collected and diluted with phosphate buffer (100 mM; pH 6) to a total volume of 10 mL, treated with 10 μL catalase (Sigma-Aldrich; thymol-free; ≥ 20 mg/mL) for 15 min to completely decompose H_2O_2, and then prepared for subsequent TC measurements by the DPD method (*see above*).

ClO_2 was measured colorimetrically using ABTS.[99] Sample aliquots (1 mL) were amended with 0.1 mL $HgCl_2$ (11 mM), diluted in phosphate buffer (100 mM; pH 6) to a total volume of 10 mL, then dosed with 0.4 mL ABTS (19 mM) and vigorously shaken prior to determination of their UV-Vis absorbances, in order to enable direct measurements of ClO_2.

2.5 THEORETICAL SIMULATION AND CALCULATION

2.5.1 *Mass-transfer rates and kinetic rates under steady state assumption*

Assume the oxidation of pharmaceutical occurs at the anode surface and the heat of reaction is negligible, then we have an essentially isothermal situation. The reaction is a first order irreversible reaction. The rate of reaction is given by:

$$R_{pharm.} = -k' C_{pharm.}$$

where $R_{pharm.}$ is the rate of pharmaceutical degradation on the anode surface, k' is the first order kinetic rate constant, $C_{pharm.}$ is the concentration of pharmaceutical.

As shown in Figure 2.4 (Gradient A & B), since the diffusion takes place in the stagnant layer, the steady stat diffusion equation reduces to

$$\frac{d^2 C_{pharm.}}{dx^2} = 0$$

with boundary conditions: (1) x = 0, $C_{pharm} = C_s$; (2) x = δ, $C_{pharm} = C_b$, where C_s is the concentration of pharmaceutical at anode surface, C_b is the bulk concentration of pharmaceutical, and δ is the thickness of the stagnant layer. Therefore, by substitute the boundary conditions to the second differential equation:

$$C_{pharm.} = \frac{C_b - C_s}{\delta} x + C_s$$

Therefore, the flux of pharmaceutical arriving to the surface at x = 0, $-J_{pharm.}|_{x=0}$ (mol/m^{2}s) is

$$-J_{pharm.}|_{x=0} = -\left(-D \frac{dC_{pharm.}}{dx}\right) = \frac{D}{\delta}(C_b - C_s)$$

where D is the diffusivity of pharmaceutical. The mass-transfer limiting rates is

$$k_{m,lim} = \frac{D}{\delta}$$

and substitute the k_m in the flux:

$$-J_{pharm.}|_{x=0} = k_m(C_b - C_s)$$

At steady state the flux of pharmaceutical to the anode surface must equal the reaction rate of pharmaceutical at the surface. Therefore,

$$-R_{pharm.} = -J_{pharm.}|_{x=0}$$

$$k_m(C_b - C_s) == k'C_s$$

$$C_s = \frac{C_b}{1 + \frac{k'}{k_m}}$$

These equations yield the actual rate of reaction:

$$-R_{pharm.} = k'C_s = \frac{C_b}{\frac{1}{k'} + \frac{1}{k_{lim}}}$$

When the reaction is purely mass transfer limiting, k' >> k_m, the mass-transfer limiting rate is given by $-R_{pharm.} = k_m C_b$. When the reaction is purely kinetically limited, k' << k_m, the kinetically limited reaction rate is given by $-R_{pharm.} = k'C_b$.

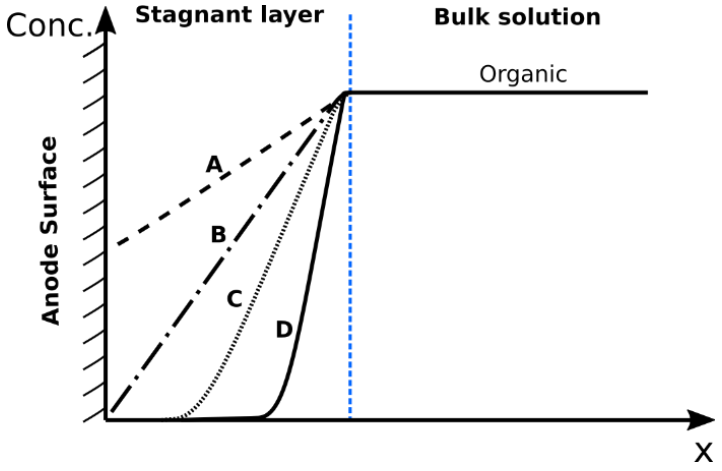

Figure 2.4 **Possible concentration gradients of pharmaceuticals in the stagnant layer** (assuming constant bulk concentration). Gradient A: oxidation that is kinetically limited by the heterogeneous reactions at the anode surface (i.e., via direct anodic oxidation and surface bound oxidants). Gradient B: the oxidation is mass-transfer-limited and the concentration is zero at the

anode surface but increases in solution. Gradient C: the oxidation is mass-transfer-limited, but in addition to heterogeneous reactions, oxidants generated at the anode desorb, diffuse outward, and react homogeneously with the pharmaceutical to drive the concentration to zero some distance away from the surface. Gradient D: the oxidation is mass-transfer-limited with a larger homogeneous reaction enhancement than gradient C.

Since the quantification of pharmaceuticals is the concentration of bulk solution, the observed pseudo first order rate constant without any homogeneous reaction enhancement (Figure 2.4, gradient A & B) can be rewritten to

$$k_{obs} = \frac{1}{\frac{1}{k'} + \frac{1}{k_{lim}}}$$

Furthermore, the kinetic rate constants can be determined for all pharmaceutical degradation rates below the mass-transfer limiting rates under our experimental condition. Thus, the limiting reaction mechanisms can be appropriately discussed based on the magnitude of k' and k_m.

2.5.2 *The Stagnant Layer Thickness and Local pH at Electrode Surface*

In the steady-state diffusion layer model, the thickness of the stagnant layer during electrolysis can be calculated by $k_c = D/\delta$, where k_c is the mass transfer coefficient, D is the diffusion coefficient, and δ is the thickness of the stagnant boundary layer. As noted above, the diffusion coefficient of $[Fe(CN)_6]^{3-}$ is 5.6 x 10^{-6} cm^2/s. Therefore, the thickness of stagnant layer thickness is 28.7 μm and 11.2 μm at stir rates of 600 rpm and 1000 rpm, respectively.

Furthermore, the local pH at the anode surface is determined. The oxidation of water at the anode results in the formation of H^+ due to the formation of $^{\bullet}OH$ and O_2. Assuming 100% Faradaic efficiency and under a current density of 10 mA/cm^2, the flus of H^+ is 1.06 x 10^{-7} $mol/(cm^2s)$. Therefore, the concertation of H^+ at the electrode surface ($C_{s,H+}$) was calculated by

Fick's first law: $J_{H+} = k_{c,H+} (C_{b,H+} - C_{s,H+})$, where J_{H+} is the flux of H^+, and $k_{c,H+}$ is the mass transfer coefficient of H^+. The $k_{c,H+}$ was derived from $k_{c,ferrocyanide}$ using equation 1. Therefore, the $k_{c,H+}$ are 0.0353 cm/min and 0.0906 cm/min for stir rates of 600 rpm and 1000 rpm, respectively. Furthermore, the diffusion coefficient of H^+ in water is 9.311 x 10^{-5} cm^2/s,[71] and the pH of the bulk solution is 6 ($[H^+]$ = 1 x 10^{-6} M). Thus, the pH at the anode surface are 0.74 and 1.15 for stir rates of 600 rpm and 1000 rpm, respectively. The pH gradient with respect to the distance from anode surface is shown in Figure 2.5.

Additionally, the local pH at the cathode surface is determined for Chapter 5. The oxidation of water at the cathode results in the formation of OH^- due to the formation of H_2. Assuming 100% Faradaic efficiency and under a current density of 10 mA/cm^2, the flus of OH^- is 1.06 x 10^{-7} $mol/(cm^2s)$. Therefore, the concertation of OH^- at the electrode surface ($C_{s,OH-}$) was calculated by Fick's first law: $J_{OH-} = k_{c,\,OH-} (C_{s,\,OH-} - C_{b,\,OH-})$, where J_{OH-} is the flux of OH^-, and $k_{c,\,OH-}$ is the mass transfer coefficient of OH^-. Therefore, the $k_{c,\,OH-}$ are 0.0353 cm/min and 0.0906 cm/min for stir rates of 600 rpm and 1000 rpm, respectively. Furthermore, the diffusion coefficient of OH^- in water is 5.27 x 10^{-5} cm^2/s,[101] and the pH of the bulk solution is 6 (i.e., $[OH^-]$ = 1 x 10^{-8} M). Thus, the pH at the anode surface is 13.25 and 12.85 for stir rates of 600 rpm and 1000 rpm, respectively.

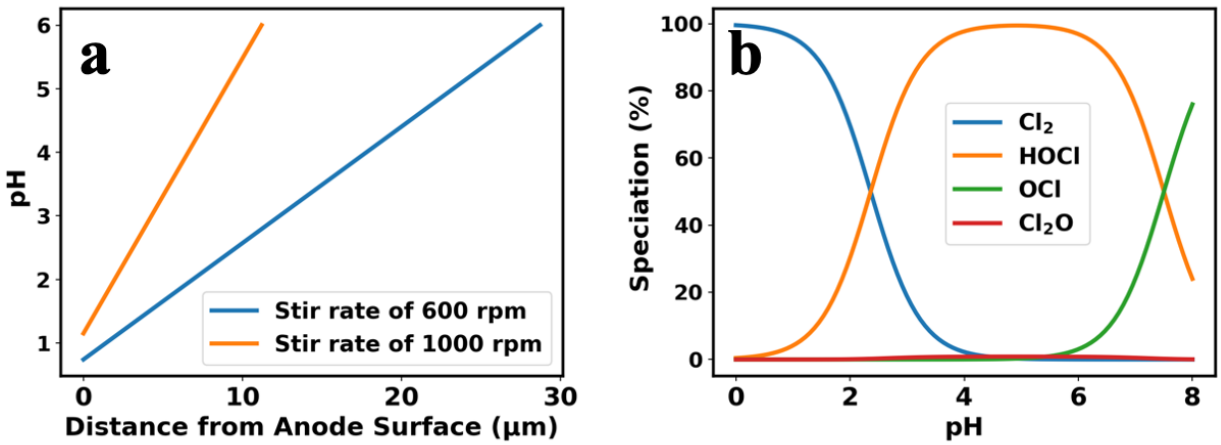

Figure 2.5 **(a) pH gradient as a function of the distance from anode surface by Fick's first law. (b) FC speciation at various pH.** The simulated speciation was calculated based on acid dissociation constant of HOCl ($K_{a,\ HOCl}$ = $10^{-7.5}$ mol/L), equilibrium constants of Cl_2 and Cl_2O with HOCl ($K_{H,\ Cl2}$ = 4.35 × 10^{-4} $(mol/L)^2$; $K_{H,\ Cl2O}$ = 8.74 × 10^{-3} $(mol/L)^{-1}$), concentration of Cl^- ($[Cl^-]$ = 100 mM), and pH.

Chapter 3. SELECTIVE OXIDATION OF PHARMACEUTICALS AND SUPPRESSIONS OF PERCHLORATE FORMATION DURING ELECTORLYSIS OF FRESH HUMAN URINE

In this chapter, we show that the unusually low second-order rate constant of urea oxidation by the hydroxyl radical (•OH) (k = 7.9×10^5 $M^{-1}s^{-1}$)[102] versus its extremely high rate constants for typical organic contaminants (e.g., k = 2×10^9 $M^{-1}s^{-1}$ for cyclophosphamide (CP)[103] and 6.2×10^9 $M^{-1}s^{-1}$ for sulfamethoxazole (SMX)[30]) actually provides a significant selectivity advantage for •OH attack on pharmaceuticals in comparison to the case in stored hydrolyzed urine. Furthermore, we show the advantages of conducting electrolysis of pharmaceuticals in fresh urine (at point of generation) as opposed to hydrolyzed (without loss of NH_3) or hydrolyzed aged urine (with loss of NH_3). We demonstrate that urea (and/or a high NH_4^+/NH_3 concentration) effectively inhibits the oxidation pathway toward ClO_3^- and ClO_4^-, likely due to scavenging of

$Cl^{\bullet}$ and/or $Cl_2^{\bullet-}$ or rapid sequestration of HOCl. Meanwhile, the urea in fresh urine inhibits the oxidation of pharmaceuticals significantly less than the NH_4^+/NH_3 and HCO_3^-/CO_3^{2-} in hydrolyzed urine due to urea's lower reactivity toward $^{\bullet}OH$, which we demonstrate using the model pharmaceutical compounds CP and SMX (a common antineoplastic agent and an antibacterial compound, respectively[104] – selected on the basis of their very different reactivities with respect to $HOCl/OCl^-$ (*vide infra*). Thus, this work provides a proof-of-concept for simple and safe point-source oxidation of pharmaceuticals in fresh human urine.

3.1 Abstract

Here, we show that the high urea content of fresh human urine suppresses the formation of oxychlorides by inhibiting formation of $HOCl/OCl^-$ during electrolysis, while still enabling pharmaceutical degradation due to the slow rate of urea oxidation by $^{\bullet}OH$. This results in improved performance compared to equivalent treatment of hydrolyzed aged urine. This electrochemical oxidation scheme is shown to degrade the model contaminants cyclophosphamide and sulfamethoxazole with surface-area-to-volume-normalized pseudo-first-order rate constants greater than 0.08 cm/min in authentic fresh human urine. It results in ~100× decrease in pharmaceutical concentrations in 2 hours while generating ~1000× lower oxychloride byproduct concentrations in synthetic fresh urine than synthetic hydrolyzed aged urine matrixes. Importantly, this proof-of-principle shows that simple and safe electrochemical methods can be used for point-source-remediation of pharmaceuticals in fresh human urine (before storage and hydrolysis), without formation of significant oxychloride byproducts.

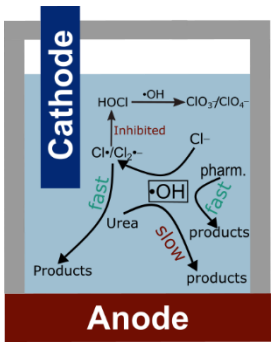

Figure 3.1 **Schematic illustration of reaction network during the electrolysis of human urine**

3.2 Understanding the Reaction Network during Electrolysis of Fresh or Hydrolyzed Urine

One of the strongest oxidant produced in EAOPs is ˙OH ($E^{0'}$ (˙OH, H^+/H_2O) = 2.32 V at pH 7),[105] which reacts rapidly with most organic molecules by either addition or hydrogen abstraction (Figure 3.2, r_3), with second-order rate constants typically in the range of $10^9 \sim 10^{10}$ $M^{-1}s^{-1}$.[102] The reactions of urea, NH_3, and carbonate species with ˙OH, in addition to associated reported second-order rate constants, are provided in Equation 3.1, Equation 3.2, Equation 3.3, and Equation 3.4.[102]

Equation 3.1

$$\text{urea} + {}^{\bullet}OH \rightarrow \text{products} \qquad k_1 = 7.9 \times 10^5\ M^{-1}s^{-1}$$

Equation 3.2

$$NH_3 + {}^{\bullet}OH \rightarrow {}^{\bullet}NH_2 + H_2O \qquad k_2 = 9.0\times10^7\ M^{-1}s^{-1}$$

Equation 3.3

$$HCO_3^- + {}^{\bullet}OH \rightarrow CO_3^{\bullet-} + H_2O \qquad k_3 = 8.5\times10^6\ M^{-1}s^{-1}$$

Equation 3.4

$$CO_3^{2-} + {}^{\bullet}OH \rightarrow CO_3^{\bullet-} + OH^- \qquad k_4 = 3.9\times10^8\ M^{-1}s^{-1}$$

For synthetic fresh urine (pH 6), [urea] = 0.25 M.[30] For synthetic hydrolyzed urine (pH 9), the concentration of total ammonium nitrogen ($[NH_4^+]_T$) is 0.5 M (72% NH_4^+, 28% NH_3, for p^cK_a = 9.25 at 25 °C, and I = 0.45 M, as calculated below), and the concentration of total inorganic carbon ($[CO_3^{2-}]_T$) is 0.25 M (88% HCO_3^-, 12% CO_3^{2-}, for $p^cK_{a,HCO3-}$ = 9.71 at 25 °C, and I = 0.45 M, as calculated below).

In synthetic fresh urine, the reaction rate of urea and •OH is $r = k_1$[urea][•OH]. Therefore, the pseudo-first order •OH-scavenging rate constant is $k' = k_1$[urea] = 2.0×10^5 s^{-1}. In synthetic hydrolyzed urine, since ammonium ions do not react with •OH,[48] the overall •OH-scavenging reaction rate is calculated as follows:

$r = k_2[NH_3][•OH] + k_3[HCO_3^-][•OH] + k_4[CO_3^{2-}][•OH]$

so that the pseudo-first order •OH-scavenging rate constant is:

$k' = k_2\alpha_{NH3}[NH_4^+]_T + k_3\alpha_{HCO3-}[CO_3^{2-}]_T + k_4\alpha_{CO32-}[CO_3^{2-}]_T$

or

$k' = k_2(K_{a,NH4+}/([H^+]+K_{a,NH4+}))[NH_4^+]_T + k_3([H^+]/([H^+]+K_{a,\ HCO3-}))[CO_3^{2-}]_T + k_4(K_{a,HCO3-}/([H^+]+K_{a,\ HCO3-}))[CO_3^{2-}]_T$

At the high ionic strength of the hydrolyzed urine matrix, corrections of $[H^+]$, $K_{a,NH4+}$, and $K_{a,NH4+}$ for ionic strength can be undertaken using the Davies equation, with:

$[H^+] = [H^+]/\gamma_{H+}$

and the concentration-based equilibrium constants for NH_4^+ and HCO_3^- dissociation:

$^cK_{a,NH4+} = [H^+][NH_3]/[NH_4^+] = K_{a,NH4+}(\gamma_{NH4+}/\gamma_{H+}) = K_{a,NH4+}$ (with $\gamma_{NH4+} = \gamma_{H+}$ for monovalent ions, where the thermodynamic $pK_{a,NH4+}$ = 9.25 at 25 °C)[71]

$^cK_{a,HCO3-} = [H^+][CO_3^{2-}]/[HCO_3^-] = K_{a,HCO3-}(\gamma_{HCO3-}/(\gamma_{H+}\ \gamma_{CO32-}))$ (where the thermodynamic $pK_{a,HCO3-}$ = 10.33 at 25 °C)[71]

and the Davies equation for each charged species, i (with A = 0.5 for water at 25 °C):[98]

$\log\gamma_i = -Az_i^2((I)^{0.5}/(1 + (I)^{0.5}) - 0.2I)$

and the ionic strength:

$I = 0.5\sum(C_iz_i^2) = 0.5([Na^+](+1)^2 + [Cl^-](-1)^2 + [NH_4^+](+1)^2 + [HCO_3^-](-1)^2 + [CO_3^{2-}](-2)^2)$

where

$I = 0.5([Na^+](+1)^2 + [Cl^-](-1)^2 + ({}^cK_{a,NH4+}/([H^+]/\gamma_{H+})+{}^cK_{a,NH4+}))[NH_4^+]_T(+1)^2 + ([H^+]/([H^+]+{}^cK_{a,HCO3-}))(-1)^2 + {}^cK_{a,HCO3-}/([H^+]+{}^cK_{a,HCO3-}))(-2)^2)$

Noting the dependence of I on γ_i, and the co-dependence of γ_i on I, this system of equations can be solved iteratively to yield:

I = 0.45 M, $\gamma_{H+} = 0.70$, $\gamma_{HCO3-} = 0.70$, $\gamma_{CO32-} = 0.24$, $[H^+] = 10^{-8.84}$ M, ${}^cK_{a,NH4+} = 10^{-9.25}$, and ${}^cK_{a,HCO3-} = 10^{-9.71}$

which can in turn be used to calculate:

k' (at T = 25 °C, I = 0.45 M) $= k_2({}^cK_{a,NH4+}/([H^+]+{}^cK_{a,NH4+}))[NH_4^+]_T + k_3([H^+]/([H^+]+{}^cK_{a,HCO3-}))[CO_3^{2-}]_T + k_4({}^cK_{a,HCO3-}/([H^+]+{}^cK_{a,HCO3-}))[CO_3^{2-}]_T = (1.3 \times 10^7 + 1.9 \times 10^6 + 1.2 \times 10^7)\ s^{-1} = 2.6 \times 10^7\ s^{-1}$

Table 3.1 Reactions in Scheme 1

Reaction Number	Reactions	Rate Constants	Reference
1	Urea + $^{\bullet}OH \rightarrow$ products	$7.9 \times 10^5\ M^{-1}s^{-1}$	[102]
2	$NH_3 + {}^{\bullet}OH \rightarrow$ products	$9.0\times10^7\ M^{-1}s^{-1}$	[102]
3	CP + $^{\bullet}OH \rightarrow$ products	$2.0 \times10^9\ M^{-1}s^{-1}$	[103]
4	CP + $Cl^{\bullet}/Cl_2^{\bullet-} \rightarrow$ products	10^7 - $10^9\ M^{-1}s^{-1}$	Assumed from [48,102,106]
5	$Cl^- \rightarrow Cl^{\bullet} + e^-$	Rapid	Assumed
6	$Cl^- + {}^{\bullet}OH \rightarrow Cl^{\bullet} + OH^-$	$3.0\times10^9\ M^{-1}s^{-1}$	[107]
7	$Cl^- + Cl^{\bullet} \rightarrow Cl_2^{\bullet-}$	$8.0\times10^9\ M^{-1}s^{-1}$	[108]
8	$Cl_2^{\bullet-} + Cl_2^{\bullet-} \rightarrow Cl_2 + 2Cl^-$ $Cl_2^{\bullet-} + Cl^{\bullet} \rightarrow Cl_2 + Cl^-$	$9.0\times10^9\ M^{-1}s^{-1}$ $2.1\times10^8\ M^{-1}s^{-1}$	[109]
9	$Cl_2 + H_2O \rightarrow HOCl + Cl^- + H^+$	$28.6\ s^{-1}$	[110]
10	$Cl_2^{\bullet-} + {}^{\bullet}OH \rightarrow HOCl + Cl^-$	$1.0 \times 10^9\ M^{-1}s^{-1}$	[111]
11	Urea or $NH_4^+/NH_3 + Cl_2^{\bullet-} \rightarrow$ -$NH^{\bullet}$ or $NH_2^{\bullet}$	$10^7\ M^{-1}s^{-1}$	Assumed from [38,112-115]

12	Urea or $NH_4^+/NH_3 + Cl^\bullet \rightarrow$ -$NH^\bullet$ or $NH_2^\bullet$	10^9 $M^{-1}s^{-1}$	Assumed from [38,112-115]
13	$HOCl + NH_3 \rightarrow NH_2Cl + H_2O$ $OCl^- + NH_4^+ \rightarrow NH_2Cl + H_2O$	3.07×10^6 $M^{-1}s^{-1}$ 5.93×10^4 $M^{-1}s^{-1}$	[116]
14	Urea + $HOCl \rightarrow$ N-chlorinated urea	0.63 $M^{-1}s^{-1}$	[117]
15	CP + $HOCl \rightarrow$ products	Sluggish	Measured in this work
16	$OCl^- + 2^\bullet OH \rightarrow ClO_2^- + H_2O$	8.8×10^9 $M^{-1}s^{-1}$	[118]
17	$ClO_2^- + 2^\bullet OH \rightarrow ClO_3^- + H_2O$	7.0×10^9 $M^{-1}s^{-1}$	[119]
18	$ClO_3^- + 2^\bullet OH \rightarrow ClO_4^- + H_2O$	$< 1 \times 10^6$ $M^{-1}s^{-1}$	[118]
19	$O2 + {}^\bullet NH2 \rightarrow NH_2O_2$	1.2×10^8 $M^{-1}s^{-1}$	[120]
20	$HCO_3^-/CO_3^{2-} + {}^\bullet OH \rightarrow HCO_3^\bullet/CO_3^{\bullet-} + OH^-$ $HCO_3^-/CO_3^{2-} + Cl^\bullet \rightarrow HCO_3^\bullet/CO_3^{\bullet-} + Cl^-$	10^7 - 10^8 $M^{-1}s^{-1}$	[121]
21	$2H^+ + ClO_4^- + e^- \rightarrow ClO_3^- + H_2O$	Very sluggish	Assumed

The unusually slow rate of urea oxidation by $^\bullet OH$ ($k = 7.9\times10^5$ $M^{-1}s^{-1}$; Figure 3.2, r_1)[102] provides improved selectivity for $^\bullet OH$ attacking pharmaceuticals ($k = 10^9 \sim 10^{10}$ $M^{-1}s^{-1}$; Figure 3.2, r_3) [30,103] in fresh urine, compared to stored hydrolyzed urine. This fact has not been discussed before despite availability of the related kinetic data. In hydrolyzed urine, the hydrolysis of urea to NH_4^+ and HCO_3^-, along with the volatilization of NH_3 and precipitation of CO_3^{2-}, can have major impacts on the oxidation pathways during electrolysis. The $^\bullet OH$ is scavenged by NH_3 and HCO_3^-/CO_3^{2-} in hydrolyzed urine much faster than by the urea in fresh urine (Figure 3.2, r_2 and r_{20};).[102,122] While the amino radical (E^0 ($^\bullet NH_2/NH_3$) = 0.6 V)[48] and carbonate radical ($E^{0'}$ ($CO_3^{\bullet-}$/ CO_3^{2-}) = 1.57 V)[105] resulting from reactions of $^\bullet OH$ with NH_3 and HCO_3^-/CO_3^{2-} provide oxidizing power, their second-order rate constants with most organics are more than 3 orders-of-magnitude smaller than for $^\bullet OH$,[48,123-125] as reflected in our experimental data (see Chapter 3.5 for detailed discussion). Further, $^\bullet NH_2$ will be rapidly scavenged by dissolved O_2 (Figure 3.2, r_{19}).[122]

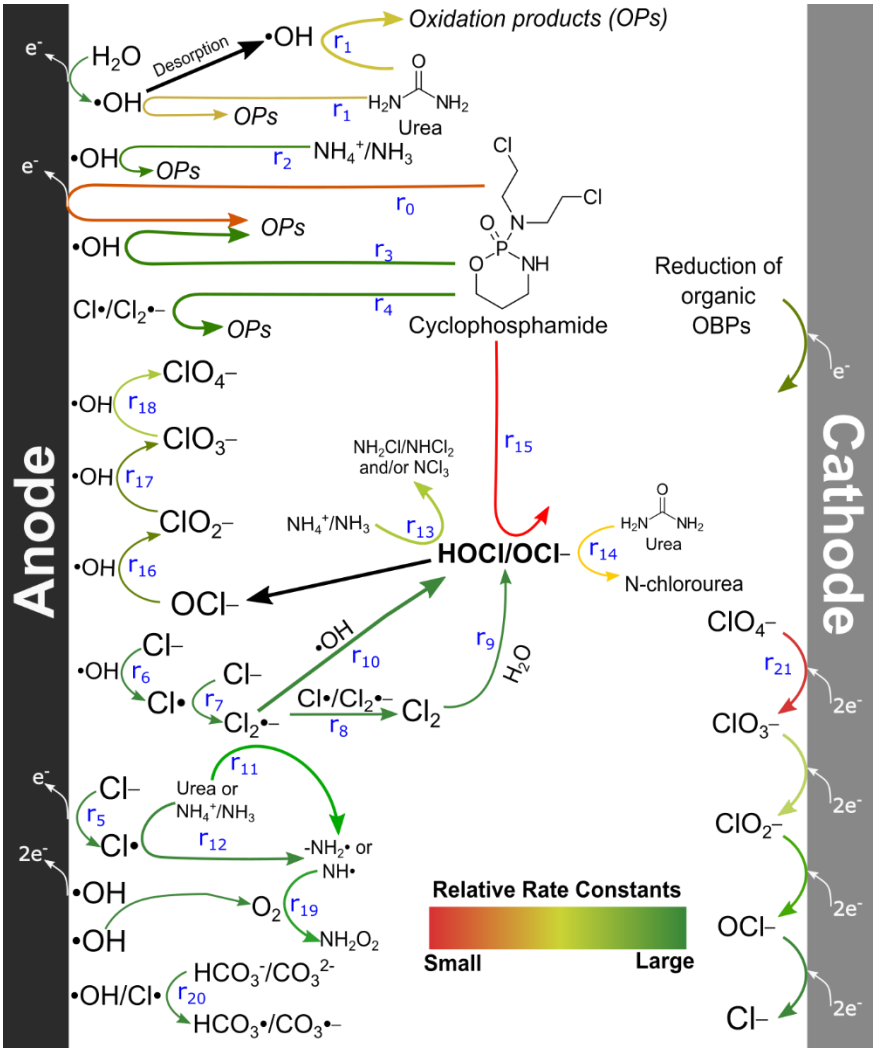

Figure 3.2 **Relative rate constants for important reactions during the electrolysis of pharmaceuticals in urine matrixes (with CP as an example pharmaceutical in an undivided cell setup).** Divided cell architectures will block r_{21} and subsequent reactions. The color coding indicates the relative range of large to small rate constants. The black arrows represent the transport of species. Furthermore, $^{\bullet}OH$, $Cl^{\bullet}$ and $Cl_2^{\bullet-}$ depicted at the anode surface may also desorb and diffuse outward through a relatively stagnant near-anode region. Likewise, Cl^-, urea, and the pharmaceuticals diffuse from bulk solution toward the anode as they are consumed at the anode or in the near-anode stagnant region. See chapter 3.5 for discussion of the importance of mass transport in galvanostatic experiments. Reactions, their rate constants and their origins are included in Table 3.1**.**

In urine matrixes with high chloride concentrations (100 mM), reaction of $^{\bullet}OH$ with Cl^{-} (Figure 3.2, r_6) and direct anodic oxidation of Cl^{-} (Figure 3.2, r_5) leads to formation of chlorine radical, $Cl^{\bullet}$ (E^0 ($Cl^{\bullet}/Cl^{-}$) = 2.43 V),[105] and dichloride radical, $Cl_2^{\bullet-}$ (E^0 ($Cl_2^{\bullet-}/Cl^{-}$) = 2.13 V).[105] They can also contribute to degradation of organics (Figure 3.2, r_4), with rate constants for $Cl^{\bullet}$ spanning a similar range as for $^{\bullet}OH$, and for $Cl_2^{\bullet-}$ 1-2 orders-of-magnitude lower than for $^{\bullet}OH$.[48,102,106] The rate constants have not been reported for reactions of $Cl^{\bullet}$ or $Cl_2^{\bullet-}$ with urea or NH_4^{+}/NH_3. However, observations from previous work suggest that these radicals likely react rapidly with both nitrogen species.[38,112-115] Therefore, both urea and NH_4^{+}/NH_3 likely serve as scavengers of $Cl^{\bullet}$ and/or $Cl_2^{\bullet-}$ (Figure 3.2, r_{11} and r_{12}). Our own observations are also consistent with these expectations (see Chapter 3.6 for detailed discussion).

In addition to their effects on pharmaceutical degradation, the concentrations of urea or NH_4^{+}/NH_3 may affect the sequence of chloride oxidation to FC and then to ClO_2^{-}, ClO_3^{-}, and ClO_4^{-}. In fresh and hydrolyzed urine, FC is formed via radical-driven or direct anodic oxidation of Cl^{-} (Figure 3.2, $r_{5\text{-}10}$).[126] As noted above, urea or NH_4^{+}/NH_3 likely effectively scavenges $Cl^{\bullet}$ and/or $Cl_2^{\bullet-}$ in either fresh or hydrolyzed urine. This could contribute to suppression of FC formation by hindering recombination and/or disproportionation reactions involving $Cl^{\bullet}$ and $Cl_2^{\bullet-}$ (several of which lead to direct formation of Cl_2).[127] In hydrolyzed urine (pH 9), NH_4^{+}/NH_3 ($k_{HOCl,NH3}$ = 3.1 × 10^6 $M^{-1}s^{-1}$ $M^{-1}s^{-1}$)[116] should react with FC with an apparent second-order rate constant of ~3 × 10^4 $M^{-1}s^{-1}$ (not corrected for ionic strength) (Figure 3.2, r_{13}). This results in an anticipated maximal pseudo-first-order FC scavenging rate constant of ~2 × 10^4 s^{-1} ($t_{1/2}$ ~ 4 × 10^{-5} s) for 500 mM NH_4^{+}/NH_3 in freshly hydrolyzed urine (with diminishing rate constant values as NH_3 volatilizes from the urine during storage). In fresh urine (pH 6), urea ($k_{HOCl,urea}$ = 0.63 $M^{-1}s^{-1}$)[117] should react with FC with an apparent second-order rate constant of ~0.6 $M^{-1}s^{-1}$ (Figure 3.2,

r_{14}). This leads to a lower, but still high pseudo-first-order FC scavenging rate constant of ~0.2 s^{-1} ($t_{1/2}$ ~ 4 s). In either case, the presence of high levels of NH_4^+/NH_3 or urea should contribute to suppression of the further oxidation of HOCl/OCl^- into ClO_2^-, ClO_3^-, and ClO_4^- (Figure 3.2, r_{16-18}).

3.3 Reactive Chlorine Species Scavenging by Urea

Cyclic voltammetry was performed in three different solutions to reveal the effects of urea on the electrocatalytic oxidation of water (primarily to O_2(g) and $^{\bullet}$OH) and chloride (primarily to Cl_2(g), HOCl, $Cl^{\bullet}$, and $Cl_2^{\bullet-}$) by BDD and iridium oxide (IrO_2) anodes. BDD was used as a model "non-active" electrode that physisorbs $^{\bullet}$OH, whereas IrO_2 was used as an "active" electrode that chemisorbs $^{\bullet}$OH, effectively forming surface hydroxyl groups. The three solutions chosen comprised: (1) 100 mM $NaClO_4$ to characterize the water oxidation without chloride oxidation; (2) 100 mM NaCl to observe the additional current from chloride oxidation; and (3) 100 mM NaCl plus 250 mM urea to observe any differences in chloride oxidation that occur with urea present. Figure 3.3a, b shows cyclic voltammograms (CV) of oxidative sweeps of these three solutions on BDD and IrO_2. The CV of BDD with $NaClO_4$ shows the expected large onset potential for O_2(g) evolution of 2.4 V vs SHE.[128] With Cl^- present, the current onset potential shifts down to 2.1 V vs SHE due to the lower overpotential for Cl_2(g) evolution (Table 3.2**)**. In contrast to BDD, the CV of IrO_2 in Figure 3.3b shows a difference in the onset potential and the magnitude of current when Cl^- is present. The IrO_2 surface oxidizes according to $IrO_2 + H_2O \rightleftharpoons IrO_3 + 2H^+ + 2e^-$.[129] In the Cl^- only solution on IrO_2, the peak seen in the cathodic sweep from 1.2 V to 0 V likely corresponds to the reduction of reactive chlorine species (RCS – a collective sum

of FC, chlorine radicals and Ir-O-Cl surface groups). Importantly, the absence of this peak when urea is present in the matrix shows that urea scavenges one or more RCS.

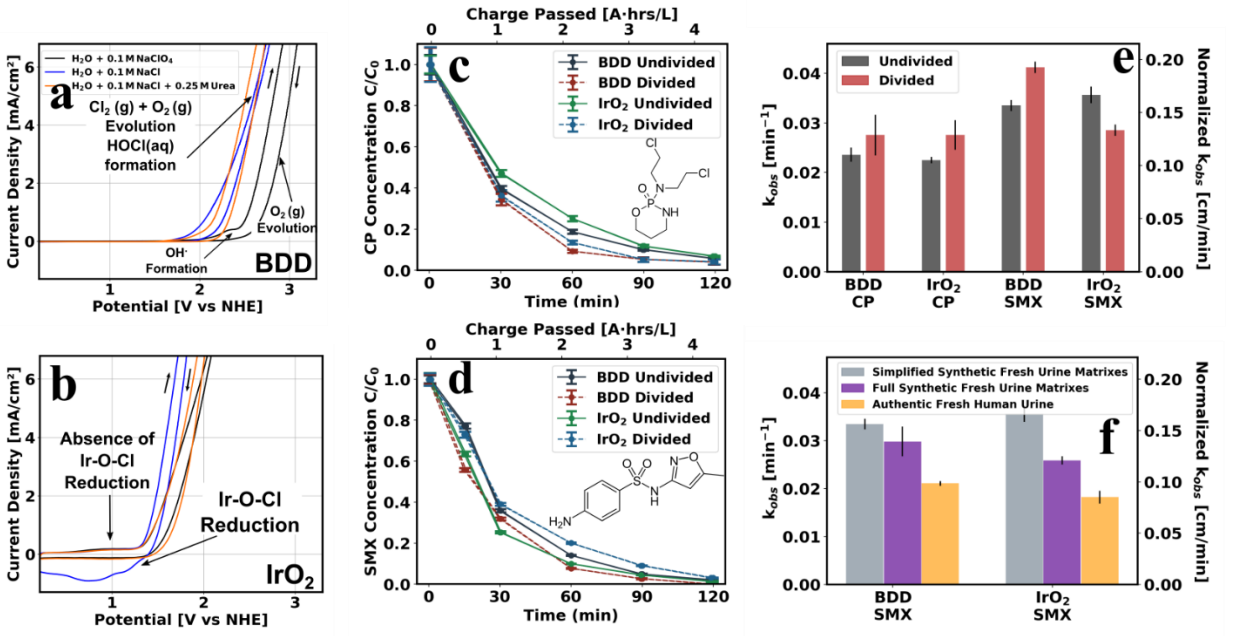

Figure 3.3 **CVs in 100 mM $NaClO_4$, 100 mM NaCl, and 100 mM NaCl + 250 mM urea on (a) BDD and (b) IrO_2 anodes. (c) Concentration of cyclophosphamide (CP) during the electrolysis in simplified synthetic fresh urine matrixes** with a starting CP concentration of 1.9 mM. Inset: The chemical structure of CP. **(d) Concentration of sulfamethoxazole (SMX) during oxidation in simplified synthetic fresh urine matrixes** with a starting SMX concentration of 0.39 mM. Inset: The chemical structure of SMX. **(e) Observed pseudo-first-order rate constants for pharmaceutical degradation. (f) Observed pseudo-first-order rate constants for SMX degradation in simplified synthetic fresh urine, full synthetic fresh urine, and authentic fresh human urine with undivided electrochemical cell setup.** The error bars represent standard deviations about the means from triplicate experiments.

Table 3.2 Significant Electrochemical Reactions during Oxidation

Oxidized	Reduced	Standard Reduction Potential [V vs SHE]	Formal Potential pH 7, $[Cl^-]$ = 0.1 M [V vs. SHE]	Formal Potential pH 2, $[Cl^-]$ = 0.1 M [V vs. SHE]	Ref.
$O_2(g) + 4\ H^+ + 4\ e^-$	$2\ H_2O$	1.23	0.81	1.11	[71]
$^{\bullet}OH + e^- + H^+$	H_2O	2.73	2.32	2.61	[71]

$Cl^{\bullet} + e^{-}$	Cl^{-}	2.43	2.49	2.49	[105]
$Cl_2^{\bullet -} + e^{-}$	$2\ Cl^{-}$	2.13	2.25	2.25	[105]
$ClO^{\bullet} + e^{-}$	OCl^{-}	1.39	1.39	1.39	[105]
$Cl_2(g) + 2\ e^{-}$	$2\ Cl^{-}$	1.36	1.42	1.42	[71]
$ClO_4^{-} + 2\ H^{+} + 2\ e^{-}$	$ClO_3^{-} + H_2O$	1.19	0.77	1.07	[71]
$ClO_3^{-} + 2\ H^{+} + e^{-}$	$ClO_2(g) + H_2O$	1.15	0.32	0.92	[71]
$ClO_2(g) + H^{+} + e^{-}$	$HClO_2$	1.28	0.86	1.16	[71]
$HClO_2 + 2\ H^{+} + 2\ e^{-}$	$HOCl + H_2O$	1.65	1.23	1.53	[71]
$HOCl + H^{+} + 2\ e^{-}$	$Cl^{-} + H_2O$	1.48	1.30	1.45	[71]

3.4 Pseudo-First-Order Kinetics and Mass Transfer

Most research examining electrolysis of pharmaceuticals has reported rates of pharmaceutical degradation in terms of observed pseudo-first-order rate constants.[39,63,130,131] As highlighted by Zöllig et al., these first-order kinetics should only be expected in galvanostatic electrolysis for mass-transfer-limited reactions (assuming only heterogeneous reactions).[39] Therefore, the pseudo-first-order rate constants for pharmaceutical degradation are highly dependent on the geometry and the mass transport in the electrochemical setup. A mass-transfer limited pseudo-first-order rate constant is directly proportional to the planar surface-area of the anode and inversely proportional to the volume of the solution. In this work, an effort was made to choose reasonable values for the ratio of the electrode surface area to electrolyte volume (A/V) based on scale-up to a practical device. The electrochemical setup used in this work (Figure 2.1**)** has an A/V of 0.21 cm^{-1} and is magnetically stirred. The hydrodynamic flow pattern in the magnetically stirred reactor is similar to that in a rotating disk electrode,[132,133] where the mass-transfer limited reaction rate is proportional to $Re^{1/2}$ (Reynolds number, $Re = \omega r^2/\nu$). To assess if the electrolysis of pharmaceuticals is mass-transfer limited in our stirred electrochemical setup, we conducted

galvanostatic oxidation experiments over a wide range of *Re* (150 < *Re* < 10,000*)*. The observed pseudo-first-order rate constant for CP degradation varied linearly with $Re^{1/2}$ (Figure 3.4). This confirms that the experiments are mass-transfer limited for CP. All experiments were performed with stir-bar radius (*r*) and rotation rates (ω) corresponding to *Re* = 1,600. This yields a mass-transfer limited electrolysis rate of 0.022 min^{-1} (i.e., 0.102 cm/min) for CP.

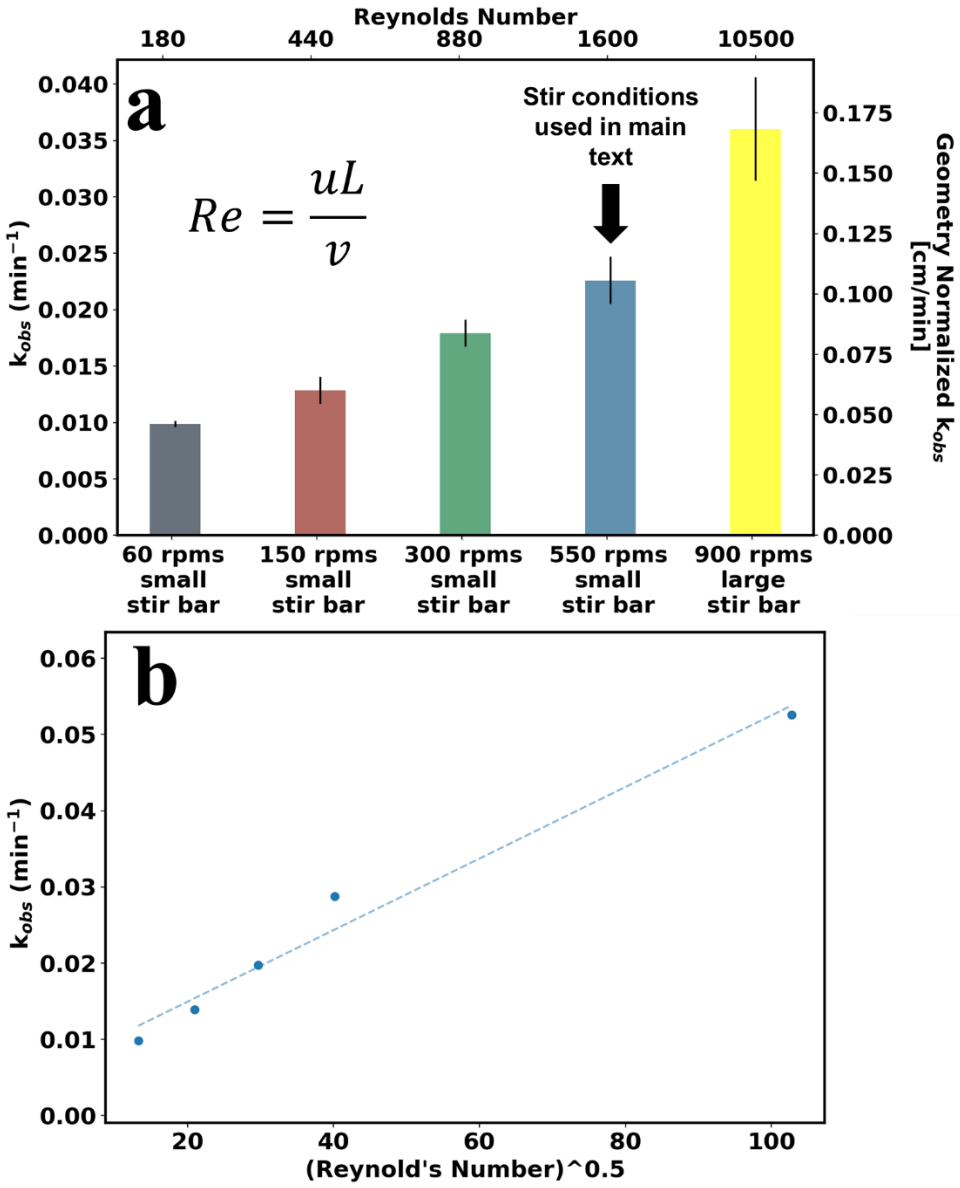

Figure 3.4 **(a) Extracted pseudo-first-order rate constants for the galvanostatic (10 mA/cm^2) degradation of cyclophosphamide as a function of different stirring conditions using a BDD electrode in an undivided cell.** (inset) Reynolds number was calculated using the linear velocity of the tip of the stir bar (u), the length of the stir bar (L), and the kinematic viscosity of water (v). **(b) A plot of the extracted pseudo-first-order rate constant vs. Re$^{1/2}$** is roughly linear, which is commensurate with the mass transfer correlation for a rotating disk electrode.[133]

To determine what pseudo-first-order rate constants are practical for a real device, we modeled expected degradation rates for various rate constants as shown in Figure 3.5. A pseudo-first-order rate constant of 0.01 min^{-1} or greater is required to lower pharmaceutical concentrations by at least three orders-of-magnitude in a 12-hour period, which is a reasonable residence time for a practical at-home situation. This corresponds to a geometry-normalized pseudo-first-order rate constant (based on A/V) of at least 0.05 cm/min to degrade pharmaceuticals at a rate reasonable for a scaled-up device.

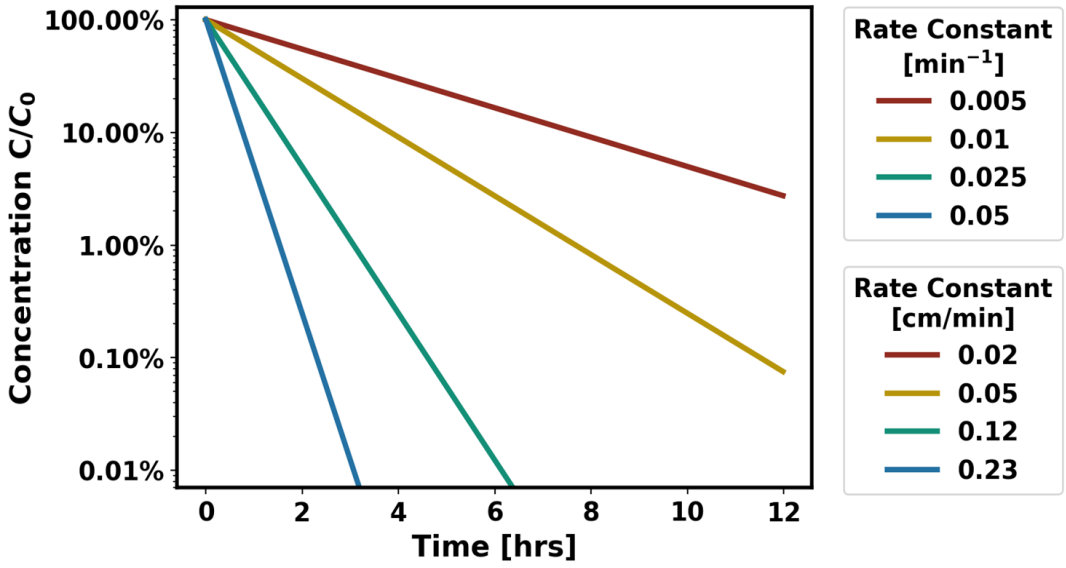

Figure 3.5 **The pseudo-first-order pharmaceutical degradation rate constant is a critical factor in the design of electrochemical devices.** Modeled degradation profiles for various pseudo-first-order rate constants suggest that a rate constant of >0.01 min^{-1} is required in a practical device. This would correspond to a decrease in pharmaceutical concentration by 3

orders of magnitude in a 12-hour period, which is a reasonable residence time for a practical at-home situation. Normalized rate constants take into account the current density, surface area, and solution volume. In this model, current density, surface area, and solution volume were respectively set as 10 mA/cm^2, 8.56 cm^2, and 40 mL to match the experimental parameters of this study.

3.5 Electrolysis of Model Pharmaceutical Compounds in Various Urine Matrixes

3.5.1 *Galvanostatic oxidation in fresh-urine matrixes*

A series of galvanostatic oxidations of SMX and CP (see chemical structures in Figure 3.3c, d insets) were performed with BDD and IrO_2 anodes. SMX and CP were chosen as model compounds because of their large differences in reactivity toward FC. SMX has a relatively high bimolecular rate constant with FC of ~10^3 $M^{-1}s^{-1}$ ($t_{1/2}$ ~ 6.9 s when reacting with 0.1 mM FC) at circumneutral pH,[134] while we measured CP to be essentially non-reactive with FC ($t_{1/2}$ ~ 4600 hr when reacting with 0.1 mM FC) (Figure 3.2, r_{15}). Cyclophosphamide (CP) reaction rates in the presence of excess FC were measured at pH values similar to full synthetic fresh urine matrixes (i.e., pH 6) with addition of 0.1 M phosphate buffer. Solutions containing 0.2 mM of cyclophosphamide were amended with 200, 400, or 600 mM FC to initiate experiments. Under these conditions, various chlorine species, including $HOCl/OCl^-$, Cl_2, and Cl_2O may contribute to observed reactions with organic compounds.[135,136] Samples were periodically collected, quenched with excess thiosulfate (4:1 thiosulfate-to-chlorine molar ratio), and analyzed for cyclophosphamide by HPLC-MS. The CP concentrations measured over the course of the experimental reaction time were used to evaluate the kinetics of CP reaction with FC species. Negligible losses of CP were observed over the course of the experiments, indicating that CP is essentially non-reactive toward FC species under the conditions evaluated.

Galvanostatic oxidations were performed in both undivided cell (working electrode (WE) and counter electrode (CE) in same compartment) and divided cell (WE and CE separated by a frit) configurations to test if cathodic reactions had any influence on SMX or CP degradation (Figure 2.1). The concentrations of SMX and CP were lowered by two orders-of-magnitude after two hours of electrolysis at 10 mA/cm^2 for all conditions in simplified synthetic fresh urine (Figure 3.3c & d). This corresponds to geometry normalized pseudo-first-order rate constants greater than 0.1 cm/min as shown in Figure 3.3e. The observed pseudo-first-order rate constants of SMX degradation were lower for full synthetic fresh urine matrixes and authentic fresh urine (Figure 3.3f). However, the reactions remained sufficiently fast to degrade SMX by four orders-of-magnitude in ~8 hours (Figure 3.5).

The rate constants for oxidation of both pharmaceuticals by both electrodes are similar in simplified synthetic fresh urine matrixes (i.e., urea + Cl^-). This suggests that mass transfer to the electrode surface is the dominant factor limiting the degradation rates (*see above*). For *Re* = 10,000, pseudo-first-order degradation rate constants up to 0.25 cm/min were achieved. However, stir speeds corresponding to *Re* = 1,600 were used for the experimental data shown in Figure 3.3, since they are easier to achieve in electrochemical devices.[137]

For the divided cell architecture, a pH gradient is established because the oxygen evolution reaction at the anode generates H^+ while the hydrogen evolution reaction at the cathode generates OH^-. On average, the pH was stabilized to 1.8 for IrO_2 and 2.3 for BDD in the anode chamber and 12.5 in the cathode chamber for both electrodes. Furthermore, this gradient is quickly established by passing 10 mA/cm^2 for 5 mins (~0.2 A·hr/L). Moreover, the electrolysis rates of CP and SMX did not show significant differences in divided and undivided cells. This suggests little to no effect of cathodic reactions (possibly leading to reduction of homogeneous oxidants)

on CP or SMX degradation, consistent with the above finding of mass-transfer limited degradation kinetics at the anode. Additionally, the effect of the bulk solution pH (a drop from 6 in the undivided cell to 2 in the divided cell) had no appreciable impact on degradation rates. This is likely because the local pH at the anode surface in the undivided cell is much lower than the bulk due to H^+ generation at the anode. Moreover, the electrolysis rates of CP and SMX were similar in the divided cell setup for both anodes under the acidic pH condition established by oxygen evolution (*vide supra*). This suggests that the contribution of FC to each pharmaceutical's degradation is negligible. This is also consistent with the Cl_2 quenching effect of urea ($k_{urea,\ Cl2}$ = 2.35 × 10^4 $M^{-1}s^{-1}$),[117] since the predominant species of FC is dissolved Cl_2 under acidic pH.

3.5.2 *Differences between Synthetic Fresh, Hydrolyzed, and Hydrolyzed-Aged Urine Matrixes*

The electrolysis rates of CP and SMX were investigated in synthetic hydrolyzed and synthetic hydrolyzed aged urine matrixes and compared to a reference mass-transfer limited rate (Figure 3.6a). Sketches of concentration profiles adjacent to the anode surface are shown in Figure 3.6b to illustrate the differences between kinetic limitation (gradient A), mass-transport limitation due to heterogenous reactions (direct electron transfer and reactions with adsorbed oxidants) (gradient B), and mass-transport limitation due to the combination of heterogeneous reactions and near-anode-surface homogeneous reactions with desorbed $^{\bullet}OH$, RCS, or other homogeneous oxidants (gradients C and D). As noted above, the mass-transfer limited electrolysis rate for CP was determined to be 0.022 min^{-1}. Given CP's slow reaction with FC and the short lifetime of $^{\bullet}OH$, 0.022 min^{-1} likely corresponds to the mass-transport limited rate with primarily heterogeneous reactions. Desorbed $^{\bullet}OH$ may exist in solution, but the homogeneous reaction zone where it may react with CP is likely less than 1 μm in thickness,[138] which is small

compared to the stagnant layer thickness of >20 μm. Additionally, the linear relationship between k_{obs} and $Re^{1/2}$ suggests the obtained mass-transfer limiting rate corresponds to gradient B.

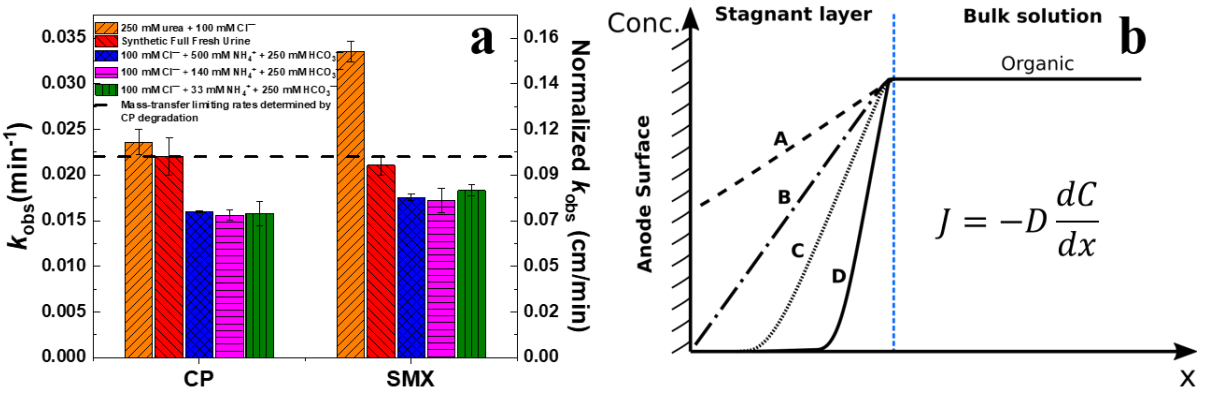

Figure 3.6 **(a) Observed and geometry-normalized pseudo-first-order rate constants for pharmaceutical degradation on BDD** with undivided cell setup in: (1) simplified urine matrixes (250 mM urea and 100 mM Cl^-, pH 6.15); (2) synthetic full fresh urine matrixes (250 mM urea, 100 mM NaCl, 16 mM Na_2SO_4, 24 mM NaH_2PO_4, 13 mM creatinine, 3 mM uric acid,**,** pH 5.87); (3) hydrolyzed, un-aged urine matrixes (100 mM Cl^-, 500 mM NH_4^+ and 250 mM HCO_3^-, pH 9.35); (4) hydrolyzed, aged urine matrixes adapted from Udert et al. [66] (100 mM Cl^-, 140 mM NH_4^+ and 250 mM HCO_3^-, pH 9.02); and (5) hydrolyzed, aged urine matrixes adapted from Hoffmann et al. (100 mM Cl^-, 33 mM NH_4^+ and 250 mM HCO_3^-, pH 8.88). The dotted line represents the mass-transfer limiting rate of pharmaceutical degradation obtained from Figure 3.4**.** The electrolytes (40 mL) were stirred at 500 rpm. The applied current density was 10 mA/cm^2. The error bars represent standard deviations about the means from triplicate experiments. **(b) Possible concentration gradients of pharmaceuticals in the stagnant layer** (assuming constant bulk concentration).

As shown in Figure 3.6a, the degradation rates of CP were mass-transfer limited in simplified and full synthetic fresh urine matrixes (orange & red bars) – likely due to reaction with electro-generated ˙OH on the BDD surface or desorbed short-lived ˙OH very near the surface (Figure 3.6b, gradient B). In contrast, the electrolysis rates of SMX in simplified urine matrixes exceeded

the "heterogenous"-reaction mass-transfer limiting rates, suggesting the contribution of homogenous reactions further from the surface with longer-lived oxidants (Figure 3.6b, gradient C or D). However, the rates of SMX oxidation in synthetic full fresh urine matrixes were at the heterogeneous-reaction mass-transfer limiting rate (Figure 3.6b**,** gradient B). This suggests that for the synthetic full fresh urine case homogeneous reactions involving either RCS and/or other homogeneous oxidants with SMX are insignificant and are consumed by additional species present in the synthetic full urine matrix (e.g., uric acid, creatinine, etc.). The electrolysis rates of both CP and SMX were significantly decreased below the mass-transfer limiting rate in synthetic hydrolyzed urine matrixes amended with varying NH_4^+/NH_3 levels to reflect different degrees of aging (blue, pink, and green bars). This suggests the electrolysis of CP and SMX are kinetically limited in hydrolyzed urine matrixes (Figure 3.6b, Gradient A) on BDD. This is attributable to HCO_3^-/CO_3^{2-} (present at the same 250 mM concentration in each hydrolyzed urine matrix) that acts as a dominant $^{\bullet}OH$ and $Cl^{\bullet}/Cl_2^{\bullet-}$ scavenger in such matrixes. This results in the formation of $CO_3^{\bullet-}$, which typically reacts with organic contaminants ~10^3-fold slower than $^{\bullet}OH$ or $Cl^{\bullet}$ and ~10-fold slower than $Cl_2^{\bullet-}$ (*see above*). Furthermore, the degradation rates of both pharmaceuticals in such matrixes were invariant with changes in the concentration of NH_4^+/NH_3, consistent with the apparent low reactivity of NH_4^+/NH_3 toward $CO_3^{\bullet-}$.[139] This likewise suggests that RCS do not contribute significantly to CP or SMX oxidation in the hydrolyzed urine matrixes, because increasing concentrations (33-500 mM) of NH_4^+/NH_3 would have been expected to increase RCS scavenging efficiency, and consequently decrease rates of pharmaceutical degradation if RCS were predominant oxidants. Based on these findings, it may be advantageous to electrochemically oxidize pharmaceuticals in fresh urine rather than in hydrolyzed urine for faster pharmaceutical removal. Although beyond the scope of the current

work, future investigations are needed to explore the identities and yields of transformation products generated upon electrolysis of CP, SMX, and other pharmaceutical compounds in urine, in addition to their potential human health and ecosystem impacts.

3.6 Generation of Oxidation Byproducts

The rates of oxidation byproduct generation in full synthetic fresh urine matrixes were compared for each combination of anode and cell configuration as shown in Figure 3.7. Both ClO_4^- and ClO_3^- were often found to be near or below the detection limits (i.e., 2 μM) for the ion chromatography techniques used in these experiments. The detection limits for both ClO_3^- and ClO_4^- were higher than in pure water due to the high concentration of Cl^- in urine matrixes. No ClO_4^- was measured in matrixes oxidized by IrO_2, consistent with previous reports.[36,70] ClO_4^- was formed in the matrixes oxidized by BDD, but at much lower concentrations than other reports.[66,70] Additionally, the ClO_4^- measured on the BDD was at a lower concentration than the ClO_3^-, consistent with other reports.[66,70] Nitrate (NO_3^-) (Figure 3.7c) and nitrite (NO_2^-) (Figure 3.7d) generation were found to be higher on IrO_2 than BDD, though in IrO_2 divided cell experiments, NO_2^- generation was below the detection limit (5 μM). These oxidized nitrogen anions could come from the oxidation of urea, creatinine, uric acid and/or the oxidation of CP or SMX. Reaction pathways involving radical-driven generation of reactive nitrogen species from NO_3^- or NO_2^- have been shown to lead to potentially harmful nitrated and nitrosated byproducts.[140,141] The suppression of NO_2^- formation when using the IrO_2 in the divided cell configuration indicates that such pathways would not be active or would be diminished and represents a potential advantage of operating in this mode.

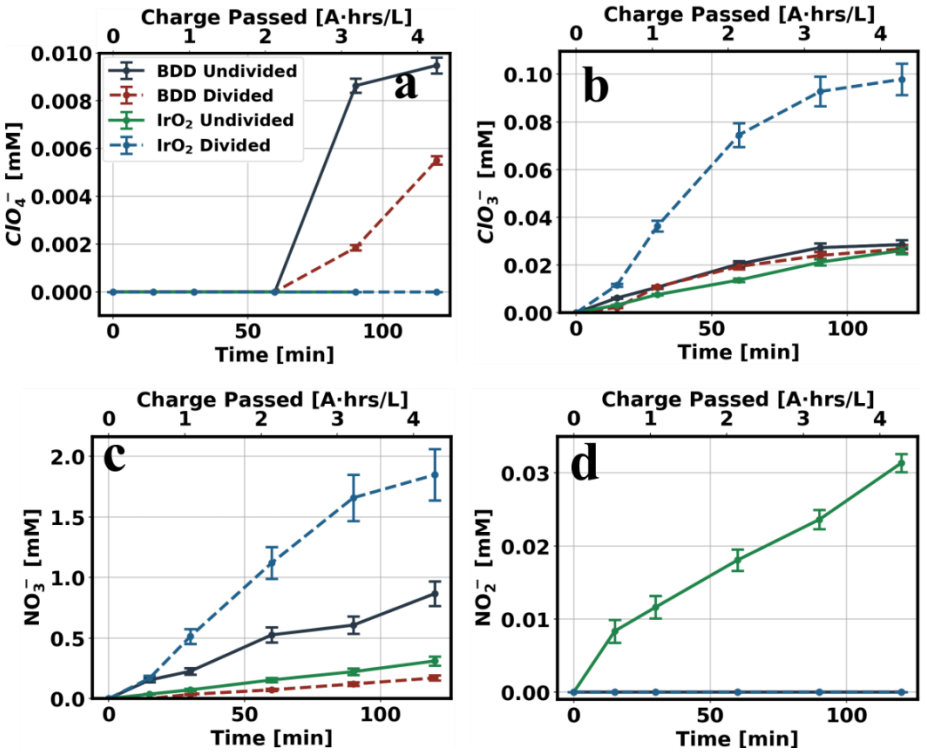

Figure 3.7 **Evolution of inorganic oxidation byproducts showing concentrations of (a) ClO_4^-, (b) ClO_3^-, (c) NO_3^-, and (d) NO_2^- during electrolysis at 10 mA/cm^2 on BDD and IrO_2 anodes in the undivided and divided setups.** Results are from oxidation of full synthetic fresh urine matrixes amended with 1.9 mM CP and 0.39 mM SMX. The error bars represent standard deviations from triplicate experiments.

3.6.1 *Inhibition of Oxychloride Formation Increases with Increased Urea or NH_4^+/NH_3*

The levels of generated OBPs shown in Figure 3.7 are substantially lower than in previous studies of authentic hydrolyzed aged urine electrolysis.[66,70] Therefore, further experiments were undertaken in several matrixes and at extended electrolysis time to evaluate potential causes of the lower rates of formation of OBPs (Figure 3.8). Fresh urine has an average concentration of 250 mM urea,[59] whereas hydrolyzed urine should exhibit maximal concentrations of 500 mM NH_4^+/NH_3 and 250 mM HCO_3^- after urea hydrolysis. Previous studies that have examined the treatment of authentic hydrolyzed aged urine have reported much lower NH_4^+/NH_3

concentrations (e.g., 34 mM[70] and 109 mM[66]) indicating substantial ammonia loss during storage (aging). As shown in Figure 3.8, ClO_3^- and ClO_4^- generation were increasingly inhibited as inorganic nitrogen species concentrations increased. For example, a 10^3-fold decrease in ClO_3^- and ClO_4^- generation was observed for a matrix of 100 mM Cl^- and 250 mM urea compared to 100 mM Cl^- alone. A full synthetic fresh urine matrix containing the other primary constituents of urine (citrate, creatinine, uric acid, SO_4^{2-}, and $H_2PO_4^-$) in addition to urea also showed exceptionally low ClO_3^- and ClO_4^- generation. The ClO_3^- was first detected after 15 A•hrs charge passed in full synthetic urine matrixes. Additionally, the generation of ClO_3^-in full synthetic urine matrixes was slightly lower than that in a matrix of 100 mM Cl^- and 250 mM urea, but it is the opposite of the generation of ClO_4^-. However, the difference of ClO_3^- and ClO_4^- formation in between these two matrixes is much less than that in between NaCl-only solution and a matrix of Cl^- and urea. It suggests that SO_4^{2-}, $H_2PO_4^-$, creatinine and uric acid at the concentration present in fresh urine matrixes has much less significant impact than urea on the generation of ClO_3^- and ClO_4^-. A matrix representing hydrolyzed (but not aged) urine (100 mM Cl^-, 500 mM NH_4^+, and 250mM HCO_3^-) yielded a roughly 10^2-fold lower ClO_3^- concentration than 100 mM Cl^- alone, whereas ClO_4^- levels generated were similar to those observed in the presence of 250 mM urea. The dashed lines in Figure 3.8 indicate concentrations 100x higher than the suggested drinking water limits for each oxychloride species. Assuming that urine is typically diluted by a factor of greater than 100 in transit to WWTFs, these lines are intended to represent thresholds below which ClO_3^- and ClO_4^- levels would not exceed the WHO drinking water guidelines of 700 μg/L for ClO_3^- or 70 μg/L for ClO_4^- even for a "worst-case" scenario of minimal WWTF effluent dilution for direct potable reuse.[142] As evident from Figure 3.8, ClO_3^- and ClO_4^- levels in all of the matrixes containing low or no NH_4^+/NH_3 exceeded these

thresholds, whereas ClO_3^- and ClO_4^- levels in the high NH_4^+/NH_3 and urea-containing matrixes were below the thresholds (except for ClO_3^- in the high NH_4^+/NH_3 matrix at the highest values of charge passed).

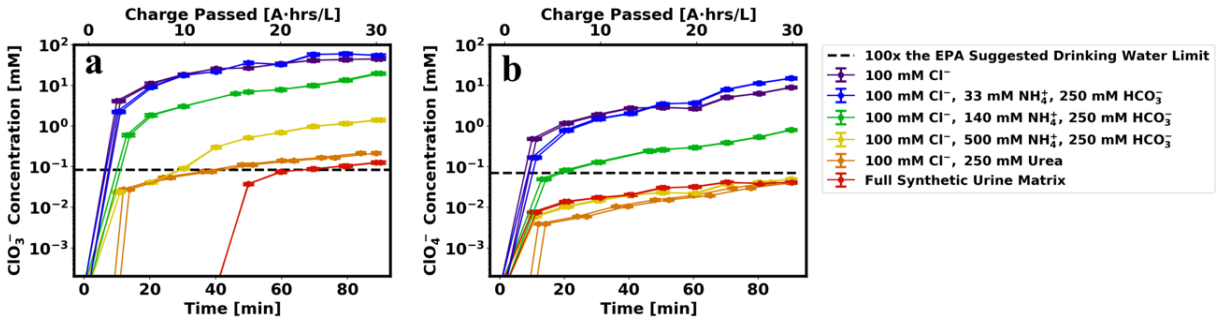

Figure 3.8 **OBPs formation in galvanostatic electrolysis experiments undertaken over extended times compared to experiments from which the Figure 3 data were obtained. Concentrations of generated (a) ClO_3^- and (b) ClO_4^- were measured for various matrixes treated using a BDD anode in the undivided setup.** For the matrixes containing NH_4^+/NH_3, the pH was 9–10. For the matrixes containing only Cl^- and/or urea, the pH was 6–7. Galvanostatic treatments were performed for 90 mins at a current density of 93 mA/cm^2 for a final charge passed of 30 A·hr/L. The dashed lines indicate concentrations 100x higher than suggested drinking water limits for each oxychloride species (see accompanying discussion in the main text).

3.6.2 *Mechanism of Inhibition of Oxychloride Formation*

The oxidation of Cl^- to $HOCl/OCl^-$ is expected to proceed through direct oxidation or reaction with $^{\bullet}OH$ at or near the anode surface (Figure 3.1, $r_{5\text{-}10}$).[50,143] Subsequently, $HOCl/OCl^-$ is oxidized at or near the BDD surface via direct electron transfer and/or reaction with $^{\bullet}OH_{ads}$ to form ClO_3^- and ClO_4^- (Figure 3.1, $r_{16\text{-}18}$).[126,144] In this study, we have shown that increasing urea or NH_4^+/NH_3 inhibits the formation of ClO_3^- and ClO_4^-. We hypothesize that high urea or NH_4^+/NH_3 concentrations effectively prevent oxychloride formation by: (1) scavenging chlorine

radicals (Figure 3.1, r_{11} and r_{12}) and/or (2) reacting with HOCl/OCl^- and thereby sequestering chlorine in the form of organic chloramines (N-chlorinated urea) or inorganic chloramines (NH_2Cl, $NHCl_2$, and/or NCl_3) (Figure 3.1, r_{13} and r_{14}). Either pathway would block key steps in the pathways of Cl^- oxidation to ClO_3^- and ClO_4^-.

Free chlorine (FC; comprising Cl_2O, HOCl, OCl^- and Cl_2), total chlorine (TC; comprising FC and chloramines), and chlorine dioxide (ClO_2) in bulk solution were quantified in full synthetic fresh urine and various synthetic hydrolyzed urine matrixes to explore the mechanism whereby ClO_3^- and ClO_4^- formation is inhibited (Figure 3.9). The key observations from these measurements are: (1) ClO_2 was not detected at measurable concentrations in any matrixes investigated, consistent with the hypothesized action of urea or NH_4^+/NH_3 on RCS involved in steps preceding formation of ClO_2 in the Cl^- to ClO_4^- oxidation sequence (e.g., $Cl^\bullet$, $Cl_2^{\bullet-}$, $ClO^\bullet$, or FC); (2) no FC was measurable in the bulk solution in any matrixes; (3) high μM to low mM levels of chloramine species (measured as the difference in TC and FC values) were present in each matrix, confirming that FC (once formed) was consumed by urea or NH_4^+/NH_3 to form chloramine species; and importantly (4) lower concentrations of chloramines were generated in the presence of higher concentrations of NH_4^+/NH_3 or urea. This last observation indicates that FC generation (followed by chloramine formation) is faster at lower concentrations of NH_4^+/NH_3. This suggests that at higher NH_4^+/NH_3 concentrations, the reaction between $Cl^\bullet/Cl_2^{\bullet-}$ and NH_4^+/NH_3 to generate $NH_2^\bullet$ (Figure 3.2, r_{12}) out-competes the reactions between $Cl^\bullet/Cl_2^{\bullet-}$, $^\bullet OH$, and H_2O to generate HOCl (Figure 3.2, $r_{8\text{-}10}$). The generated $NH_2^\bullet$ is then scavenged by dissolved O_2,[122] $^\bullet OH$,[145] $CO_3^{\bullet-}$,[146] etc. without formation of chloramines. A satisfactory explanation must also reconcile the fact that the rates of generation of ClO_3^- and ClO_4^- were found to be similar in NaCl-only electrolyte (no urea, no ammonium, no bicarbonate, etc.) and in

synthetic hydrolyzed urine with low NH_4^+/NH_3 concentration (33 mM NH_4^+) (Figure 3.8), even though bulk-solution FC was effectively sequestered as chloramine in the latter matrix (Figure 3.9b).

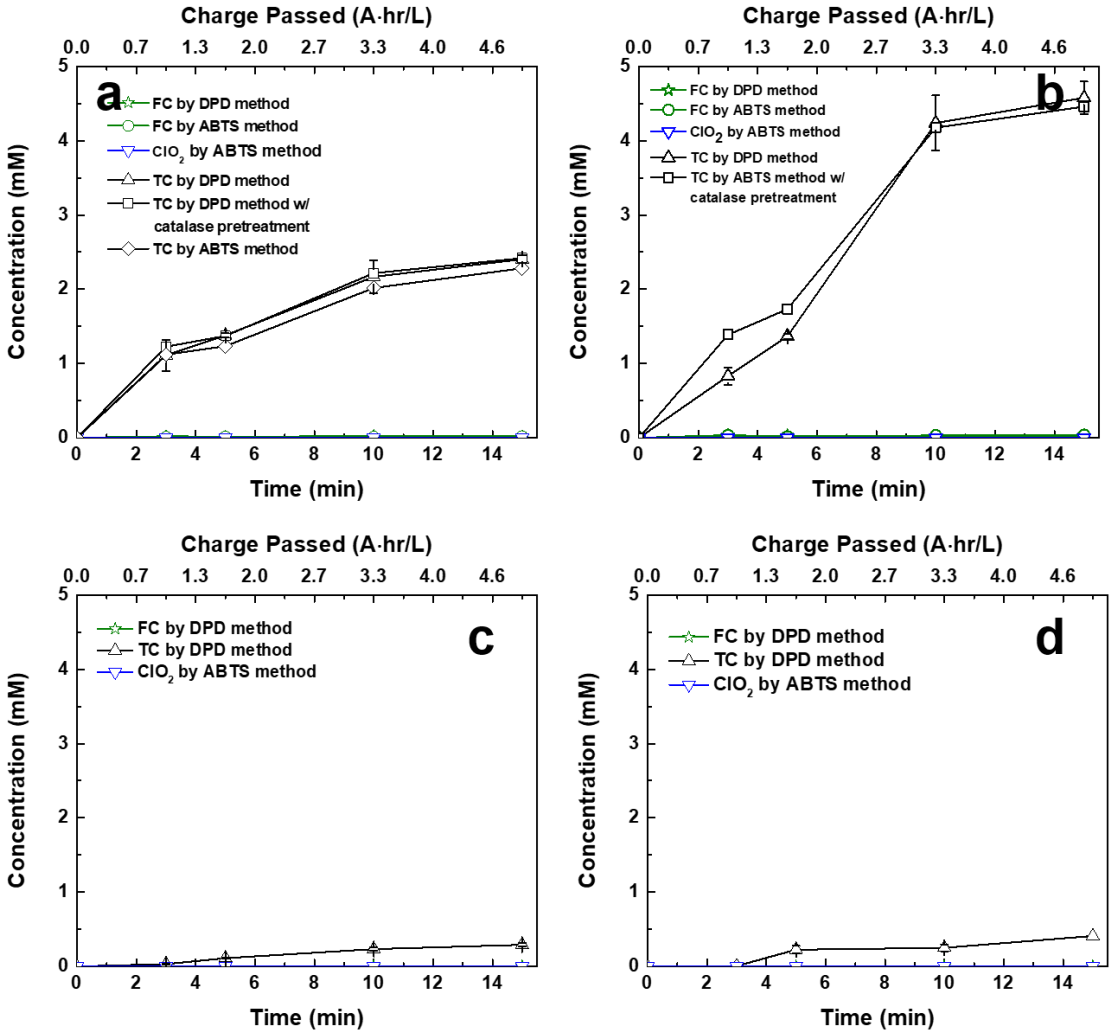

Figure 3.9 **Concentration profiles of various chlorine species during electrolysis on the BDD anode in four different matrixes.** Starting from a baseline solution 100 mM Cl^-, 33 mM NH_4^+, 250 mM HCO_3^-, the four solutions were: (a) baseline solution at pH 6.75. (b) baseline solution at pH 8.88; (c) baseline solution with high ammonium (500 mM NH_4^+) at pH 9.35; (d) Full synthetic fresh urine matrix (no ammonium and bicarbonate but with urea, creatine, uric acid, etc.) at pH 5.87). The current densities were 93.3 mA/cm^2; the stir rate was 500 rpm. FC and ClO_2 were not measurable in any of the four matrixes investigated. FC measurements via DPD were verified by ABTS in matrixes (a) and (b). The measurement of total chlorine via DPD was

checked by ABTS in matrix (a). Potential interference of H_2O_2 with the measurements of TC was investigated by pretreating diluted samples with catalase to decompose any H_2O_2 that may have been present. The absence of any effect from catalase treatment indicates that H_2O_2 was not present at concentrations sufficient to interfere with TC measurements. Error bars represent standard deviation about the means from triplicate experiments.

Taken together, these observations suggest that: (1) generation of ClO_3^- and ClO_4^- in these systems involves oxidation of FC at or near the anode surface (as opposed to the bulk solution), consistent with DFT calculations in previous work;[126,144,147] (2) lower levels of FC formation for high urea and NH_4^+/NH_3 concentrations are linked to lower levels of ClO_3^- and ClO_4^- formation; and (3) suppression of ClO_3^- and ClO_4^- formation by urea and NH_4^+/NH_3 derives from their $Cl^\bullet$ and/or $Cl_2^{\bullet-}$ scavenging effects at or near the anode interface that precede formation of $HOCl/OCl^-$ (Figure 3.2, $r_{11\text{-}12}$), rather than from FC scavenging effects in bulk solution or at the interface (Figure 3.2, r_{16}). Considering the much lower reactivity of urea than NH_4^+/NH_3 toward $^\bullet OH$ (Chapter 3.2), scavenging of $^\bullet OH$ is unlikely to be the primary mechanism for the suppression of oxychloride formation. This also points to scavenging of $Cl^\bullet$ or $Cl_2^{\bullet-}$ involved in FC formation as a more likely explanation for the similar effects of urea and NH_4^+/NH_3 on ClO_4^- formation, and the even somewhat greater effectiveness of urea in suppressing ClO_3^- formation. Finally, the fact that similar amounts of ClO_3^- and ClO_4^- are formed in both NaCl-only and low NH_4^+/NH_3 (Figure 3.8) solutions suggests that NH_4^+/NH_3 becomes depleted near the anode surface at low concentrations. This shuts-down the amino radical pathway (Figure 3.2, $r_{11\text{-}12}$) leaving $Cl^\bullet$ or $Cl_2^{\bullet-}$ to form HOCl (Figure 3.2**,** $r_{6\text{-}10}$), which is then oxidized to form ClO_3^- and ClO_4^-.

The use of appropriately-selective probe compounds for quantification of $Cl^\bullet$, $Cl_2^{\bullet-}$, and/or $ClO^\bullet$ could provide more definitive evidence of the relative effects of urea and NH_4^+/NH_3 on

chlorine radical scavenging. Unfortunately, the probe compounds most commonly accepted for such uses in AOPs, such as nitrobenzene,[148-150] benzoic acid,[151] and 1,4-dimethoxybenzene,[152,153] are unsuitable for electrolysis in either divided or undivided cells due to potential artifacts from their direct oxidation on anodes.[154-158]

Overall, these results indicate that the protective effect of ammonia in mitigating oxychloride formation during electrolysis of hydrolyzed aged urine is likely to be lower than that afforded by urea in fresh urine due to ammonia losses following urea hydrolysis.

3.7 CONCLUSIONS

In this chapter, we demonstrate that urea (or NH_4^+/NH_3 from hydrolyzed urea) at the concentrations present in human urine can suppress the pathway(s) of Cl^- oxidation to ClO_3^- and ClO_4^- during EAOPs. This fortuitous effect greatly inhibits the formation of the highly stable ClO_3^- and ClO_4^-, which are two of the most recalcitrant OBPs formed during EAOPs. Our findings also show that pharmaceuticals can be degraded to less than 5% of their starting concentrations with less than 10 µM ClO_4^- and 100 µM ClO_3^- generated following 2 hours of electrolysis in matrixes containing 250 mM urea. These data demonstrate the feasibility of applying EAOPs to eliminate pharmaceuticals in fresh (as opposed to stored hydrolyzed) urine at the source of generation while generating minimal oxidation byproducts.

"Non-active" BDD[50] has been the anode of choice for EAOPs because of high oxidizing power, but is prohibitively expensive to use in a practical device. The observations here and by others that "active" IrO_2 [50] is sufficiently oxidizing to degrade CP (a particularly recalcitrant pharmaceutical) in simplified synthetic fresh urine matrixes at reasonably high rates of ~0.1 cm/min highlights a large opportunity for the further development of both "non-active" and "active" low-cost anodes that have long service lifetime. Estimation of the electricity cost alone

to implement an EAOP in source-separated urine is supposed to be much less than $57.60/year/person (Chapter 1.4). Future research aiming at device development (based on this chemistry) and energy saving could provide an important contribution to mitigating the release of pharmaceuticals and other contaminants into the environment.

Chapter 4. ELECTROCHEMICAL OXIDATION OF PHARMACEUTICALS IN SYNTHETIC FRESH HUMAN URINE: USING SELECTIVE RADICAL QUENCHERS TO REVEAL THE DOMINANT DEGRADATION PATHWAYS AND THE SCAVENGING EFFECTS OF INDIVIDUAL URINE CONSTITUENTS

In this chapter, we reveal the significance of specific electrogenerated oxidants ($^{\bullet}OH$, IrO_{2+1}, $Cl^{\bullet}/Cl_2^{\bullet-}$, Cl_2, HOCl, and IrO_3-Cl) by using selective radical quenchers during the electrochemical degradation of pharmaceuticals in partial synthetic fresh urine matrixes (i.e, chloride only solution) (see Chapter 4.4). The experiments were also conducted in different combinations of synthetic fresh urine constituents with BDD and IrO_2 to evaluate the scavenging effect of individual constituent (see Chapter 4.5 & 4.6). The limiting mechanisms of pharmaceutical degradation (i.e., mass-transfer and/or kinetically limited) are evaluated in each matrix. We assess the performance of representative “active” electrodes (IrO_2) and “inactive” electrodes (BDD) for pharmaceutical oxidation in FUM (see Chapter 4.7). Furthermore, we evaluate the strategies for achieving faster rates of pharmaceutical degradation in FUM (see Chapter 4.8). The observed pseudo-first-order rate constants were obtained and reported along with geometry-normalized rate constants accounting for the electrode-surface-area-to-electrolyte-volume ratio

(A/V) of the electrochemical cell (normalized k_{obs} = k_{obs}/(A/V)). The study sheds mechanistic insight on the electrolysis of pharmaceuticals in synthetic fresh urine and will be useful in the development and design of inexpensive and effective anode materials EAOPs for point-source urine treatment.

4.1 ABSTRACT

Here, we evaluate the importance of electro-generated oxidants and direct anodic oxidation for degradation of four pharmaceutical (cyclophosphamide (CP), carbamazepine (CBZ), sulfamethoxazole (SMX) and ibuprofen (IBP)) accounting for the scavenging effect of urine constituents using boron-doped diamond (BDD) and IrO_2 electrodes. Allyl alcohol and tert-butanol were used as selective quenchers for adsorbed and dissolved radicals, respectively. In electrolyte containing only chloride and pharmaceuticals, we found that CBZ and SMX are primarily oxidized by electro-generated Cl_2 in the fluid boundary layer is the dominant oxidant for oxidation, and CP and IBP are primarily oxidized by physisorbed $^{\bullet}OH$ or chemisorbed chlorine (IrO_3-Cl). Regarding the effects of other fresh urine constituents, urea, creatinine, and uric acid quench the dissolved reactive chlorine species ($Cl^{\bullet}/Cl_2^{\bullet-}$, HOCl, Cl_2, etc.). However, SO_4^{2-} shows no effect on pharmaceutical degradation while $H_2PO_4^-$ and citrate ions quench IrO_3-Cl resulting in a mixed kinetic and mass-transfer limiting oxidation of pharmaceuticals on IrO_2. Citrate ions only quench the dissolved oxidants (surface adsorbed radicals are the dominant oxidants) leading to the pharmaceutical degradation limited by the mass transfer of pharmaceutical to BDD surface. This work provides an understanding of the significance of various pathways for pharmaceutical degradation, scavenging effect of urine constituents, and strategies for rapid pharmaceutical degradation in human urine.

4.2 Using Selective Radical Quenchers to Reveal the Dominant Degradation Pathways

Allyl alcohol (AA, CH_2=$CHCH_2OH$) was used to quench both surface adsorbed radicals (e.g. $Cl^{\bullet}_{ads}$ and $^{\bullet}OH_{ads}$) and dissolved radicals (e.g. $Cl^{\bullet}/Cl_2^{\bullet-}$ and $^{\bullet}OH$ in the solution phase)[94] due to: (1) its strong interaction with the anode surface via its π-orbitals[159] and (2) its high reactivity with radicals ($k_{\bullet OH,\ AA}$ = 5.9 × 10^9 $M^{-1}s^{-1}$ [160], $k_{Cl\bullet,\ AA}$ = 6 × 10^8 $M^{-1}s^{-1}$ [94]) (Figure 4.1a, r_3 - r_5). As shown in Figure 4.1b, c, the electro-generation of FC species were completely inhibited due to AA quenching adsorbed and dissolved $^{\bullet}OH$ and $Cl^{\bullet}/Cl_2^{\bullet-}$ along with IrO_3-Cl and IrO_{2+1}. Therefore, the only degradation pathway available to pharmaceuticals is DET in the presence of excess AA. By contrast, tert-butanol (t-BuOH) has been found to not readily react with surface adsorbed radical species.[94,161]

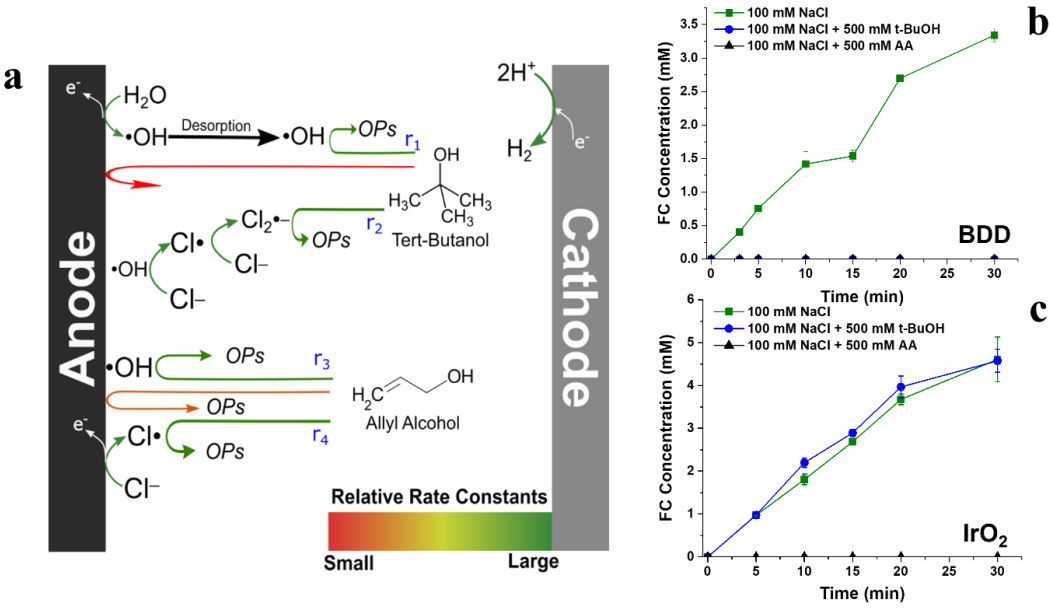

Figure 4.1 **(a) Scheme of relative rate constants for reactions of selective quenchers (AA and t-BuOH) with radicals.** The black arrows represent the transport of species. The color coding indicates the relative range of large to small rate constants. **Free chlorine (FC) production on**

(b) BDD and (c) Ti/IrO_2 anodes in a 100 mM chloride electrolyte in the presence of quenchers. Error bar represents the standard deviation from triplicate measurements.

However, t-BuOH can still effectively quench dissolved radicals in the solution phase (e.g. dissolved $Cl^{\bullet}/Cl_2^{\bullet-}$ and $^{\bullet}OH$) given the large homogeneous second-order rate constants ($k_{\bullet OH,\ t\text{-}BuOH} = 4.8 \times 10^8\ M^{-1}s^{-1}$, $k_{Cl\bullet,\ t\text{-}BuOH} = 3 \times 10^8\ M^{-1}s^{-1}$) (Figure 2.4a, r_1 & r_2).[162,163] The formation of FC with IrO_2 anodes was not quenched by t-BuOH (Figure 2.4c), but it was quenched with BDD (Figure 2.4b). This is consistent with that FC is generated via surface absorbed chlorine (IrO_3-Cl) with IrO_2, but it is formed via dissolved chlorine radicals which are quenched by t-BuOH.[38] Consequently, the degradation of pharmaceuticals is ascribed to DET and reaction with surface adsorbed radicals with excess t-BuOH.

4.3 Mass Transfer Limiting Pseudo-First-Order Rate Constants

The electrolysis rate of pharmaceuticals is typically reported as a pseudo-first-order rate constant (k_{obs}), which is the multiplicative product of a second order rate constant (for the reaction of the pharmaceutical with all the oxidants) and the concentration of oxidants.[39] Pseudo-first-order kinetics can be justified since: (1) the direct anodic oxidation and oxidation by reactive chlorine species (RCS) or reactive oxygen species (ROS) on the surface are all first order with respect to pharmaceutical concentration and (2) the concentrations of oxidants in solution phase are assumed to be constant with time (steady-state generation and consumption) and at much lower concentration than the pharmaceutical. Using pseudo-first-order kinetics significantly simplifies a complex coupled reaction and mass transport system. The pseudo-first-order rate constant captures the rate of pharmaceutical degradation due to the electrode surface chemistry, the applied potential, the electrolyte composition, and the fluid mechanics in the reactor. The role of the fluid mechanics (i.e, k_m) and reactor geometry (i.e., A/V) are significant

barriers to universally using observed pseudo-first order rate constants obtained in laboratory experiments since the rate constants may not be accurate for other reactor geometries and flow situations.

In this work, we compare the k_{obs} with the mass-transfer-limited pseudo-first-order rate constant (k_m) in our experiment setup to understand the limiting mechanisms of oxidation. k_m was determined by the "limiting current" technique with different mass-transfer conditions (Chapter 2.3.5)**.**[79] The corresponding mass-transfer coefficient was determined to be 0.130 ± 0.0028 cm/min, which corresponds to a pseudo-first-order rate constant of 0.028 min^{-1} for the electrochemical cell used in this work (A/V = 0.214 cm^{-1}). If $k_{obs} = k_m$, it indicates that the rate of pharmaceutical degradation is limited by transport of pharmaceutical molecules to the anode surface where reactions occur via direct anodic oxidation, surface adsorbed radicals and dissolved oxidants in the vicinity of electrode surface (before diffusing into the stagnant layer) (Figure 2.4**,** Gradient B). If $k_{obs} > k_m$, oxidants generated at the anode desorb and react homogeneously with the pharmaceuticals (Figure 2.4, Gradient C and D). By contrast, if $k_{obs} < k_m$, the pharmaceutical degradation has some kinetic limitations along with the mass-transfer resistance (Figure 2.4, Gradient A; see Chapter 2.5 for detailed discussion).[39]

4.4 Electrochemical Oxidation Pathways of Pharmaceuticals in Chloride only Solution

To reveal the scavenging effects of each constituent in the urine matrix, it is important to first determine the electrochemical oxidation pathways of pharmaceutical in Cl^- only solution. The possible pathways are direct electron transfer (DET) and reaction with electro-generated oxidants including physisorbed and dissolved $^{\bullet}OH$, free chlorine (FC, primarily HOCl and OCl^-, and to a lesser extent Cl_2 and/or Cl_2O at pH 6), chemisorbed chlorine (IrO_3-Cl) and chlorine radicals

($Cl^{\bullet}_{ads}$, $Cl^{\bullet}$, $Cl_2^{\bullet-}$).[50,57] However, few studies have evaluated the proportion of these oxidation pathways of pharmaceutical removal in the Cl^- only electrolyte at pH 6. Mechanistic studies of various classes of pharmaceuticals degradation were conducted to gain insight into the role of various degradation pathways during electrolysis.

The contribution of each oxidation pathway was determined by the electrolysis rates of pharmaceuticals in various electrolytes containing excess quenchers (Table 4.1). The individual contribution of each of the following oxidation pathway was evaluated by $COP_i = k_i/k_{obs,Cl-}$, where COP_i is the contribution of oxidation pathway i, k_i is the rate constant of oxidation pathway via i and $k_{obs,Cl-}$ is the k_{obs} in 100 mM Cl^- electrolyte. Therefore, (1) the rate constant of direct electron transfer (DET) was the electrolysis rate in electrolyte containing Cl^- and AA; (2) the rate constant of oxidation via $^{\bullet}OH_{diss}$ was determined as the difference between electrolysis rates in ClO_4^- (an inert supporting electrolyte that yields no anodic reactive chlorine species) and ClO_4^- + t-BuOH; (3) Oxidation due to $^{\bullet}OH_{ads}/IrO_{2+1}$ was determined as the difference between the rate constant in ClO_4^- and the rate constants of DET and $^{\bullet}OH_{diss}$ obtained from (1) and (2), respectively; (4) the rate constant of oxidation via $Cl^{\bullet}_{ads}$ with BDD was determined as the difference between rate constants due to ClO_4 + t-BuOH and Cl^- + t-BuOH; (5) Oxidation due to dissolved $Cl^{\bullet}/Cl_2^{\bullet-}$ and FC with BDD was determined as the difference between observed rate constants in Cl^- and Cl^- + t-BuOH with elimination of rate constants of $^{\bullet}OH_{diss}$ obtained from (2); and (6) The rate constant of oxidation via FC and IrO_3-Cl were distinguished by mass-transfer limiting mechanism (*see below*).

Table 4.1 Constituents of Pseudo-first-order Rate Constants due to Different Electrolytes

Components of Observed Rate Constants	Electrolyte
$k_{obs} = k_{DET} + k_{\bullet OHads} + k'_{\bullet OHdiss} + k_{Cl\bullet ads} + k'_{Cl\bullet diss} + k'_{FC}{}^{b}$	100 mM Cl^-

$k_{obs} = k_{DET}$	100 mM Cl^- + 500 mM AA
$k_{obs} = k_{DET} + k_{\bullet OHads} + k'_{\bullet OHdiss}$ [a]	100 mM ClO_4^-
$k_{obs} = k_{DET} + k_{\bullet OHads}$	100 mM ClO_4^- + 500 mM t-BuOH
$k_{obs} = k_{DET} + k_{\bullet OHads} + k_{Cl\bullet ads}$ (BDD) $k_{obs} = k_{DET} + k_{\bullet OHads} + k_{Cl\bullet ads} + k'_{FC}$ (IrO_2)	100 mM Cl^- + 500 mM t-BuOH

[a] $k''_{\bullet OHdiss} = k^{\bullet}_{OH,\,pharm}[^{\bullet}OH]$. [b] $k'_{Cl^{\bullet}diss} = k_{Cl^{\bullet},\,pharm}[Cl^{\bullet}]$; $k'_{FC} = k_{FC,\,pharm}[FC]$;

4.4.1 *Rate of Degradation Due to Direct Electron Transfer (DET)*

The contribution of DET to pharmaceutical oxidation was evaluated by comparing rate constants in Cl^- solution with and without excess AA. As shown in Figure 4.2 (green *vs.* orange columns), the substantial difference between the electrolysis rates of pharmaceuticals indicates that the contribution of DET accounts for less than 3% for the degradation of CP, CBZ and SMX with both electrodes. The contribution from DET to pharmaceutical oxidation was calculated and are shown in Table 4.2. The degradation of pharmaceutical via DET on both electrodes was mainly kinetically limited ($k' << k_m$, where k' is the true kinetic rate constant of pharmaceutical oxidation). This suggests a significant kinetic barrier for direct electron transfer from pharmaceuticals to the anode. The observed rate constants of SMX degradation are higher than other three pharmaceuticals indicating the faster degradation of SMX via DET.

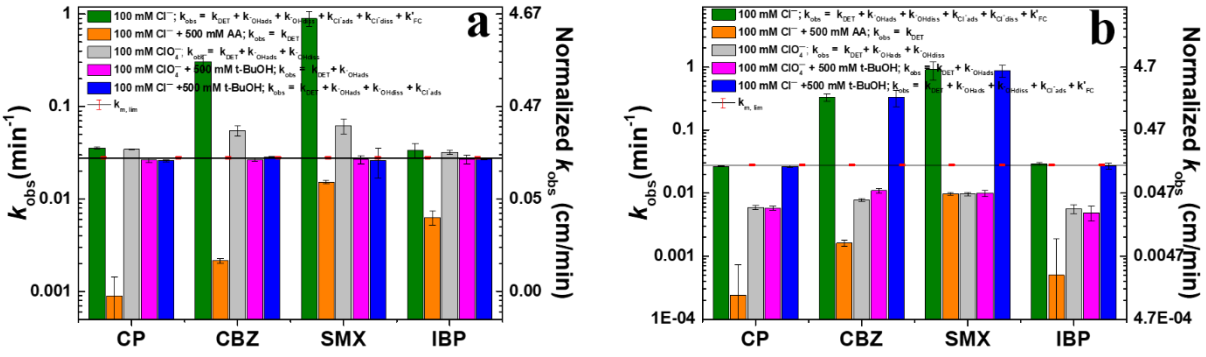

Figure 4.2. **Pseudo-first-order electrolysis rates of target pharmaceuticals on (a) BDD anodes and (b) IrO_2 anodes.** Error bars represent standard deviations from triplicate

measurements. As shown in Table 4.1, the electrolysis rates of pharmaceuticals shown in green column consist of the contribution of DET, dissolved and adsorbed $^{\bullet}OH$ and $Cl^{\bullet}/Cl_2^{\bullet-}$ and FC; the orange columns indicate the contribution of DET only; the red columns represent the electrolysis rates from DET, dissolved and adsorbed $^{\bullet}OH$; the pink columns indicate the electrolysis rates from DET and adsorbed $^{\bullet}OH$; and the blue columns reveal the electrolysis of pharmaceuticals via DET and adsorbed $^{\bullet}OH$ and $Cl^{\bullet}/Cl_2^{\bullet-}$.

Table 4.2. Contribution to Pharmaceutical Oxidation in 100 mM Cl^- with BDD and IrO_2 Electrodes. The contribution to pharmaceutical degradation from $Cl_2^{\bullet-}$ and FC with BDD cannot be distinguished due to the quenching effect of t-BuOH on both oxidants.

	BDD					**IrO_2**					
Compounds	**DET**	**$^{\bullet}OH_{ads}$**	**$^{\bullet}OH_{diss}$**	**$Cl^{\bullet}_{ads}$**	**$Cl_2^{\bullet-}{}_{diss}$ & FC**	**DET**	**IrO_{2+1}**	**$^{\bullet}OH_{diss}$**	**IrO_3-Cl**	**FC**	**$Cl^{\bullet}_{diss}$**
CP	2.5%	71.6%	23.4%	0.0%	3.4%	0.9%	20.8%	0.9%	78.0%	0%	0%
CBZ	0.7%	8.0%	9.3%	0.6%	81.4%	0.5%	2.8%	0.0%	4.6%	91.7%	0.4%
SMX	1.7%	1.3%	3.9%	0.0%	93.2%	1.1%	0%	0.0%	2.9%	92.1%	4.0%
IBP	18.6%	61.0%	15.1%	0.3%	5.0%	1.7%	15.1%	2.7%	76.0%	0%	4.5%

4.4.2 *Rate of Degradation Due to $^{\bullet}OH_{diss}$*

The difference between the electrolysis rates of pharmaceuticals in 100 mM ClO_4^- with and without t-BuOH indicates the contribution of $^{\bullet}OH_{diss}$ to the pharmaceutical degradation (Figure 4.2, grey *vs.* pink columns). $^{\bullet}OH_{diss}$ contributes 23.4%, 9.3%, 3.9%, and 15.1% to the degradation of CP, CBZ, SMX and IBP with BDD, respectively (Table 4.2). However, the electrolysis rates of pharmaceutical with IrO_2 are unaltered with the addition of t-BuOH. It suggests that $^{\bullet}OH_{diss}$ barely contributes to the pharmaceutical degradation with IrO_2, consistent with previous reports of low $^{\bullet}OH_{diss}$ production for active anodes.[60,94] Furthermore, the electrolysis rates of pharmaceuticals are at mass-transfer limiting rates on BDD with the addition of t-BuOH, consistent with that t-BuOH does not readily react with surface adsorbed radical species (*see above*, Figure 4.1a, r_1 & r_2).

4.4.3 *Rate of Degradation Due to Adsorbed •OH and Chemisorbed Oxygen (IrO_{2+1})*

The kinds of surface adsorbed $^{\bullet}OH$ are varied due to the anode materials.[164] Physisorbed $^{\bullet}OH$ is generated on BDD, while chemisorbed oxygen is formed on IrO_2 surface ($\underline{IrO_{2+1}}$). The significance of $^{\bullet}OH_{ads}$ and IrO_{2+1} for pharmaceutical degradation in Cl^- only electrolyte was evaluated by the difference among the electrolysis rates of pharmaceuticals in ClO_4^- ($k_{obs} = k_{DET} + k_{\bullet OHads} + k'_{\bullet OHdiss}$), ClO_4^- + t-BuOH ($k_{obs} = k_{DET} + k_{\bullet OHads}$) and Cl^- + AA ($k_{obs} = k_{DET}$) (Figure 4.2, green *vs.* pink *vs.* orange columns). The $^{\bullet}OH_{ads}$ is the dominant oxidant for the electrolysis of CP (71.6%) and IBP (61.0%) with BDD (Table 4.2). However, IrO_{2+1} is not the dominant oxidant for the oxidation of CP and IBP due to the less reactivity of IrO_{2+1} as compared to $^{\bullet}OH_{ads}$. Furthermore, only less than 8% of the electrolysis of CBZ and SMX is ascribed to $^{\bullet}OH_{ads}$ or IrO_{2+1} with both electrodes due to their favored chlorine mediated pathways (*see below*). The degradation of pharmaceuticals with IrO_2 in the absence of Cl^- is at rates lower than mass-transfer limiting rates. This implies that the pharmaceutical degradation has some kinetic limitations ($k' < k_m$) due to the formation of chemisorbed oxygen on IrO_2.

4.4.4 *Rate of Degradation Due to IrO_3-Cl, Dissolved $Cl^{\bullet}/Cl_2^{\bullet-}$, and Free Chlorine (FC) with IrO_2*

The electrolysis rates of all pharmaceuticals were unaltered with excess t-BuOH present in Cl^- solution with IrO_2 (Figure 4.1b). It suggests little contribution of dissolved $Cl^{\bullet}/Cl_2^{\bullet-}$ to the pharmaceutical degradation with IrO_2 (Table 4.2). This is consistent with previous literature that it has not yet been reported for IrO_2 to generate significant amount of dissolved $Cl^{\bullet}/Cl_2^{\bullet-}$ to affect the pharmaceutical degradation.[38,50,60,94]

Chemisorbed chlorine (IrO_3-Cl) and/or FC are the dominant oxidants for the degradation of pharmaceuticals (Table 4.2). The generation of FC is via chemisorbed chlorine (IrO_3-Cl),

evidenced by the observation that the generation of FC is unaltered in the presence of excess t-BuOH during electrolysis (Figure 4.1c). Therefore, the addition of t-BuOH cannot separate the individual importance of IrO_3-Cl and FC. The difference between the electrolysis rates of pharmaceuticals in ClO_4^- + t-BuOH and Cl^- + t-BuOH is ascribed to the essential contribution of both IrO_3-Cl and FC to the pharmaceutical degradation (Figure 4.2b, pink *vs.* blue columns). However, the heterogeneous reactions of pharmaceuticals (via direct anodic oxidation and with surface adsorbed oxidants) have a maximum pseudo-first-order rate constant (k_m = 0.028 min^{-1}) when the oxidation kinetics are faster than the rate of transport of pharmaceutical to the anode surface from the bulk solution. This results in a clear distinction between the contribution from surface adsorbed oxidants (IrO_3-Cl) and the solution phase oxidants (FC).

Taken all together, the IrO_3-Cl is the dominant oxidant for the oxidation of CP (78.0%) and IBP (76.0%), while its contribution to the degradation of CBZ (4.6%) and SMX (2.9%) is small (Table 4.2). By contrast, the contribution of FC to CP and IBP degradation is negligible (~0%) with IrO_2, consistent with that CP and IBP have been found to be recalcitrant to FC.[67,165] The electrolysis rates of CBZ and SMX in Cl^- solution are much higher than k_m (Figure 4.2b), suggesting a substantial contribution of the homogenous reaction enhancement to their degradation (Figure 2.4; Gradient C or D). CBZ reacts with HOCl at very slow rates ($k \sim 10^{-4}$ $M^{-1}s^{-1}$) as compared to SMX ($k = 1.1 \times 10^3$ $M^{-1}s^{-1}$),[134] but reacts with Cl_2 and Cl_2O at very fast rates ($k \sim 10^4$ $M^{-1}s^{-1}$).[47] Furthermore, an equilibrium of HOCl with Cl_2 and Cl_2O can be established due to the electro-generation of Cl_2 and HOCl and pH. The speciation of FC with respect to the pH is shown in Figure 2.5b, and the local pH at the anode surface is approximately 0.74 (Chapter 2.5.2) at which the dominant FC species is dissolved Cl_2. Although the proportion of Cl_2 decreases due to the increasing pH away from the anode surface (Figure 2.5b), the role of

dissolved Cl_2 is not negligible in the stagnant layer. Thus, the primary degradation pathways of CBZ in Cl^- only solution is via dissolved Cl_2 which has not been reported or known for pharmaceutical degradation during electrolysis.[60,94] Although the reactivity of Cl_2 with SMX has not been reported, the Cl_2 is assumed to react with SMX at similar rates as with CBZ due to the presence of alkene in their molecular structures (Table 4.3). Besides the presumed oxidation of SMX by dissolved Cl_2, HOCl could contribute significantly to the SMX degradation due to: (1) increasing proportion of HOCl in FC species away from the anode (Figure 2.5) and (2) similar reactivity of HOCl with SMX as Cl_2. Taken all together, FC (primarily HOCl and/or Cl_2) is the dominant oxidant for the degradation of CBZ (91.7%) and SMX (92.1%) in electrolyte containing only Cl^-.

4.4.5 *Rate of Degradation Due to $Cl^{\bullet}_{ads}$, Dissolved $Cl_2^{\bullet-}$ and Free Chlorine (FC) with BDD*

Several studies have reported that $Cl^{\bullet}$ reacts with most organic molecules at similar rates as $^{\bullet}OH$.[60,102] However, electro-generated $Cl^{\bullet}$ is known as physisorbed radical but rapidly combine with local $Cl^{\bullet}$ or Cl^- to generate Cl_2 or dissolved $Cl_2^{\bullet-}$ in the stagnant layer, respectively.[166] The experimental results showed that the contribution of $Cl^{\bullet}_{ads}$ to all pharmaceutical degradation with BDD is negligible (~0%) when compares the k_{obs} between ClO_4^- + t-BuOH and Cl^- + t-BuOH (Figure 4.2a, pink *vs.* blue columns). The electrolysis rates of organic compounds in Cl^- solutions have been correlated to reaction rates with dissolved $Cl^{\bullet}$ and $Cl_2^{\bullet-}$ previously.[38,94,167] This indicates that $Cl^{\bullet}/Cl_2^{\bullet-}$ ($E^0(Cl^{\bullet})$ = 2.41 V, $E^0(Cl_2^{\bullet-})$ = 2.09 V)[44,48] contributes to the transformation of organic contaminants.

At Cl^- concentrations of human urine (100 mM), $Cl_2^{\bullet-}$ is expected to be the dominant species of chlorine radical generated with BDD electrodes: under the experimental conditions investigated in this work (i.e., [urea] = 0.27 M, [Pharm] ~ 4×10^{-4} M, [uric acid] = 0.003 M, [t-

BuOH] = 0.5 M and [AA] = 0.5 M), $^{\bullet}$OH will preferentially react with uric acid, t-BuOH and allyl alcohol (AA). The $^{\bullet}$OH has selectivity towards pharmaceutical degradation with the presence of urea.

$$\frac{k_{\bullet OH,\,pharm}[Pharm]}{k_{\bullet OH,\,urea}[urea]} = \frac{(10^{10}\ M^{-1}s^{-1})(4\times10^{-4}\ M)}{(7.9\times10^{5}\ M^{-1}s^{-1})(0.27\ M)} = 18.7$$

$$\frac{k_{\bullet OH,\,pharm}[Pharm]}{k_{\bullet OH,\,uric\ acid}[uric\ acid]} = \frac{(10^{10}\ M^{-1}s^{-1})(4\times10^{-4}\ M)}{(7.2\times10^{9}\ M^{-1}s^{-1})(0.003\ M)} = 0.185$$

$$\frac{k_{\bullet OH,\,tBuOH}[tBuOH]}{k_{\bullet OH,\,pharm}[Pharm]} = \frac{(4.8\times10^{8}\ M^{-1}s^{-1})(0.5\ M)}{(10^{10}\ M^{-1}s^{-1})(4\times10^{-4}\ M)} = 60$$

$$\frac{k_{\bullet OH,\,AA}[AA]}{k_{\bullet OH,\,pharm}[Pharm]} = \frac{(5.9\times10^{9}\ M^{-1}s^{-1})(0.5\ M)}{(10^{10}\ M^{-1}s^{-1})(4\times10^{-4}\ M)} = 737.5$$

Given the experimental conditions employed (i.e., $[Cl^-]$ = 0.1 M, $[OH^-] = 10^{-8}$ M at pH 6), $Cl_2^{\bullet-}$ is preferred to form in the bulk solution after the formation of $Cl^{\bullet}$:[94]

$^{\bullet}ClOH^- + H^+ \leftrightarrow H_2O + Cl^{\bullet}$ $\quad K_1 = 10^{7.2}\ M^{-1}$ Equation 4.1

$Cl^{\bullet} + Cl^- \leftrightarrow Cl_2^{\bullet-}$ $\quad K_2 = 10^{5.2}\ M^{-1}$ Equation 4.2

$$\frac{[Cl_2^{\bullet-}]}{[Cl^{\bullet-}]} = \frac{K_2[Cl^{\bullet}]}{K_1[H^+]} = \frac{(10^{5.2}\ M^{-1})(0.1\ M)}{(10^{7.2}\ M^{-1})(10^{-8}\ M)} = 10^{4.2}$$

Furthermore, the generation pathway of FC with BDD is via dissolved $Cl_2^{\bullet-}$. Hence, t-BuOH not only quenches $Cl_2^{\bullet-}$, but also prevents the formation of FC (Figure 4.1b). Therefore, the significance of dissolved $Cl_2^{\bullet-}$ and FC were evaluated in group for the pharmaceutical degradation. Unfortunately, the method of distinguishing IrO_3-Cl and FC discussed above for IrO_2 is not valid for BDD since both dissolved $Cl_2^{\bullet-}$ and FC are present in solution phase. As noted above, Cl_2 is the dominant oxidant for the oxidation of CBZ while both Cl_2 and HOCl are the dominant oxidants for the oxidation of SMX. The k_{obs} of CBZ and SMX in Cl^- solution with BDD much above k_m was observed. It suggests that $Cl_2^{\bullet-}{}_{diss}$ and Cl_2 are the dominant oxidants

for the degradation of CBZ (81.4%), while $Cl_2^{\bullet-}{}_{diss}$ and $HOCl/Cl_2$ are the dominant oxidants for the degradation of SMX (93.2%) (Table 4.2).

Table 4.3 Molecular Structures of Investigated Pharmaceuticals and Their Reactivities towards Oxidants and Radicals

Compounds	Molecular Structure	Overall Reactivity with HOCl ($M^{-1}s^{-1}$)	Overall Reactivity with Cl_2 ($M^{-1}s^{-1}$)	Functional Group	Chemical Symbol	Reactivity with $^{\bullet}OH$ or $Cl^{\bullet}$ ($M^{-1}s^{-1}$)	Reactivity with HOCl ($M^{-1}s^{-1}$)	Reactivity with Cl_2 ($M^{-1}s^{-1}$)
CP	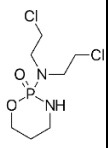	$< 10^{-4}$ *a*		Alkane	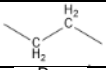	~ 10^{9} *e*	N/A	Assumed to be slow *f*
				Cyclic ether		2.9 × 10^{9} *e*	1.5 × 10^{-2} *g*	~ 10^{5} *g*
				Alkyl halide		~ 10^{8} *e*	N/A	N/A
				Phosphate	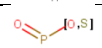	~ 10^{8} *e*	N/A	N/A
				Mustard	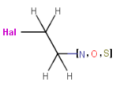	~ 10^{9} *e*	N/A	N/A
				Secondary Amine	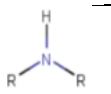	~ 10^{7} *e*	2.3 × 10^{2} *h*	3.0 × 10^{5} *q*
				Tertiary Amine		3.5 × 10^{9} *e*	4.0 *p*	1.82 × 10^{-8} *r*
CBZ	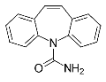	~10^{-4} *b*	10^{3} *c*	Alkene	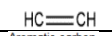	~ 10^{9} *e*	< 1 *i*	$10^{4} - 10^{6}$ *i*
				Aromatic carbon	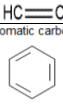	~ 10^{9} *e*	8.1× 10^{-2} *j*	6.3 × 10^{-3} *s*
				Amide	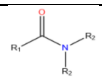	4.0 × 10^{5} *e*	3.3 × 10^{-2} *k*	2.0 – 10^{2} *t*
				Primary Amine		9.0 × 10^{7} *e*	2.77 × 10^{2} *h*	6.7 × 10^{5} *q*
				Tertiary Amine		3.5 × 10^{9} *e*	4.0 *p*	1.8 × 10^{-8} *r*
SMX	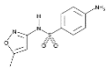	1.1 × 10^{3} *d*	N/A	Aromatic Carbon	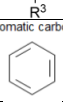	~ 10^{9} *e*	8.1× 10^{-2} *j*	6.3 × 10^{-3} *s*
				Aromatic Amine		4.0 × 10^{9} *e*	3.0 × 10^{4} *l*	0.11 *m*
				Aryl Sulfonamide		1.9 × 10^{9} *e*	10^{9} *v*	N/A
				Aromatic carbon-alkane		~ 10^{9} *e*	0 *o*	5.8 × 10^{1} *o*
				Isoxazole		N/A	N/A	N/A
IBP	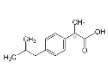	< 0.1 *b*	N/A	Alkane	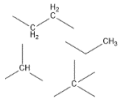	~ 10^{9} *e*	N/A	Assumed to be slow *f*

				Aromatic carbon	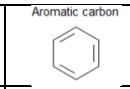	~ 10^{9} [e]	8.1× 10^{-2} [j]	6.3 × 10^{-3} [s]
				Carboxylic acid	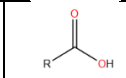	7.0 × 10^{5} [e]	1.1 [n]	2.9 × 10^{-5} [u]
				Aromatic carbon-alkane	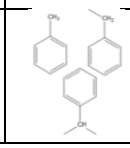	~ 10^{9} [e]	0 [o]	5.8 × 10^{1} [o]

"N/A" represents that the kinetics data has not been reported previously. [a] From ref. [168]. [b] From ref. [169]. [c] From ref. [47]. [d] From ref. [47]. [e] From ref. [170] and Cl• is assumed to have similar reactivities with respect to different functional groups as •OH. [f] The halogenation of alkane by Cl_2 requires UV light to generate Cl• as the initial step for the reaction. [g] Assumed based on the reactivity with aromatic ether from ref. [135]. [h] Assumed based on the reactivity with $NHCl_2$ from ref. [171]. [i] From ref. [172]. [j] From ref. [173]. [k] From ref. [174]. [l] From ref. [175]. [m] Assumed based on the reactivity of ClO_2 with from ref. [176]. [n] From ref. [177]. [O] Assumed based on the reactivity with p-xylene from ref. [178]. [p] Assumed based on the reactivity with trimethylamine from ref. [179]. [q] Assumed based on the reactivity with methylamine or dimethylamine from ref. [180]. [r] Assumed based on the reactivity with trimethylamine from ref. [181]. [s] Assumed based on the reactivity with benzene from ref. [182]. [t] Assumed based on the reactivity with N-substituted amides from ref. [183]. [u] Assumed based on the reactivity with acetic acid from ref. [184]. [v] From ref. [185]. It is noteworthy that all assumed reactivities of oxidants with functional groups based on the reaction with similar compounds are not accurate due to the effect of different neighboring groups.

Based on the observation above, the oxidation pathways of pharmaceuticals with alkene functional groups (present in CBZ and SMX but not in CP and IBP; Table 4.3) are primarily via reactions with Cl_2 or HOCl with both "active" and "inactive" electrodes during electrolysis in electrolyte only containing Cl^-. This is consistent with the well-known rapid reactions of alkenes with halogens.[172] By contrast, the pharmaceuticals which are sluggish towards FC are oxidized mainly via surface adsorbed oxidants (•OH or chemisorbed chlorine). Therefore, further experiments were undertaken to understand the scavenging effect of urine constituents on pharmaceutical degradation based upon the understanding of dominant degradation pathways for each pharmaceutical.

4.5 The Scavenging Effect of Organic Urine Constituents on Pharmaceutical Degradation

The synthetic fresh urine matrixes contain significant organic constituents including urea (270 mM), creatinine (13 mM), and uric acid (3 mM), and inorganic constituents such as sulfate (SO_4^{2-}; 15 mM), dihydrogen phosphate ($H_2PO_4^-$; 20 mM), and citrate ions (3 mM). The oxidant scavenging effects of these compounds may dramatically alter the rates of pharmaceutical degradation. The scavenging effect of each constituent is shown below.

4.5.1 *Urea*

Urea (270 mM) is the most abundant organic compound present in fresh human urine. The electrolysis rates of SMX and CBZ in the simplified synthetic fresh urine matrixes (SUM; 270 mM urea + 100 mM Cl^-) were significantly decreased as compared to that in Cl^- solution with both IrO_2 and BDD anodes (Figure 4.3a, b, green *vs.* orange columns). This suggests the large quenching effect of urea on dissolved reactive chlorine species (RCS; $Cl_2^{\bullet-}$, HOCl, Cl_2 and etc.). Urea reacts with HOCl with a rate constant of $k_{urea,HOCl} = 0.63\ M^{-1}s^{-1}$,[186] while the rate constant of HOCl with SMX is 3 orders-of-magnitude higher than with urea. The rest of the pharmaceuticals investigated react slower with HOCl than urea.[168,169] Moreover, the reactivity of dissolved Cl_2 with urea is similar to that with CBZ and SMX ($k_{Cl2,\ urea} = 2.35 \times 10^4\ M^{-1}s^{-1}$).[117] Therefore, the oxidation of pharmaceutical via FC are suppressed due to the high urea content in SUM. The reactivities of dissolved $Cl_2^{\bullet-}$ with urea and pharmaceuticals have not yet been reported. However, the rate constants of $Cl_2^{\bullet-}$ with most organic molecules are $\sim 10^7\ M^{-1}s^{-1}$.[48] Therefore, $Cl_2^{\bullet-}$ likely has similar reactivity towards urea and pharmaceutical with rate constants of 10^7

$M^{-1}s^{-1}$. Thus, $Cl_2^{\bullet-}$ is also quenched by urea that for the pharmaceutical degradation with BDD due to the high concentration of urea.

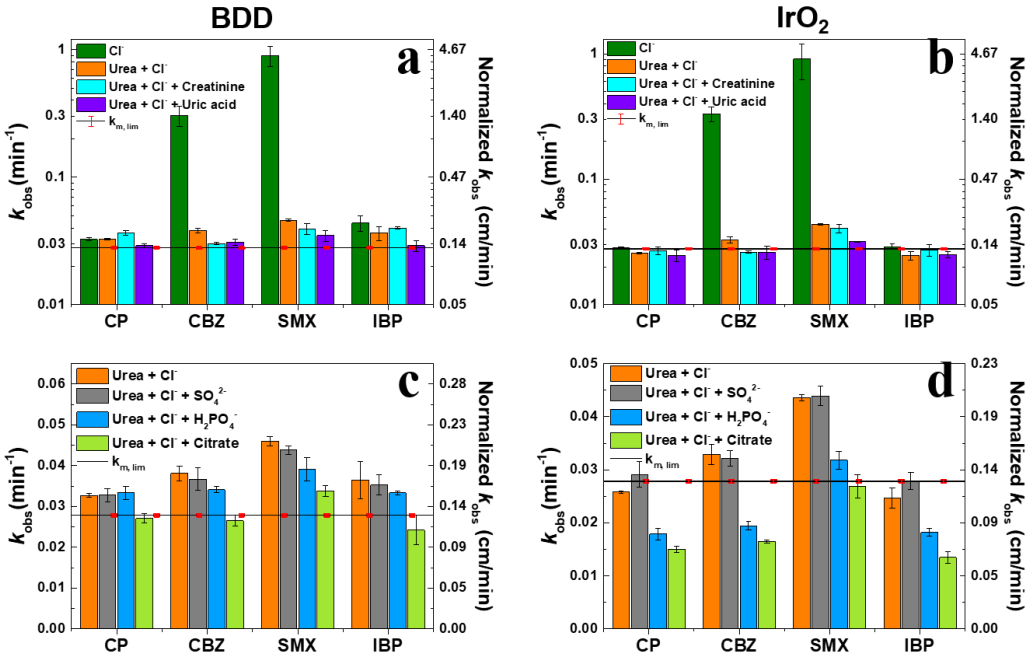

Figure 4.3 **Observed and normalized pseudo-first order rate constants during electrolysis of CP, CBZ, SMX, and IBP with the addition of individual constituent from synthetic urine matrixes with (a) & (c) BDD and (b) & (d) IrO_2.** The black horizontal line of observed rate constants represents mass-transfer limiting rates, including the measured standard deviation k_m.

The addition of urea has little impact on the electrolysis rates of CP and IBP with BDD (Figure 4.3a, green *vs.* orange columns**)** due to that: (1) the $^{\bullet}OH$ is the dominant oxidant for the degradation of CP and IBP (Table 4.2); $^{\bullet}OH$ can selectively oxidize pharmaceutical due to the unusual slow reaction of $^{\bullet}OH$ with urea;[67] and (3) contribution of RCS to their degradation is negligible (*see above*), even dissolved RCS are quenched by urea. The reactivity of $^{\bullet}OH$ with urea ($k = 7.9 \times 10^5$ $M^{-1}s^{-1}$) is much lower than with most pharmaceuticals ($k \sim 10^{10}$ $M^{-1}s^{-1}$),[187] which creates an effective selectivity of $^{\bullet}OH$ towards pharmaceutical degradation. The electrolysis rates of CP and IBP were unaltered with IrO_2 in the presence of urea (Figure 4.3b,

green *vs.* orange columns), although IrO_3-Cl (the dominant oxidant for the oxidation of CP and IBP) as one of the RCS is presumed to be quenched by urea. This is likely due to that: (1) the degradation of CP and IBP is already mass-transfer-limited reacting with IrO_3-Cl occurring at the anode surface and (2) the electro-generation of IrO_3-Cl is sufficient to degrade CP and IBP albeit urea also reacts with IrO_3-Cl.

4.5.2 *Creatinine*

Creatinine (13 mM) is a waste product of muscle metabolism and is present in human urine. As shown in Figure 4.3a, b (cyan *vs.* orange columns), the electrolysis rates of CP and IBP were not substantially changed in the presence of creatinine with both electrodes. It is because the radical quenching effect of creatinine is similar to that of urea,[23] although the rate constants of $^{\bullet}OH$ with creatinine have not been reported. Hence, $^{\bullet}OH$ can selectively oxidize pharmaceuticals with the addition of creatinine to SUM. However, the electrolysis rates of CBZ were further decreased when creatinine is added to SUM likely due to the larger scavenging effect of creatinine on dissolved Cl_2. Although the reaction rates of Cl_2 with creatinine is unknown, the second-order rate constant of Cl_2 and creatinine is speculated to be ~10^6 $M^{-1}s^{-1}$. It is because Cl_2 has been found to react with dimethenamid at 1.21×10^6 $M^{-1}s^{-1}$ via chlorination of the alkene group[136] and creatinine has alkene functional group analogous to dimethenamid. Thus, dissolved Cl_2 is further quenched with the addition of creatinine (13 mM) to SUM, consistent with the experimental data. By contrast, the rates of SMX degradation were not changed with both electrodes. This suggests the contribution of Cl_2 to SMX is insignificant, and HOCl is not further quenched by creatinine, consistent with the rate constant of HOCl with creatinine ($k_{HOCl,\ Creatinine}$ = 0.25 $M^{-1}s^{-1}$)[188] similar to that with urea ($k_{urea,HOCl}$ = 0.63 $M^{-1}s^{-1}$).[186]

4.5.3 *Uric Acid*

The normal excretion of uric acid in human urine is 1.06 - 3.1 mM. In this work, 3 mM uric acid was used to maximize the worst case of scenario of oxidants scavenging effect. As shown in Figure 4.3a, b (violet *vs.* orange columns), the addition of uric acid to SUM resulted in a decrease of electrolysis rates of CBZ to k_m due to a significant HOCl and Cl_2 quenching effect of uric acid. The uric acid scavenges HOCl with an estimated rate constant 3×10^5 $M^{-1}s^{-1}$.[180] Additionally, uric acid has an alkene group analogous to dimethenamid so that it likely reacts with Cl_2 at ~10^6 $M^{-1}s^{-1}$ (*see above discussion for creatinine*). The rates of SMX degradation were decreased but slightly above k_m (Figure 4.3a, b, violet columns). The reaction of SMX is mass-transfer-limited with very low homogenous reaction enhancement due to the reaction competition between uric acid and SMX with HOCl. Moreover, the degradation rates of CP and IBP were decreased to mass-transfer limiting rates due to the $^{\bullet}OH_{diss}$ quenching effect of uric acid in solution phase with BDD (Figure 4.3a). Uric acid is reported to react with $^{\bullet}OH$ at near diffusion controlled rate ($k_{^{\bullet}OH,\ uric\ acid} = 7.2 \times 10^9$ $M^{-1}s^{-1}$).[189] It results in the competition between uric acid and pharmaceuticals for $^{\bullet}OH$ in the solution phase. Furthermore, the oxidation of CP and IBP is also observed at mass-transfer limiting rates with IrO_2 (Figure 4.3b). It's possibly due to that: (1) the reaction of $^{\bullet}OH_{abs}$ (on BDD) and IrO_3-Cl (on IrO_2) with uric acid is mass-transfer-limited and (2) the $^{\bullet}OH_{abs}$ and IrO_3-Cl are sufficient to react with pharmaceuticals and maintain pharmaceutical concentration at zero on the surface.

The organic constituents (urea, creatinine and uric acid) in synthetic fresh urine substantially quench the dissolved RCS. It results in a significant decrease of electrolysis rates of CBZ and SMX with both electrodes. Urea and creatinine do not effectively change the electrolysis rates of CP and IBP due to the selectivity of $^{\bullet}OH$ towards pharmaceutical oxidation. By contrast, uric

acid quenching all dissolved radicals results in the oxidation of CP and IBP limited by the mass transfer of pharmaceuticals to the anode surface.

4.6 The Effect of Inorganic Urine Constituents on Pharmaceutical Degradation

4.6.1 *SO_4^{2-}*

SO_4^{2-} (15 mM) is an abundant anion in synthetic fresh urine matrixes. The addition of SO_4^{2-} can produce new oxidants, $SO_4^{\bullet-}$ and $S_2O_8^{2-}$ (Table 1.1, eqs. 5-7).[50] $SO_4^{\bullet-}$ is an intermediate and responsible for the formation of $S_2O_8^{2-}$, but many studies have suggested its participation in the oxidation of organics.[190-193] Additionally, $S_2O_8^{2-}$ is a less reactive oxidant than $SO_4^{\bullet-}$ ($<10^4$ $M^{-1}s^{-1}$).[194] The electrolysis rates of all pharmaceuticals were unchanged with the addition SO_4^{2-} to SUM due to the similar reactivity of $SO_4^{\bullet-}$ (product of quenching $^{\bullet}OH$ and $Cl^{\bullet}$ by SO_4^{2-}) as $^{\bullet}OH$ and $Cl^{\bullet}$ (Figure 4.3c, d, gray *vs.* orange columns). The reactivities of $SO_4^{\bullet-}$ with most pharmaceuticals have been reported to be greater than 10^8 $M^{-1}s^{-1}$,[195-197] and the reactivity of urea with $SO_4^{\bullet-}$ is similar to that with $^{\bullet}OH$ ($k_{SO4\bullet-,\,urea} = 6.35\times 10^5$ $M^{-1}s^{-1}$).[198] Thus, $SO_4^{\bullet-}$ should have a selectivity towards pharmaceutical oxidation analogous to $^{\bullet}OH$. Nonetheless, the electrolysis rates of CBZ and SMX were hypothesized to decrease with the addition of SO_4^{2-} due to the $Cl^{\bullet}$-quenching effect of SO_4^{2-} that inhibits the formation of FC (Table 1.1, eq. 9). However, this process is suppressed due to high content of Cl^- in the matrixes (Table 1.1, eq. 10).

4.6.2 *$H_2PO_4^-$*

$H_2PO_4^-$ (20 mM) may affect electrolysis rates of pharmaceuticals due to the generation of $H_2PO_4^{\bullet}$ (Table 1.1, eqs. 11-12).[53,54] However, the electrolysis rates of pharmaceuticals were unchanged in the presence of $H_2PO_4^-$ with BDD (Figure 4.3c, blue column). This is likely due to

that (1) the reaction rate constant of $^{\bullet}OH$ with $H_2PO_4^-$ ($k = 2.0 \times 10^4$ $M^{-1}s^{-1}$) is 5 to 6 orders-of-magnitude lower than that with CP and IBP ($k \sim 10^{9\text{-}10}$ $M^{-1}s^{-1}$) and (2) $H_2PO_4^-$ does not likely scavenge $Cl^{\bullet}$ because of the high reactivity of $H_2PO_4^{\bullet}$ with Cl^- ($k = 2.2\times 10^6$ $M^{-1}s^{-1}$) and the high concentration of Cl^-. However, the addition of $H_2PO_4^-$ decreased electrolysis rates of CP, CBZ and IBP below k_m with IrO_2 (Figure 4.3d, blue column). This is unexpected because the electro-generation of $H_2PO_4^{\bullet}$ via direct anodic oxidation is supposed to facilitate production of more RCS (Table 1.1, eq. 12). We hypothesize that the diminished rates of the degradation of CP, CBZ and IBP suggest that the IrO_3-Cl is quenched by $H_2PO_4^-$ with the generation of less reactive oxidant ($H_2PO_4^{\bullet}$) albeit the reactivity of IrO_3-Cl with $H_2PO_4^-$ is unclear. It results in a mixed kinetically and mass-transfer limiting degradation of pharmaceuticals with IrO_2. However, the rates of SMX degradation were decreased but still above k_m with both electrodes. It suggests that (1) the kinetic between $H_2PO_4^{\bullet}$ (IrO_3-Cl scavenging product) and SMX is faster than the mass transport and (2) the homogenous reaction of HOCl with SMX despite the diminished generation of HOCl due to the hypothesized IrO_3-Cl scavenging effect of $H_2PO_4^-$.

4.6.3 *Citrate ions*

Sodium citrate (3 mM) is a derivative of citric acid in urine matrixes. Its radical scavenging effect ($k_{\bullet OH,\ citrate\ ion} = 2.4 \times 10^8$ $M^{-1}s^{-1}$) (Table 1.1, eqs. 13-14)[55] changes the oxidation rates of the pharmaceuticals due to the low reactivity of citrate radicals (– radical scavenging product) with organic contaminants (E^0 ($Na_3Citrate$) = –0.18 V).[199] The reaction rate constant of $Cl_2^{\bullet-}$ with citrate ions has not been reported previously. As a reference, (1) standard reduction potential of chlorine radicals ($E^0(Cl_2^{\bullet-}/Cl^-)$ = 2.24 V)[200] is close to that of $^{\bullet}OH$ at pH 6 ($E^{0\prime}(^{\bullet}OH/OH^-)$ = 2.38 V)[200] and (2) $Cl_2^{\bullet-}$ reacts with most organics at rates 10^7 $M^{-1}s^{-1}$.[201] Thus, these suggest that the reactivity of $Cl_2^{\bullet-}$ and citrate ion is possibly around 10^7 $M^{-1}s^{-1}$. As shown in Figure 4.3c (green

vs. orange columns), the electrolysis rates of CP and IBP decreased to k_m on BDD with the addition of citrate ions, consistent with the presumable radical-scavenging effect of citrate ions. The rates of CP and IBP degradation were decreased below k_m with IrO_2 (Figure 4.3d, green *vs.* orange columns). It suggests the degradation of CP and IBP is controlled by mass-transfer as well as kinetic rates with IrO_2 due to the IrO_3-Cl quenching effect by citrate ions in analogues to $H_2PO_4^-$. Furthermore, the oxidation rates of CBZ and SMX were decreased with the addition of citrate ions with both electrodes (Figure 4.3c, d). Specifically, the observed electrolysis rate of CBZ is down to k_m while it is still above k_m for SMX degradation with BDD. The oxidation rates are observed below and near k_m for CBZ and SMX oxidation with IrO_2, respectively. Taken together, these observations suggest: (1) citrate ions slightly quench $Cl_2^{\bullet-}$ resulting in less FC formation with BDD; (2) IrO_3-Cl is largely quenched by citrate, resulting in a mixed kinetic and mass-transfer limit of reaction of CBZ with IrO_2; (3) the homogeneous reaction of HOCl with SMX adds up to the electrolysis rates, consistent with the reactivity of HOCl with citrate ($k = 5.5 \times 10^{-3}$ $M^{-1}s^{-1}$)[56] lower than with SMX ($k = 1.1 \times 10^3$ $M^{-1}s^{-1}$);[134] and (4) the Cl_2 is quenched by citrate significantly leading to no homogeneous reaction enhancement for CBZ degradation with both electrodes, although the reactivity has not been reported (Table 1.1, eq. 16).

4.7 Electrolysis of Pharmaceutical in Full Synthetic Fresh Urine Matrixes (FUM)

The scavenging effects of individual urine constituents were further consolidated and verified by experiments conducted in the full synthetic fresh urine matrixes (FUM). The electrolysis of FUM with relatively low current densities (10 mA/cm^2) did not significantly change the pH of the electrolyte. All pharmaceuticals were degraded greater than 90% within 1.5 hr treatment with BDD (Figure 4.4a), while they were eliminated greater than 80% with IrO_2 (Figure 4.4b). In

addition, the observed and normalized pseudo-first-order rate constants were obtained to assess the performance of pharmaceuticals degradation in FUM (Figure 4.4c). Similar rapid degradation rates of CP, CBZ and IBP were observed corresponding to k_m with BDD electrode. This suggests the pharmaceutical degradation in FUM takes place at mass-transfer limiting conditions, consistent with the dissolved oxidant scavenging effect of citrate and uric acid. By contrast, the electrolysis rates of CP, CBZ and IBP were substantially lower than k_m with IrO_2. It suggests a mixed kinetic and mass-transfer limit of pharmaceutical degradation, consistent with the scavenging effect of $H_2PO_4^-$ and citrate discussed above. While the SMX is degraded the fastest among all pharmaceuticals at rates slightly above k_m by both electrodes. The high reactivity of SMX with HOCl in solution phase leads to the electrolysis rates greater than or near the k_m.

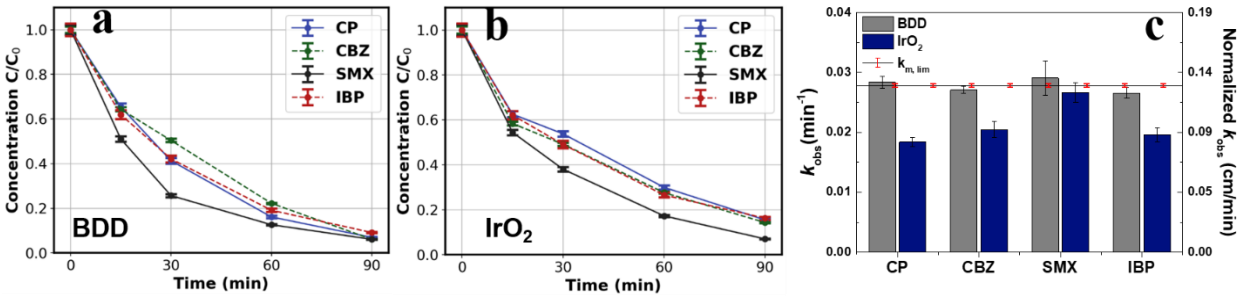

Figure 4.4 **Target pharmaceuticals removal during electrolysis in FUM matrixes on (a) BDD electrode; (b) Ti/IrO_2 electrode. (c) Observed and geometry normalized pseudo-first order rate constants of target pharmaceutical electrolysis in FUM on BDD and Ti/IrO_2.** The black horizontal line represents the measured mass-transfer limiting rate constants with uncertainties. Error bars represent the standard deviation of replicate experiments.

In our electrochemical setup, the concentration of pharmaceuticals can be removed by 3 orders-of-magnitude within 9 hr treatment on IrO_2 electrodes (normalized k_{obs} greater than 0.075 cm/min) (Figure 3.5). BDD outperformed IrO_2 with normalized $k_{obs} \geq 0.124$ cm/min for all pharmaceuticals. This results in presumable 3 orders-of-magnitude reduction in concentration

within 6 hours (Figure 3.5). The discrepancy between the electrolysis rates of pharmaceuticals with both anodes is as expected and reported previously due to the kinds and yields of oxidants generated on BDD and IrO_2 electrodes (*see above*).[36,128,202]

4.8 Strategies of Faster Pharmaceutical Degradation by Active and Inactive Anodes

To investigate the best strategies for achieving faster degradation of pharmaceuticals with both active and inactive anodes, multiple approaches were tested such as increasing mass transfer rates, increasing the applied current densities, and increasing the initial chloride concentration.

4.8.1 *Increasing Mass Transfer Rates*

The observed rate constants of pharmaceutical degradation are determined by the mass-transfer-limiting rate (k_m) and the true kinetic rate constant of pharmaceutical degradation (k') when oxidation only occurs at the anode surface (Figure 2.4, gradient A and B), given by $k_{obs} = \frac{1}{\frac{1}{k'}+\frac{1}{k_m}}$ (Chapter 2.5). Therefore, increasing k_m should result in the increase of k_{obs} theoretically. It agrees with the observation shown in Figure 4.5a, b, increasing the mass transfer rates leads to higher oxidation rates of pharmaceuticals with both electrodes, although the electrolysis rates are below their corresponding k_m (*Re* = 11050). It suggests the oxidation of pharmaceuticals at *Re* = 11050 is both kinetically and mass-transfer-limited for our experimental setup. Additionally, the pseudo-first-order true kinetic rate constants (k') of each pharmaceutical with BDD and IrO_2 can be determined in our electrochemical setup (measured potential ~2.5V). The k' reflects the kinetics of pharmaceutical oxidation on the electrode surface controlled only by the applied potential regardless of electrochemical cell geometry and mass transfer conditions. As shown in Table 4.4, the k' is higher for all pharmaceuticals with BDD than IrO_2, consistent with the

presumed $H_2PO_4^-$ and citrate ion quenching effect on IrO_3-Cl with IrO_2 (*see above*). Furthermore, the k' is highest for the oxidation of SMX with both electrodes due to the faster degradation of SMX via DET.

Table 4.4 Geometry-normalized Pseudo-first-order True Kinetic Rate Constants (k') Obtained from k_{obs} at *Re* =11050 in Figure 5a, b, given by the equation $k_{obs} = \frac{1}{\frac{1}{k'}+\frac{1}{k_m}}$ (Chapter 2.5).

	CP *k' (cm/min)*	*CBZ* *k' (cm/min)*	*SMX* *k' (cm/min)*	*IBP* *k' (cm/min)*
BDD	0.94	0.82	1.09	0.82
IrO_2	0.25	0.27	0.34	0.28

4.8.2 *Increasing Current Densities*

As shown in Figure 4.5c, d, increasing current densities (equivalent to increasing the applied potential) increases the generation rates of oxidants and facilitates the direct electron transfer. The electrolysis rates of pharmaceuticals with 100 mA/cm^2 were significantly higher than the determined k_m at *Re* = 2977. Cotillas[23] ascribed the similar observation to the twice generation of oxidants in solution phase due to the higher current densities in Cl^- only solution. However, it is doubtful due to the oxidant-scavenging effect of urine constituents as noted above. The plausible explanation is that a 1-order-of-magnitude increase in applied current density leads to significantly more gas evolution, and thus increases k_m during electrolysis which further increases the observed oxidation rates of pharmaceuticals. It explains why the electrolysis rates of pharmaceuticals are higher than k_m (*Re* = 2977) with 100 mA/cm^2 applied current densities. The degradation rate of SMX is much higher than the other pharmaceuticals. It is likely due to the higher rates for SMX degradation via DET (*see above*).

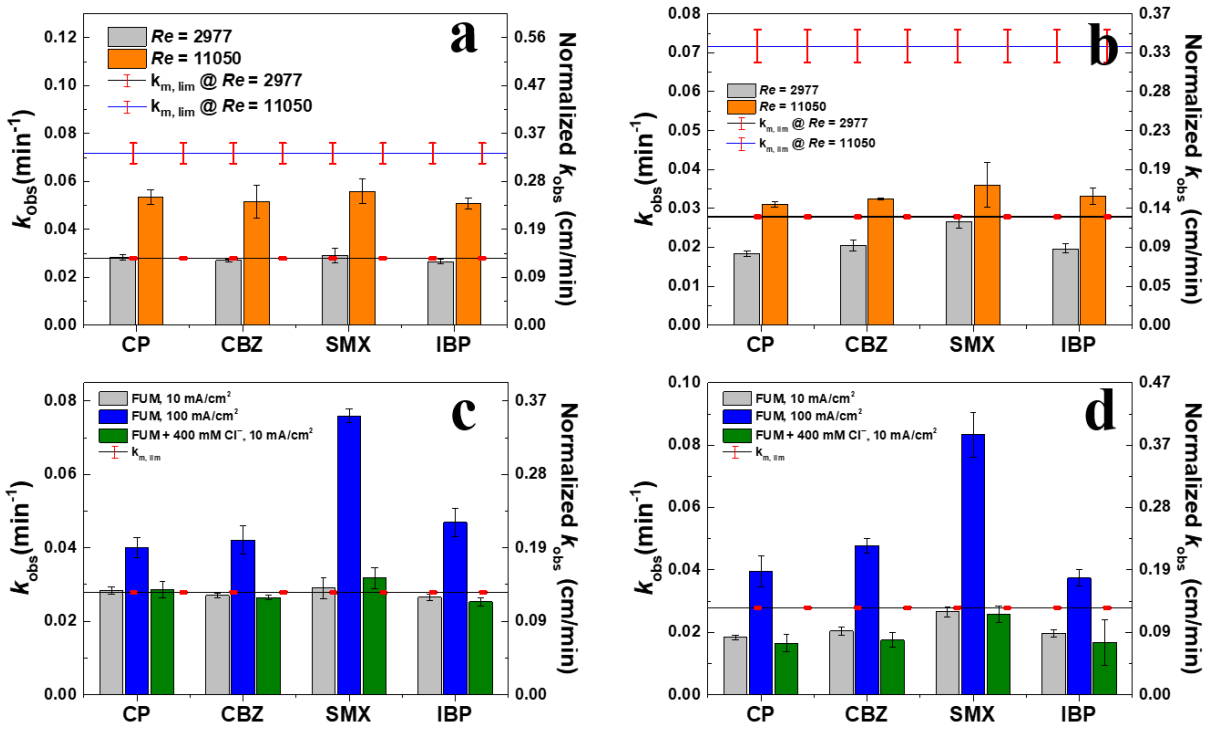

Figure 4.5 **Electrolysis rates of test pharmaceuticals in FUM investigated in this work with different stir rates by (a) BDD and (b) IrO_2. Electrolysis rates of four pharmaceuticals in FUM under a stir rate of 600 rpm (*Re* = 2977) with various applied current densities and initial Cl^- concentration by (c) BDD and (d) IrO_2.**

4.8.3 *Increasing the Concentration of Chloride Ions*

The electrolysis rates of pharmaceuticals were unchanged with the addition of 400 mM Cl^- to FUM (Figure 4.5 c, d). The stoichiometric excess of Cl^- (as compared to urea) did not effectively accelerate the degradation of pharmaceuticals. It suggests that (1) the generation of dissolved RCS is not rapid enough to reach the chlorination breakpoint and (2) the electro-generation of IrO_3-Cl is not sufficient to outweigh the quenching effect of $H_2PO_4^-$ and citrate ions.

Increasing the mass-transfer rates is important for faster degradation of pharmaceuticals in FUM for both "active" and "inactive" types of electrodes. However, the electrolysis rates of pharmaceuticals with "inactive" type anode (e.g., BDD) outcompete that with "active" type

anode (e.g., IrO_2) due to the higher kinetic rates achieved by "inactive" anode in our experimental setup. Nonetheless, for EAOPs with low k_m (i.e., much smaller than k' on IrO_2), the oxidation of organic contaminants with IrO_2 could occur at mass-transfer controlled rates in the absence of dissolved oxidants. Under this circumstance, the electrolysis rates could be similar for BDD and IrO_2 electrodes since the rates are controlled by the mass transfer of organic contaminants from bulk to the electrode surface. Additionally, increasing the applied current densities can result in similar electrolysis rates of pharmaceuticals by BDD and IrO_2 by enabling the true kinetic rates on IrO_2 similar to that on BDD. However, increasing the current densities decreases the Faradaic efficiency and costs more energy, however, it enhances mass-transfer rates likely due to the intense gas evolution. The stoichiometric excess Cl^- (as compared to urea) does not impact the oxidation of pharmaceuticals in FUM due to that the generation rates of FC are not sufficient to reach chlorination breakpoint.

4.9 CONCLUSIONS

In this chapter, we show that electro-generated dissolved Cl_2 has been overlooked for the oxidation of organic contaminants in previous literature. Dissolved Cl_2 is the dominant oxidant for the rapid degradation of CBZ while HOCl is the dominant oxidant for the oxidation of SMX in electrolyte only containing Cl^-. By contrast, the surface adsorbed oxidants ($^{\bullet}OH$ or IrO_3-Cl) are the dominant oxidants for the degradation of CP and IBP. Additionally, urea, creatinine and uric acid significantly quench dissolved RCS in the solution phase. This results in a mass-transfer limit of pharmaceutical degradation. Citrate ions and $H_2PO_4^-$ possibly quench IrO_3-Cl resulting in a mixed kinetic and mass-transfer controlled degradation of pharmaceuticals with IrO_2. However, $H_2PO_4^-$ and SO_4^{2-}ions do not alter the electrolysis rates of pharmaceuticals that

are primarily degraded by •OH. The degradation of pharmaceuticals in full synthetic fresh urine matrixes (FUM) occurs at mixed kinetic and mass-transfer control with IrO_2 but occurs at mass-transfer controlled rates with BDD (for our experimental setup). Increasing the mass-transfer rate is particularly important for both types of anodes for faster pharmaceutical degradation in FUM. The true kinetic rate constants for pharmaceutical oxidation are higher with BDD than with IrO_2. However, for industrial EAOPs in a flow reactor (*Re* < 3000), the oxidation of organic contaminants with IrO_2 could occur at mass-transfer controlled rates in the absence of dissolved oxidants. Furthermore, BDD is prohibitively expensive and IrO2 contains rare earth elements. Therefore, the development of economic, stable and environmentally friendly anodes is desirable. Furthermore, future work aimed at designing devices that allows fast mass transfer with minimum byproduct formation could provide significant contribution to mitigating the release organic contaminants into the environment.

4.10 SUPPLEMENTARY INFORMATION

Table 4.5 Pseudo-first-order Rate Constants of Pharmaceutical Removal during Electrolysis on BDD used for the electrolytes in Figure 4.2a.

	Cl^- + AA (min^{-1})	ClO_4^- (min^{-1})	Cl^- (min^{-1})	ClO_4^- + t-BuOH (min^{-1})	Cl^- + t-BuOH (min^{-1})
CP	9.00×10^{-4}	3.47×10^{-2}	3.26×10^{-2}	2.64×10^{-2}	2.60×10^{-2}
CBZ	2.14×10^{-3}	5.51×10^{-2}	0.31	2.67×10^{-2}	2.84×10^{-2}
SMX	1.52×10^{-2}	6.19×10^{-2}	0.90	2.68×10^{-2}	2.63×10^{-2}
IBP	6.30×10^{-3}	3.21×10^{-2}	3.38×10^{-2}	2.69×10^{-2}	2.70×10^{-2}

Table 4.6 Pseudo-first-order Rate Constants of Pharmaceutical Removal during Electrolysis on Ti/IrO_2 used for the electrolytes in Figure 4.2b.

	Cl^- + AA (min^{-1})	ClO_4^- (min^{-1})	Cl^- (min^{-1})	ClO_4^- + t-BuOH	Cl^- + t-BuOH (min^{-1})

				(min^{-1})	
CP	2.40×10^{-4}	5.98×10^{-3}	2.75×10^{-2}	5.74×10^{-3}	2.64×10^{-2}
CBZ	1.61×10^{-3}	7.78×10^{-3}	0.33	1.09×10^{-2}	0.33
SMX	9.76×10^{-3}	9.72×10^{-3}	0.91	0.010	0.87
IBP	5.00×10^{-4}	5.66×10^{-3}	2.90×10^{-2}	4.88×10^{-3}	2.69×10^{-2}

Table 4.7 Pseudo-first-order Rate Constants of Pharmaceutical Removal during Electrolysis on BDD used for the electrolytes in Figure 4.3a and Figure 4.3c.

	Urea + Cl^- (min^{-1})	Urea + Cl^- + Creatinine (min^{-1})	Urea + Cl^- + Uric Acid (min^{-1})	Urea + Cl^- + SO_4^{2-} (min^{-1})	Urea + Cl^- + $H_2PO_4^-$ (min^{-1})	Urea + Cl^- + Citrate (min^{-1})
CP	0.033	0.036	0.029	0.033	0.033	0.027
CBZ	0.038	0.030	0.030	0.034	0.034	0.026
SMX	0.046	0.039	0.035	0.037	0.039	0.034
IBP	0.036	0.040	0.029	0.035	0.033	0.024

Table 4.8 Pseudo-first-order Rate Constants of Pharmaceutical Removal during Electrolysis on IrO_2 used for the electrolytes in Figure 4.3b and Figure 4.3d.

	Urea + Cl^- (min^{-1})	Urea + Cl^- + Creatinine (min^{-1})	Urea + Cl^- + Uric Acid (min^{-1})	Urea + Cl^- + SO_4^{2-} (min^{-1})	Urea + Cl^- + $H_2PO_4^-$ (min^{-1})	Urea + Cl^- + Citrate (min^{-1})
CP	0.027	0.027	0.025	0.029	0.018	0.015
CBZ	0.033	0.026	0.026	0.032	0.019	0.016
SMX	0.043	0.040	0.031	0.035	0.032	0.027
IBP	0.027	0.027	0.024	0.028	0.018	0.013

Table 4.9 Pseudo-first-order Rate Constants of Pharmaceutical Removal during Electrolysis with BDD used for the electrolytes in Figure 4.5a, c.

	Re =2977 10 mA/cm^2 100 mM Cl^- (min^{-1})	*Re* =11050 10 mA/cm^2 100 mM Cl^- (min^{-1})	*Re* =2977 100 mA/cm^2 100 mM Cl^- (min^{-1})	*Re* =2977 10 mA/cm^2 500 mM Cl^- (min^{-1})
CP	0.028	0.053	0.040	0.029
CBZ	0.027	0.051	0.042	0.026
SMX	0.029	0.055	0.076	0.032
IBP	0.027	0.051	0.047	0.025

Table 4.10 Pseudo-first-order Rate Constants of Pharmaceutical Removal during Electrolysis with IrO_2 used for the electrolytes in Figure 4.5b, d.

	Re =2977 10 mA/cm^2 100 mM Cl^- (min^{-1})	*Re* =11050 10 mA/cm^2 100 mM Cl^- (min^{-1})	*Re* =2977 100 mA/cm^2 100 mM Cl^- (min^{-1})	*Re* =2977 10 mA/cm^2 500 mM Cl^- (min^{-1})
CP	0.018	0.031	0.040	0.017
CBZ	0.020	0.032	0.048	0.018
SMX	0.027	0.036	0.083	0.026
IBP	0.019	0.033	0.037	0.017

Chapter 5. ENHANCING RATES OF PHARMACEUTICAL DEGRADATION AND SUPPRESSION OF CHLORINATED BYPRODUCTS FORMATION BY ALTERNATING SCHEME OF OXIDATION AND REDUCTION DURING ELECTROLYSIS OF FRESH HUMAN URINE

In this chapter, we examine two alternating schemes of oxidation and reduction: (1) using two WEs from a bipotentiostat and forced convection to move fluid from an anodic WE to a cathodic WE and (2) using alternating current electrolysis to change the polarity of electrode, alternating the same surface between WE and CE. Both alternating schemes use an interdigitated working electrode (IWE) where Ti/IrO_2 is used for both sides of the IWE as a proof of principle (Figure 5.1). The first alternating scheme using convection incorporates: (i) mass transport of the pharmaceuticals from bulk solution to the anode surface for their oxidation and (ii) mass transport of the electro-generated CBPs from anode to cathode under magnetic stirring. We show that the oxidation of pharmaceuticals is accelerated in various urine matrixes with the application of this alternating scheme. Moreover, the formation of inorganic CBPs (i.e., ClO_3^-) and organic CBPs (i.e., MCAA, DCAA, TCAA and $CHCl_3$) is significantly decreased with a cathodic

potential of -2V (*vs.* Ag/AgCl) applied in the alternating scheme during electrolysis of different urine matrixes. Furthermore, increasing the mass-transfer rates (*Re*) further suppresses the formation of organic and inorganic CBPs. The second alternating scheme using AC electrolysis shows adverse effect on the degradation rates of pharmaceuticals due to the instant reduction of surface-adsorbed oxidants. This work provides a proof-of-concept for a simple alternating scheme of point-source remediation of pharmaceuticals in fresh human urine for the acceleration of pharmaceutical degradation and suppression of oxidation byproducts formation.

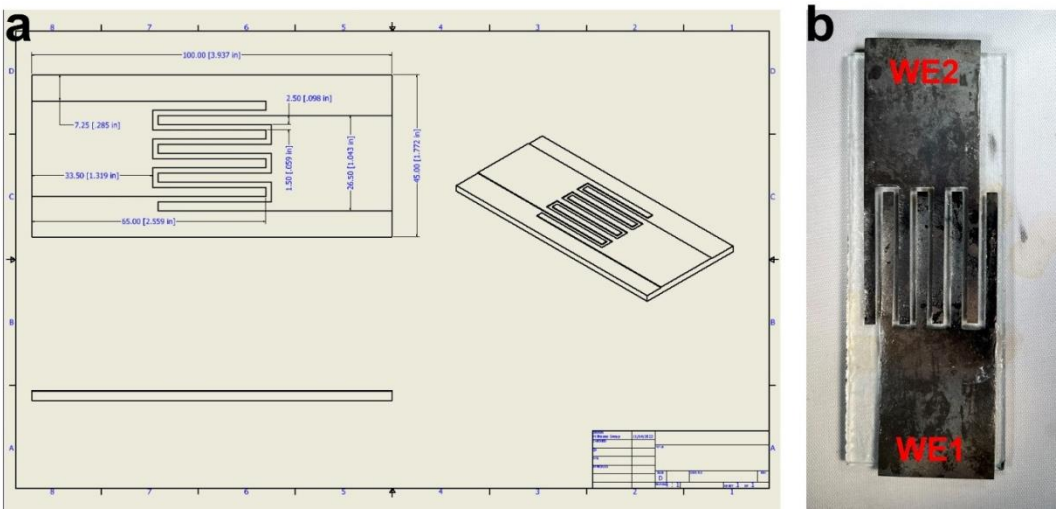

Figure 5.1 **(a) Schematics for the dimensions of the Ti/IrO_2 interdigitated working electrodes (IWEs) attached on a 40 x 100 mm clean soda-lime glass substrate. (b) Photograph of the Ti/IrO_2 IWEs fabricated.**

5.1 ABSTRACT

We propose an in-situ alternating scheme of oxidation and reduction for the electrochemical oxidation of pharmaceuticals in fresh urine. The alternating scheme is examined for simultaneous oxidation of pharmaceuticals and reduction of electro-generated CBPs. The two working electrodes (both Ti/IrO_2) are fabricated in an interdigitated planar geometry. These interdigitated working electrodes (IWEs) are used in two ways to create situations where a region

of solution is oxidized then quickly reduced by using: (1) a convention method where a bipotentiostat applies a constant anodic potential to one side of the IWE and a cathodic potential to the other side of the IWE while a stir bar directly on top of the planar IWEs moves fluid across the IWE (with separate counter and reference electrodes in the cell) and (2) an alternating current method where at any given time one side of the IWE is the working electrode and the other side is the counter electrode but over time the WE and CE are alternated by the potentiostat at a rate of up to 100 Hz. In this work, we also introduce a metric, i.e., normalized yield of chlorinated byproducts (CBPs), to evaluate the generation of CBPs per percentage of pharmaceutical degraded. We show that the degradation of pharmaceuticals is accelerated with the convection method (1) for both synthetic fresh urine matrixes (FUM) and synthetic hydrolyzed aged urine matrixes (HUM). Furthermore, the formation of ClO_3^-, $CHCl_3$ and chlorinated acetic acids (CAAs) are increasingly suppressed with increasing cathodic potentials or mass-transfer rates. The electrolysis rates of pharmaceuticals in HUM are substantially lower than that in FUM. It results in a greater normalized yield of CBPs in HUM. Therefore, it is advantageous to treat fresh urine rather than hydrolyzed aged urine. When using the alternative method (2), the electrolysis rates of pharmaceutical and the CBPs formation are dramatically decreased with increasing alternating frequency. This decrease is due to the rapid electrochemical reduction of chemisorbed oxidants during the cathodic potential that precedes the anodic potential on the same electrode surface. It leads to a low level of normalized yield of CBPs at even low *Re*. In addition, the total energy (~ 180 J) wasted on the charge/discharge of double layer capacitance between each alternating cycle is unwanted. Importantly, this proof-of-principle shows that a flow cell using IWEs under high mass transfer conditions can be used for point-source-remediation of

pharmaceuticals in fresh human urine less formation of CBPs when compared with conventional single WE setups.

5.2 INTRODUCTION

Electrochemical advanced oxidation processes (EAOPs) in human urine shows promise for providing wastewater treatment for the mitigation of pharmaceutical occurrences in the aquatic environment. Despite several studies show the feasibility of the EAOPs in both fresh and hydrolyzed aged urine matrixes,[39,60,67,75,203] the biggest hurdle for the successful application is the oxidation byproducts (OBPs) formation during the electrolysis of urine. These OBPs formed during EAOPs includes chlorate (ClO_3^-), perchlorate (ClO_4^-), haloaceitc acids (HAAs), trihalomethanes (THMs) etc.[50] Owing to their potential health effects and widespread occurrences in chlorinated water, HAAs in conjunction with THMs, ClO_3^-, ClO_4^- and bromate, are regulated under the promulgated United States Environmental Protection Agency (US EPA) Disinfectants and Disinfection Byproducts rule.[204,205]

In Chapter 3, we have shown that employing the electrolysis of pharmaceuticals in fresh human urine is more advantageous than in hydrolyzed aged urine matrixes (due to the volatilization of NH_3).[67] It is because the HCO_3^- in synthetic hydrolyzed aged urine matrixes (HUM) quenches the electro-generated $^{\bullet}OH$ and/or $Cl^{\bullet}$ with the formation of $HCO_3^{\bullet}$ (less reactive with respect to pharmaceutical). It results in a lower oxidation rates of pharmaceuticals in HUM as compared to that in synthetic fresh human urine matrixes (FUM).[67] Additionally, the generation of ClO_3^- and ClO_4^- is suppressed in FUM due to the presence of high urea content which quenches the $Cl^{\bullet}$ preventing the formation of ClO_3^- and ClO_4^-.[67] Although the generation

of ClO_3^- and ClO_4^- is suppressed during electrolysis of FUM, the further development is needed to minimize the formation of ClO_3^- and ClO_4^-.

In addition to the inorganic CBPs, the remediation of the organic CBPs has been investigated previously. Reductive dehalogenation has been considered as an attractive option to remove HAAs in water. However, it often requires an addition of reducing agents, such as zerovalent iron,[206] hydrogen,[207] and sodium sulfite[208]. Therefore, the electrochemically advanced reductive processes (EARPs) in the remediation of organic CBPs has received growing attention.[209,210] Electrochemical reduction could effectively dechlorinate the organic CBPs without producing toxic byproducts.[211-213] For instance, Mao, et. al. has reported an efficient electrochemical dechlorination of TCAA using a graphene-Cu foam electrode. The dechlorination is via direct cathodic reduction and reduction by adsorbed atomic hydrogen (H-rad) generated on the cathode.[209] Furthermore, EARPs can be easily employed as a continuous treatment in the continued stirred reactor in parallel with EAOPs without the addition of other chemical agents. However, the similar generation of HAAs and THMs has been reported in undivided and membrane-divided cell configurations.[214] It suggests the reductive dechlorination on the cathode is negligible in a traditional undivided electrolytic cells. It is because the generation rates of organic CBPs are substantially higher than the rates of reductive dechlorination. The slow reduction of organic CBPs can be ascribed to (1) the sluggish kinetics of reduction on the cathode and/or (2) the slow mass transport of organic CBPs to the cathode surface. Therefore, the cathode materials, cathodic potentials and the mass transfer conditions play important roles in the EARPs of organic CBPs.

5.3 THE REACTIONS DURING ELECTROLYSIS OF FRESH HUMAN URINE IN THE PRESENCE OF ALTERNATING SCHEME OF OXIDATION AND REDUCTION

The alternating scheme of oxidation and reduction is achieved by using a convention method where a bipotentiostat applies a constant anodic potential on the anode and a constant cathodic potential on the cathode while a stir bar directly on top of the planar IWEs (Figure 5.2a, b) moves fluid across the IWEs. Importantly, the convection of the products generated on the anode to the cathode is expected to suppress the formation of CBPs. Specifically, the electrochemically generated chemisorbed oxygen (Figure 5.2c, r_1) and chemisorbed chlorine (Figure 5.2c, r_6) on IrO_2 could oxidize the pharmaceuticals (e.g., CP) (Figure 5.2c, r_2 & r_3). Furthermore, $HOCl/OCl^-$ can be formed via the reaction of H_2O and Cl_2 (Figure 5.2c, r_8). In analogous to the formation of ClO_3^- on BDD electrode,[126] the $ClO_3^-$is hypothesized to be generated via the sequential oxidation of OCl^- by chemisorbed oxygen on IrO_2 (Figure 5.2c, r_9 & r_{10}). For the oxidation of organic constituents of urine, urea reacts with $HOCl/OCl^-$ (Figure 5.2c, r_{15}) and chemisorbed chlorine (not shown in Scheme 1c) to generate N-chlorourea, resulting in an ultimate generation of chloramines.[38] The reactions of citrate, creatinine and uric acid with $HOCl/OCl^-$ (Figure 5.2c, r_{13}) and/or chemisorbed chlorine (Figure 5.2c, r_{11}) are speculated to result in the formation of unknown intermediates which may further be oxidized by active chlorine to generate CBPs (Figure 5.2c, r_{14} & r_{12}).[215] On the cathode surface, the reduction of H_2O generates adsorbed hydrogen (Figure 5.2c, r_{29}) and H_2 (Figure 5.2c, r_{28}). The convection of CBPs from anode to cathode enables the reduction of CBPs via direct electron transfer and/or reactions with adsorbed hydrogen (Figure 5.2c, $r_{16\text{-}22}$). In addition, the electrochemically generated dissolved O_2 and $HOCl/OCl^-$ (on the anode) can be reduced to chemisorbed oxygen (Figure 5.2c, r_{26}) and chemisorbed chlorine **(**Figure 5.2c, r_{21}) on the cathode, respectively. The formation of

chemisorbed oxygen and chemisorbed chlorine on the cathode could further contribute to the oxidation of pharmaceuticals (Figure 5.2c, r_{23} & r_{25}).

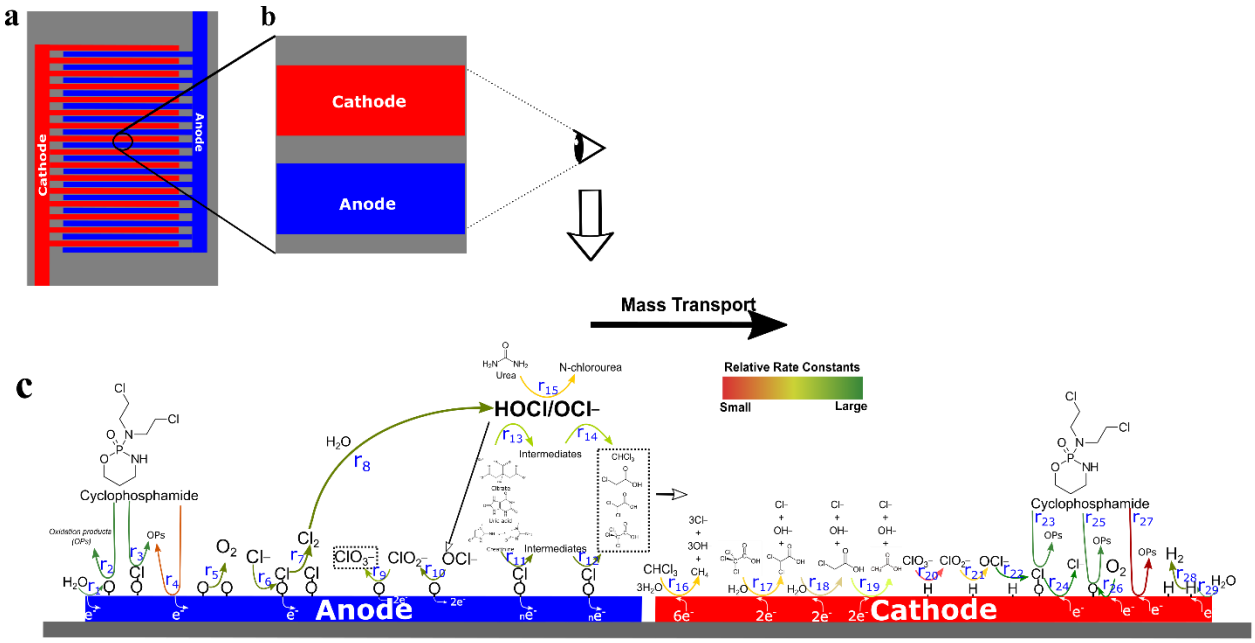

Figure 5.2 **(a) Schematic view of planar IWEs using Ti/IrO_2; (b) the detailed schematic view of one pair of the anode and cathode in IWEs, (c) side view of (b) as well as the relative rate constants for reactions that have been reported or speculated during the electrolysis of pharmaceuticals in urine matrixes (with CP as an example pharmaceutical)**. The compounds in the dash rectangles are the CBPs generated during the oxidation of human urine.

5.4 THE EFFECT OF CATHODE POTENTIALS AND MASS TRANSPORT CONDITIONS ON THE APPLICATION OF ALTERNATING SCHEME IN SYNTHETIC FRESH URINE MATRIXES (FUM)

To examine the alternating scheme as a proof-of-concept of the oxidation of pharmaceuticals while minimizing the generation of CBPs, the effect of cathode potential and mass transport were studied. It is critical to lower the formation of CBPs without significantly compromising the rates of pharmaceutical oxidation. Therefore, the rates of pharmaceutical degradation and the

generation of inorganic and organic CBPs were measured. Most research examining electrolysis of pharmaceuticals has reported rates of pharmaceutical degradation in terms of observed pseudo-first-order rate constants (k_{obs}).[39,63,130,131] In analogous to our previous work,[67,78] we also report the corresponding reactor-geometry-normalized k_{obs} accounting for the electrode-surface-area-to-electrolyte-volume ratio (A/V) of the electrochemical cell (normalized $k_{obs} = k_{obs}/(A/V)$).

5.4.1 *Rates of Pharmaceutical Degradation in FUM due to Various Cathode Potentials*

The control experiment (i.e., without alternating scheme) was the electrolysis of pharmaceuticals in FUM with an anodic potential of 2.5 V (*vs.* Ag/AgCl) applied to working electrode 1 (WE1, Figure 5.2b) and open circuit at working electrode 2 (WE2, Figure 5.2b) at stirring rates of 600 (*Re* = 2977) or 1000 rpm (*Re* = 11050). As shown in Figure 5.3a, the electrolysis rates of all pharmaceuticals in the control experiments were consistent with previous study.[78] Furthermore, the k_{obs} was roughly doubled with the potential of 2.5 V applied to both WE1 and WE2 as compared to the electrolysis with open circuit at WE2 (Figure 5.3a, dark grey *vs.* red columns). It is owing to the double surface area of working electrodes. However, it is noteworthy that the normalized k_{obs} is not shown properly for the electrolysis experiments with the potential of 2.5V applied to both WE1 and WE2 (Figure 5.3a, dark gray column). It is because the universal conversion of k_{obs} to normalized k_{obs} in this work only accounts for the surface area of WE1.

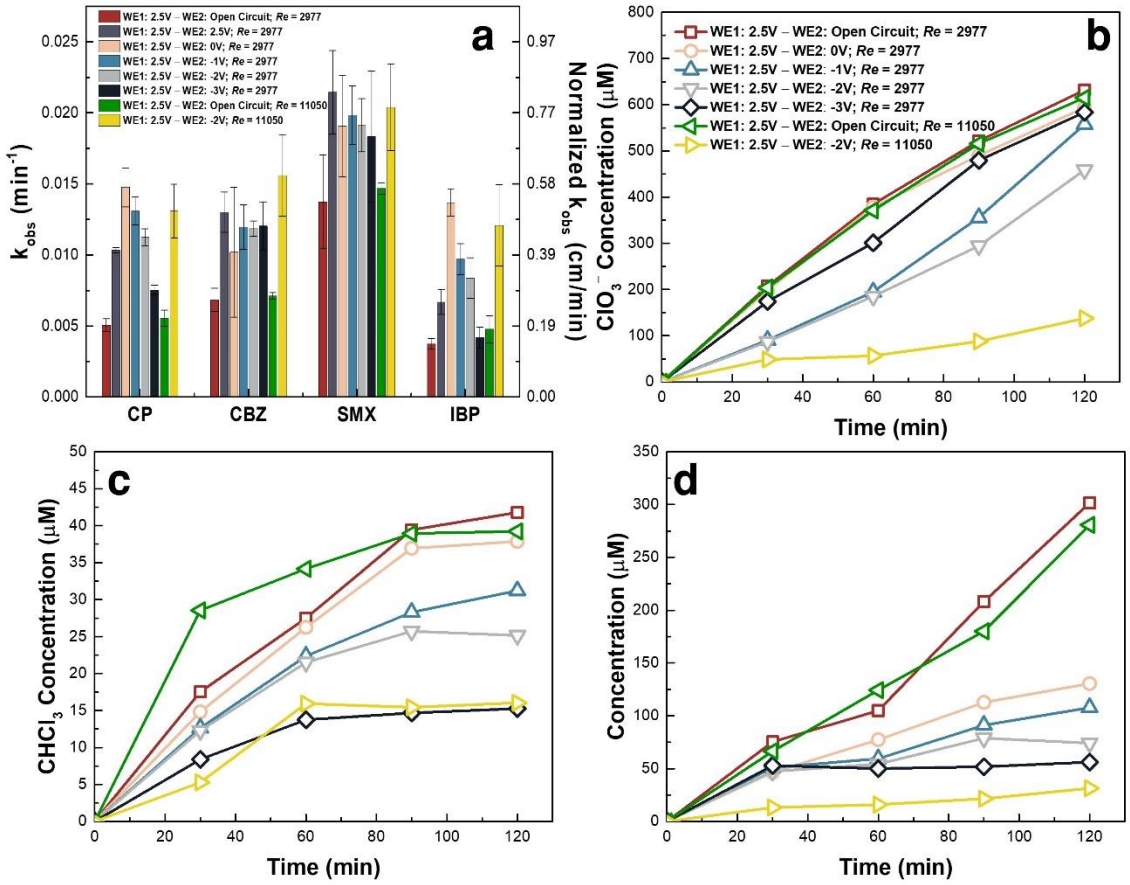

Figure 5.3 **(a) The observed pseudo-first order rate constants (k_{obs}) and normalized k_{obs} of the pharmaceutical degradation** obtained with the potential of 2.5 V (*vs.* Ag/AgCl) applied to working electrode 1 (WE1) and (1) open circuit, (2) 2.5 V, (3) 0 V, (4) -1 V, (5) -2 V, and (6) -3 V (*vs.* Ag/AgCl) applied to working electrode 2 (WE2). **The generation of (a) ClO_3^-, (b) $CHCl_3$, and (c) total chlorine in the chlorinated acetic acid** (− total count of chlorine in MCAA, DCAA, and TCAA) in full synthetic fresh urine matrixes (FUM) at stir rates of 600 (*Re* = 2977) or 1000 rpm (*Re* = 11050).

The electrolysis rates of all pharmaceuticals were enhanced when cathodic potentials were applied to WE2 as compared to that with open circuit at WE2 at *Re* = 2977 (Figure 5.3a; peach orange/blue/light grey/black column *vs.* red column). We hypothesize that the dissolved oxidants (e.g., O_2 and free chlorine) generated on the anode surface are transported to the cathode by

stirring and reduced to chemisorbed oxygen or chlorine (i.e., IrO_{2+1} or IrO_3-Cl) (Figure 5.1c, $r_{23\text{-}26}$). These chemisorbed oxidants (on the cathode) further contribute to the oxidation of pharmaceuticals. The standard reduction potentials of O_2 and free chlorine to chemisorbed oxidants have not yet been reported. However, the formal potentials of similar reduction reactions can be calculated as a reference for the rationale of the above hypothesis. The thickness of the stagnant layer (i.e., 28.7 μm) and local pH at the anode surface (i.e., 0.74) at *Re* = 2977 have been reported in our previous work.[78] The local pH at the cathode surface is calculated to be 13.25 due to the hydrogen evolution (Chapter 2.5.2). Therefore, OCl^- is the major species of free chlorine near the cathode surface (Figure 5.4a). As a reference, the formal potentials of the reduction of O_2 to OH^- and OCl^- to Cl^- are determined based on the local pH at cathode surface: $O_2(g) + 2H_2O + 4\ e^- \rightarrow 4OH^-$ ($E^{0'}$ = 0.24 V *vs.* Ag/AgCl); $ClO^- + H_2O + 2e^- \rightarrow Cl^- + 2OH^-$ ($E^{0'}$ = 0.67 V *vs.* Ag/AgCl).[71] Hence, it is thermodynamically feasible to reduce O_2 and OCl^- to chemisorbed oxygen and chlorine even with 0 V (*vs.* Ag/AgCl) applied to the WE2. Importantly, the reduction of dissolved O_2 and OCl^- was observed in the cyclic voltammograms of O_2 saturated 100 mM $NaClO_4$ and 10 mM NaOCl in N_2 saturated 100 mM $NaClO_4$ (Figure 5.4b). Further evidence of the reduction of dissolved oxidants on the cathode is the observation of the suppressed formation of FC in 100mM NaCl solution with the application of alternating scheme in which a cathodic potential of -2V is used (Figure 5.4c).

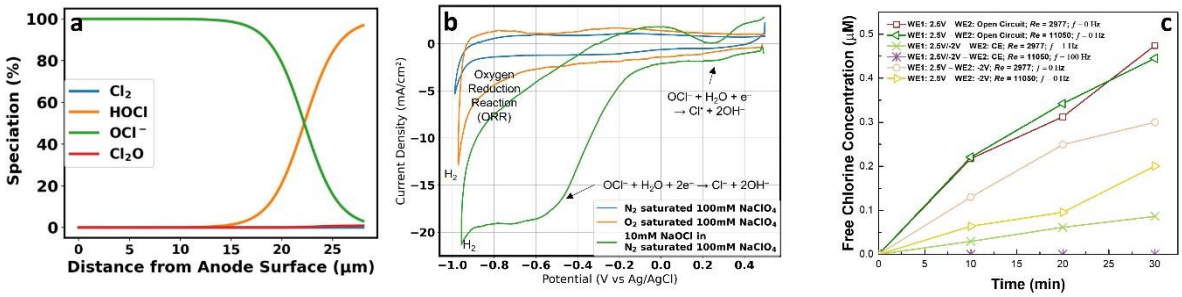

Figure 5.4 **(a) Free chlorine speciation as a function of the distance away from the cathode.** The simulated speciation was calculated based on acid dissociation constant of HOCl ($K_{a,\ HOCl}$ = $10^{-7.5}$ mol/L), equilibrium constants of Cl_2 and Cl_2O with HOCl ($K_{H,\ Cl2}$ = 4.35 × 10^{-4} $(mol/L)^2$; $K_{H,\ Cl2O}$ = 8.74 × 10^{-3} $(mol/L)^{-1}$), concentration of Cl^- ([Cl^-] = 100 mM), and pH. **(b) Cyclic voltammograms (CVs)** in (1) N_2 saturated 100 mM $NaClO_4$, (2) O_2 saturated 100 mM $NaClO_4$, and (3) 10 mM NaOCl in N_2 saturated 100 mM $NaClO_4$; **(c) Free chlorine (FC) production on Ti/IrO_2 IWEs** in a 100 mM chloride electrolyte (1) without the alternating scheme at the stirring rate of 600 rpm (□) and 1000 rpm (◁), (2) with the application of alternating scheme at the stirring rate of 600 rpm (▽) and 1000 rpm (▷), and (3) AC electrolysis with alternating frequencies of 1 Hz (×) and 100 Hz (∗) at the stirring rate of 600 rpm.

Increasing the cathode potentials (more negative potential) applied to WE2 resulted in a gradual decrease in the rates of CP and IBP degradation (Figure 5.3a). It is likely due to that the reduction of H^+ to H_2 competes with the presumable reduction of O_2 and OCl^- on the cathode, and thus results in lower rates of CP and IBP degradation. The hypothesis is supported by that (1) CP and IBP are degraded dominantly via IrO_3-Cl in electrolyte only containing Cl^-;[78] (2) the reduction of OCl^- to IrO_3-Cl could need the participation of H^+ or atomic hydrogen; and (3) increasing the cathodic potential leads to more intensive reduction of H^+ to H_2 on the cathode. By contrast, the degradation rates of CBZ and SMX remained similar with various cathodic potentials applied to WE2 at *Re* = 2977 (Figure 5.3a). It is possibly because the direct cathodic reduction of CBZ[216] and SMX[217] compensates for the presumable less generation of chemisorbed

oxidants on the cathode when the cathode potentials increase. It is supported by the observation of direct cathodic reduction peaks in the cyclic voltammograms of CBZ or SMX in 100 mM $NaClO_4$ electrolyte (Figure 5.5b, c). Taken all together, the degradation of pharmaceuticals is accelerated with the application of alternating scheme under the same mass transfer conditions.

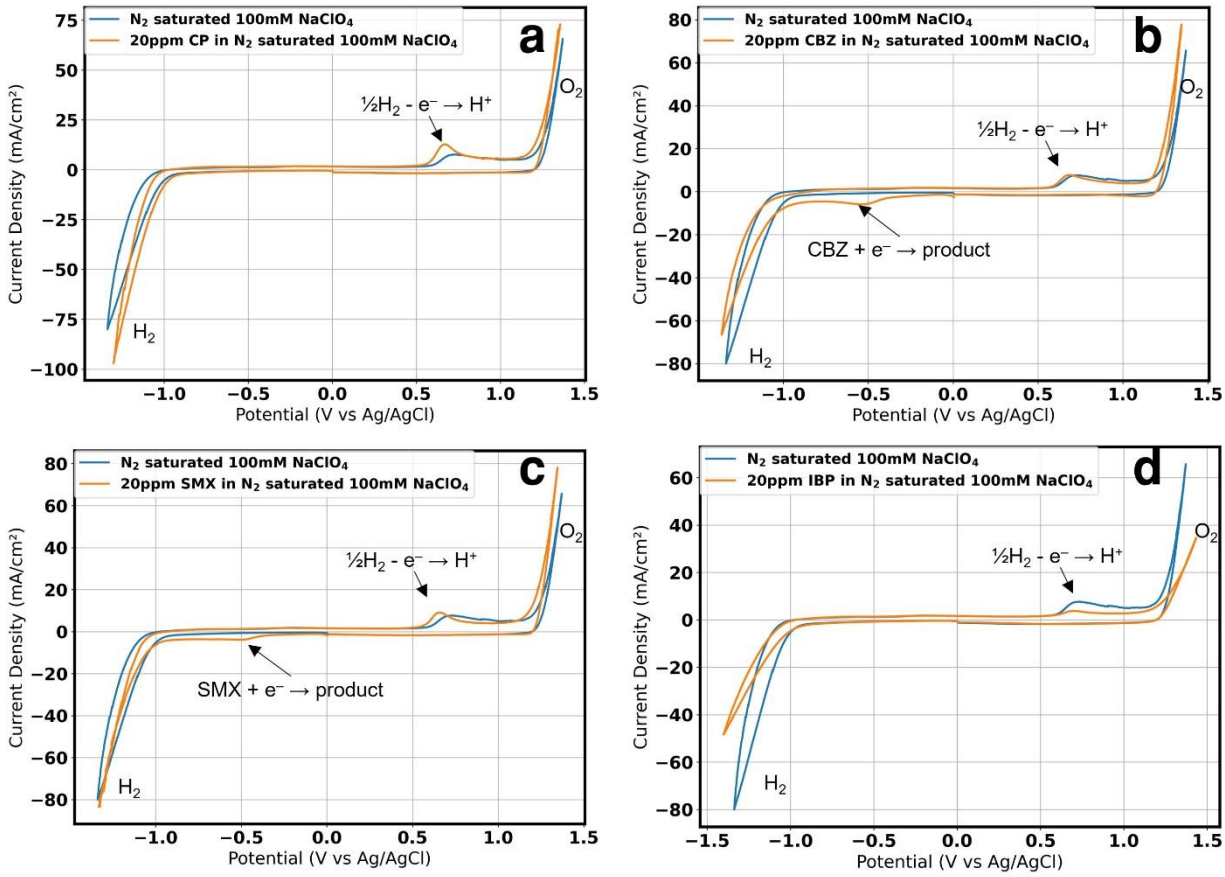

Figure 5.5 **Cyclic voltammograms (CVs) of the N_2 saturated 100 mM $NaClO_4$ with the addition of 20 ppm of (a) CP, (b) CBZ, (c) SMX, and (d) IBP.** The scan started from 0 V to -1.5 V and then swept to 1.5 V and finally returned to 0 V at a scan rate of 100 mV/s. The direct cathodic reduction peaks were observed in CVs of 20 ppm CBZ and SMX in 100 mM $NaClO_4$ electrolyte, consistent with our hypothesis that the direct cathodic reduction could contribute to the degradation of CBZ and SMX with the application of alternating scheme.

5.4.2 *Rates of Pharmaceutical Degradation in FUM due to Mass Transfer Rates*

Consistent with previous literature,[78] increasing the mass transfer rates resulted in higher oxidation rates of pharmaceuticals in the absence of alternating scheme (Figure 5.3a, green *vs.* red columns). The degradation rates of pharmaceuticals were increased with the application of alternating scheme as compared to the electrolysis without the alternating scheme at *Re* = 11050 (Figure 5.3a, yellow *vs.* green column). It is consistent with the degradation rates comparison between the electrolysis with and without the alternating scheme at *Re* = 2977. Furthermore, the electrolysis rates were increased at higher *Re* when the identical cathodic potential was applied (Figure 5.3a, yellow *vs.* light grey column). It is due to the (1) enhanced mass transport of pharmaceuticals towards the electrodes[78] and (2) enhanced mass transport of O_2 and OCl^- from anode to cathode resulting in more chemisorbed oxidants generation, which is supported by the observation of further suppression of FC formation with increasing the mass transfer rates (Figure 5.4c)

5.4.3 *Generation of Chlorinated Byproducts*

The generation of chlorinated byproducts (CBPs) including ClO_3^-, chloroform ($CHCl_3$), monochloroacetic acid (MCAA), dichloroacetic acid (DCAA), and trichloroacetic acid (TCAA) were measured and compared for each combination of cathodic potentials and mass transfer rates as shown in Figure 5.3b, c & d. In this work, we use the total count of chlorine atoms that are associated with chlorinated chloroacetic acid (CAA) ($[Cl_{CAA}]_{total}$ = 1 × [MCAA] + 2 × [DCAA] + 3 × [TCAA]) as an indicator of the chlorination level of CAAs. The interpretation of the generation of CAAs is very challenging in the presence of alternating scheme due to the lack of fundamental understanding of (1) the underlying chemistry of the CAAs formation and (2) the

mechanisms that suppress CAAs formation. However, it has been reported that CAAs can be reduced via reductive dechlorination step by step: TCAA + H_2O + $2e^-$ → DCAA + Cl^- + OH^-; DCAA + H_2O + $2e^-$ → MCAA + Cl^- + OH^-; MCAA + H_2O + $2e^-$ → acetic acid + Cl^- + OH^- .[209,218] Taken all together, the $[Cl_{CAA}]_{total}$ is used as a metric to determine the effectiveness of the reductive dechlorination with the application of alternating scheme. Nonetheless, the generation of MCAA, DCAA and TCAA during the electrolysis in each single experiment are shown in Figure 5.9 as a reference.

As shown in Figure 5.3b & d (red *vs.* green lines), the generation of ClO_3^- and Cl_{HAA} was similar *in the absence* of alternating scheme at *Re* = 2977 and *Re* = 11050. It suggests that their formation is dominantly kinetically controlled. By contrast, the generation of $CHCl_3$ is initially fast and then slows down for the electrolysis at *Re* = 11050 as compared to that at *Re* = 2977 (Figure 5.3c**;** red *vs.* green lines). It results in a slightly lower concentration of $CHCl_3$ after 2hr electrolysis. That is likely due to the volatilization of $CHCl_3$ under vigorous stirring conditions.[66] As shown in Figure 5.3c & d, the formation of $CHCl_3$, and Cl_{HAA} was increasingly suppressed with the increasing cathode potentials *in the presence* of alternating scheme. Therefore, the reduction of $CHCl_3$ and CAAs and/or the intermediates of their formation is a kinetically controlled reaction. Due to the lack of information of the formation pathways, the reduction reactions on the cathode (WE2) that lead to the suppression of $CHCl_3$ and CAAs formation are unknown. The generation of ClO_3^- was decreased by increasing cathode potentials from open circuit to -2V (Figure 5.3b). However, further increase of the cathode potential to -3V resulted in a less suppression of ClO_3^- formation (Figure 5.3b, black *vs.* grey lines). We hypothesize that the reduction of the ClO_3^- and/or the intermediate oxidants (i.e., HOCl/OCl^- or ClO_2^-) (Figure 5.1c, $r_{20\text{-}22}$) competes with H_2 evolution on the cathode resulting in a less suppression of ClO_3^-

formation at the potential of -3V. The hypothesis is supported by the facts that (1) generation of oxychloride is via the sequential chloride oxidation to HOCl/OCl^- and then to ClO_2^-, ClO_3^- during electrolysis;[126,144] and (2) the reduction of HOCl/OCl^-, ClO_2^- and ClO_3^- needs the participation of H^+.[71]

The generation of CBPs was also measured for the electrolysis with alternating scheme at *Re* = 11050. After 2hr electrolysis, the concentrations of ClO_3^-, $CHCl_3$, and Cl_{CAA} were 137 μM, 16 μM, and 31 μM, respectively (Figure 5.3b, c & d; yellow line). Increasing the mass transfer rates results in a further suppression of CBPs formation *in the presence* of alternating scheme (Figure 5.3b, c & d; yellow *vs.* light grey lines). It is likely due to that the faster mass transport of CBPs and/or the intermediates of CBP formation to the cathode surface results in enhanced rates of reduction. In this work, we introduce a new metric (i.e., normalized yield of CBPs) for the evaluation of the "side-effect" of EAOPs in various urine matrixes. The normalized yield of CBPs is defined as CBPs formation per percentage of pharmaceutical degradation: $Y_i = [i]_{t=2hr}/[100 \times (1 - [Pharm.]_{t=2hr}/[Pharm.]_{t=0})]$, where i represents the kind of CBPs. The SMX was chosen as the reference pharmaceutical due to (1) it has the highest degradation rates among all pharmaceuticals in any matrixes and experimental setups and (2) it is the most investigated pharmaceutical for EAOPs among previous literature. As shown in Table 5.1, the normalized yield of CBPs during electrolysis of FUM was substantially lower *in the presence* of the alternating scheme than that without the alternating scheme. Additionally, the least normalized yield of ClO_3^- at *Re* = 2977 (i.e., 5.10 μM) was achieved by the application of alternating scheme with the potential of -2V applied to WE2. ClO_3^- as an endocrine disruptor is one of the most concerned oxidation byproducts due to its high toxicity and large difficulty to remediate. Consequently, the potential of -2V was used for following experiments when alternating scheme

was applied. Furthermore, increasing the *Re* to 11050 with the application of alternating scheme substantially decreases the normalized yield of ClO_3^-, $CHCl_3$, and CAAs down to 1.51 µM, 0.17 µM, and 0.34 µM, respectively (Table 5.1).

Table 5.1 The normalized yield of CBPs after 2hr electrolysis in FUM with or without the alternating scheme.

	WE1: 2.5V – WE2: Open Circuit; *Re* = 2977	**WE1: 2.5V – WE2: 0V; *Re* = 2977**	**WE1: 2.5V – WE2: -1V; *Re* = 2977**	**WE1: 2.5V – WE2: -2V; *Re* = 2977**	**WE1: 2.5V – WE2: -3V; *Re* = 2977**	**WE1: 2.5V – WE2: Open Circuit; *Re* = 11050**	**WE1: 2.5V – WE2: -2V; *Re* = 11050**
Y_{ClO3-} (µM)	7.82	6.61	6.14	5.10	6.56	7.42	1.51
Y_{CHCl3} (µM)	0.51	0.42	0.34	0.28	0.17	0.50	0.17
Y_{CAAs} (µM)	3.73	1.45	1.19	0.82	0.63	3.39	0.34

5.5 THE EFFECT OF SYNTHETIC HYDROLYZED AGED URINE MATRIXES (HUM) FOR THE APPLICATION OF ALTERNATING SCHEME.

The rates of pharmaceutical degradation and CBPs generation during electrolysis in synthetic hydrolyzed aged urine matrixes (HUM) were investigated as a comparison with the FUM. This direct comparison can provide the evidence and guidance for the choice of electrolyte when employing the alternating scheme for the electrolysis of pharmaceuticals.

5.5.1 *Rates of Pharmaceutical Degradation in HUM*

The electrolysis rates of all pharmaceuticals were increased by increasing the mass transfer rates during electrolysis of HUM (**Figure 5a**; yellow *vs.* light blue columns). It is consistent with the equation derived in the previous report:[78] $k_{obs} = \frac{1}{\frac{1}{k'}+\frac{1}{k_m}}$, where k' is the true kinetic rate constant of pharmaceutical degradation, k_m is the mass-transfer-limiting rate. Moreover, the oxidation of pharmaceuticals was accelerated *in the presence* of alternating scheme as compared to the oxidation without the alternating scheme at *Re* = 2977 and *Re* = 11050, respectively

(Figure 5.6a, dark blue *vs.* light blue columns & orange *vs.* yellow columns). It is consistent with the observation of electrolysis in FUM. It is owing to the presumable formation of IrO_{2+1} and IrO_3-Cl on the cathode via the reduction of O_2 and OCl^- that are initially formed on the anode. Additionally, increasing the *Re* only results in the slight increase of the oxidation rates of pharmaceuticals with or whithout the application of alternating scheme (Figure 5.6a**,** yellow *vs.* light blue columns & orange *vs.* dark blue columns). It is due to the oxidation of pharmaceuticals is dominantly kinetically limited resulted from the chemisorbed oxidant scavenging effect by HCO_3^-.[67] The electrolysis rates of all pharmaceuticals in HUM are substantially lower than that in the FUM with or without an alternating scheme applied. It is consistent with the comparison between the pharmaceutical oxidation in FUM and HUM on the boron-doped diamond electrode.[67]

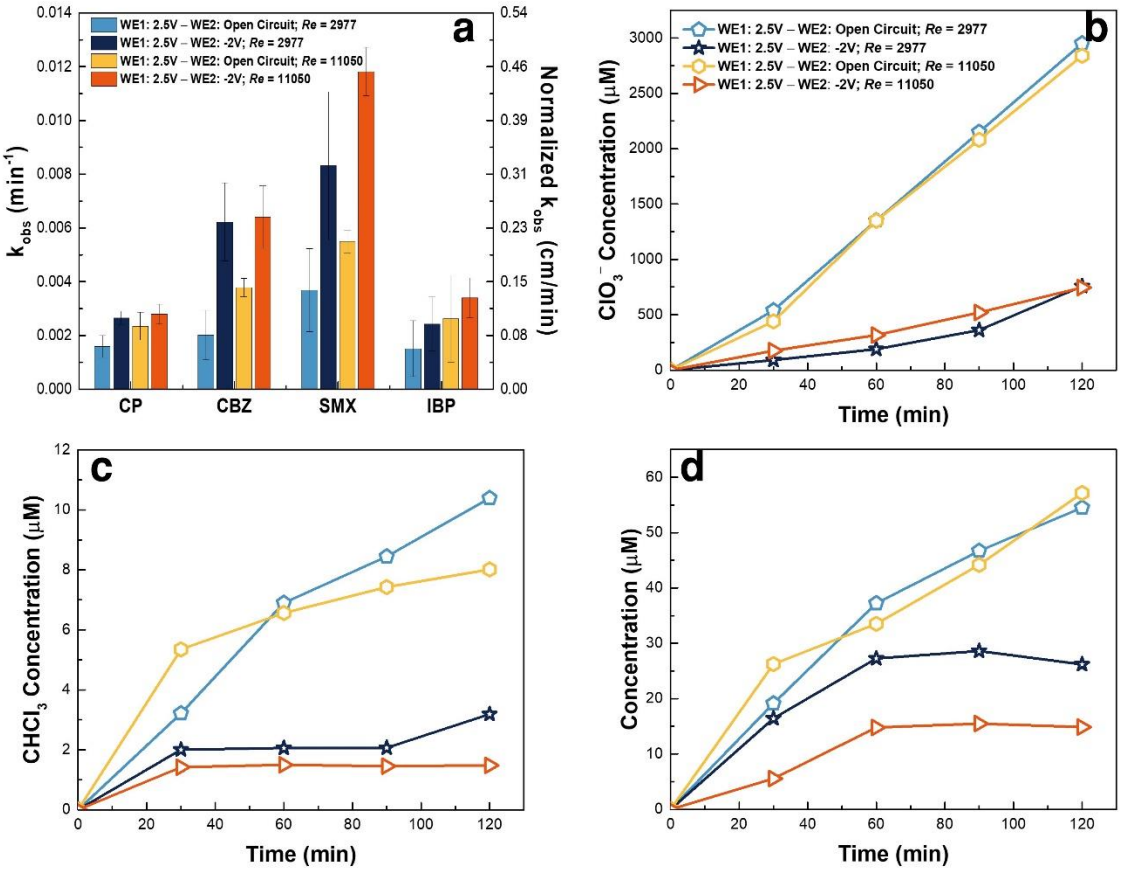

Figure 5.6 **(a) The observed pseudo-first order rate constants (k_{obs}) and normalized k_{obs} of the pharmaceutical degradation** obtained with the applied potential of 2.5 V (*vs.* Ag/AgCl) at working electrode 1 (WE1) and (1) open circuit, and (2) -2V (*vs.* Ag/AgCl) applied to working electrode 2 (WE2). **The generation of (b) ClO_3^-, (c) $CHCl_3$, and (d) total chlorine in the chlorinated acetic acid** (− total count of chlorine in MCAA, DCAA, and TCAA) in synthetic hydrolyzed aged urine matrixes (HUM) under stirring rates of 600 (*Re* = 2977) or 1000 rpm (*Re* = 11050).

5.5.2 *Generation of Chlorinated Byproducts:*

In analogous to the electrolysis in FUM, the generation of ClO_3^-, $CHCl_3$, and CAAs were measured during electrolysis in HUM (Figure 5.6b, c & d). The concentration of ClO_3^- is nearly 3000 μM after 2 hr electrolysis in HUM without alternating scheme applied at *Re* = 2977 and *Re*

= 11050 (Figure 5.6b, light blue & yellow lines). The generation of ClO_3^- in HUM is approximately an order of magnitude higher than that in FUM (Figure 5.3b; red & green lines). It is due to that the high nitrogen content in the FUM (250 mM urea as compared to only 33 mM NH_4^+ in HUM) scavenges $Cl^\bullet$ and/or $Cl_2^{\bullet-}$ at or near the anode interface that precede formation of $HOCl/OCl^-$ for further oxidation to ClO_3^-.[67] Furthermore, the generation of ClO_3^- shows no significant difference when increasing the stirring rate to 1000 rpm (*Re* = 11050) (Figure 5.6b; light blue *vs.* yellow lines). It suggests that the formation of ClO_3^- is dominantly controlled by the kinetics of the sequential oxidation of Cl^- to ClO_3^- on IrO_2. As expected, the generation of ClO_3^- was dramatically suppressed *in the presence* of alternating scheme at the *Re* of either 2977 and 11050 (Figure 5.6b; dark blue *vs.* light blue lines & orange *vs.* yellow lines). As discussed above, we hypothesize that the suppression of ClO_3^- formation is via the direct cathodic reduction of ClO_3^- and/or the reduction of FC that precedes the formation of ClO_3^- (Figure 5.2c, $r_{20\text{-}22}$). Furthermore, the generation of ClO_3^- is similar at *Re* = 2977 and *Re* = 11050 in the presence of the alternating scheme (Figure 5.6b; dark blue *vs.* orange lines). It is likely due to that the reduction of FC and/or ClO_2^- on the cathode is dominantly kinetically controlled so that increasing the mass transfer rates shows minimum effect on the suppression of ClO_3^- formation. Nonetheless, the measured concentration of ClO_3^- is 500 μM in HUM which is much greater than that in FUM after 2 hr electrolysis. Therefore, it is more advantageous to treat fresh urine rather than hydrolyzed aged urine for a faster pharmaceutical oxidation and less generation of ClO_3^- with or without the alternating scheme employed.

The generation of $CHCl_3$ is 11 μM after 2hr electrolysis in HUM in the absence of alternating scheme at *Re* = 2977 (Figure 5.6c, light blue line). It is substantially lower than the $CHCl_3$ formation in FUM under the same stirring rate. That is due to less total organic carbon

present in the HUM than in the FUM. The formation rate of $CHCl_3$ was initially higher at *Re* = 11050, but it then dramatically decreased as compared to that at *Re* = 2977 (Figure 5.6c; light blue *vs.* yellow lines). It is consistent with the observation of $CHCl_3$ formation during electrolysis in FUM with the same experimental setups. It is likely due to the volatilization of $CHCl_3$ under vigorous stirring condition.[66] The formation of $CHCl_3$ was suppressed when the alternating scheme is applied (Figure 5.6c). It is due to the presumable reduction of (1) $HOCl/OCl^-$, and/or (2) the intermediate of $CHCl_3$ formation,[215] and/or (3) $CHCl_3$ directly on the cathode. However, increasing the mass transfer rates did not significantly decrease the generation of $CHCl_3$ (Figure 2c; orange *vs.* dark blue lines). It suggests that the reduction of $CHCl_3$ and/or the intermediates for $CHCl_3$ formation is dominantly kinetically controlled.

By contrast, the measured total number of chlorine atoms associated with acetic acid ($[Cl_{CAA}]_{total}$) is roughly the same at *Re* = 2977 and *Re* = 11050 without the alternating scheme (Figure 5.6d, yellow *vs.* light blue lines). It is consistent with the observation of the electrolysis in FUM. It suggests that the formation of nonvolatile CAAs is dominantly kinetically controlled. Consistent with the observation in FUM, the application of the alternating scheme significantly decreased the $[Cl_{CAA}]_{total}$ at *Re* = 2977 and *Re* = 11050, respectively (Figure 5.6d, dark blue *vs.* light blue lines & orange *vs.* yellow lines). Additionally, increasing the mass transfer resulted in a further dechlorination of CAAs (Figure 5.6d, orange *vs.* dark blue lines). It indicates that the direct reduction of CAAs and/or the intermediates for the CAAs formation is a mixed kinetically and mass-transfer controlled reaction. As shown in Table 5.2, the normalized yield of CBPs during EAOPs in HUM was determined and evaluated as a comparison with FUM. Although the normalized yield of $CHCl_3$ and CAAs is slightly lower in HUM than in FUM, the high normalized yield of ClO_3^- can be a huge hurdle for employing the electrolysis in HUM with or

without the alternating scheme. Nonetheless, it is still beneficial to employ the alternating scheme at high mass transfer rates in the HUM if one cannot access the fresh urine (Table 5.2).

Table 5.2 The normalized yield of CBPs after 2 hr electrolysis in HUM with or without the alternating scheme.

	WE1: 2.5V – WE2: Open Circuit; *Re* = 2977	**WE1: 2.5V – WE2: -2V; *Re* = 2977**	**WE1: 2.5V – WE2: Open Circuit; *Re* = 11050**	**WE1: 2.5V – WE2: -2V; *Re* = 11050**
Y_{ClO3^-} (μM)	82.65	12.01	58.85	9.84
Y_{CHCl3} (μM)	0.29	0.05	0.16	0.02
Y_{CAAs} (μM)	1.52	0.41	1.18	0.20

5.6 THE EFFECT OF AC ELECTROLYSIS DURING ELECTROLYSIS OF FUM

An alternative method of implementing the alternating scheme during electrolysis is to apply AC voltages or a square-wave function of positive and negative potentials to the electrode. In this work, we evaluate the performance of employing the square-wave potentials (to what we refer as AC electrolysis) as described in Figure 5.7 **Voltages applied to the electrode in the AC electrolysis with the frequency of (a) 1 and (b) 100 Hz.**.

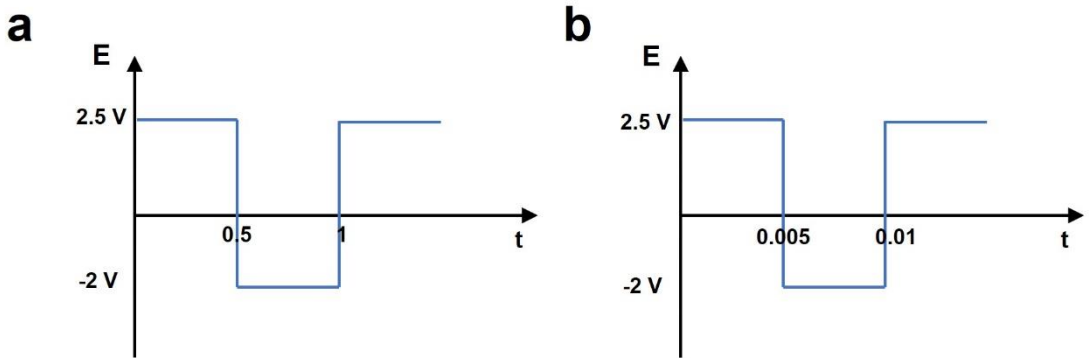

Figure 5.7 **Voltages applied to the electrode in the AC electrolysis with the frequency of (a) 1 and (b) 100 Hz.**

5.6.1 *Rates of Pharmaceutical Degradation in Synthetic Fresh Urine Matrixes (FUM)*

The electrolysis rates of all pharmaceuticals were decreased with the increasing alternating frequency (f) (Figure 5.8a). We hypothesize that chemisorbed oxidants are rapidly reduced when the AC electrolysis undergoes the cycle of negative potentials. It is supported by the observation that the formation of FC (in 100 mM NaCl) significantly decreases with the increasing alternating frequency of AC electrolysis (Figure 5.4c). The chemisorbed oxidants (primarily IrO_{2+1} and IrO_3-Cl) have been reported to be (1) the intermediate oxidants for the formation of FC[167] and (2) the dominant oxidants for the oxidation of pharmaceutical on IrO_2 electrode in FUM.[78] Thus, the decreased rates of pharmaceutical oxidation with increasing f in FUM can be ascribed to the less generation of chemisorbed oxidants during AC electrolysis.

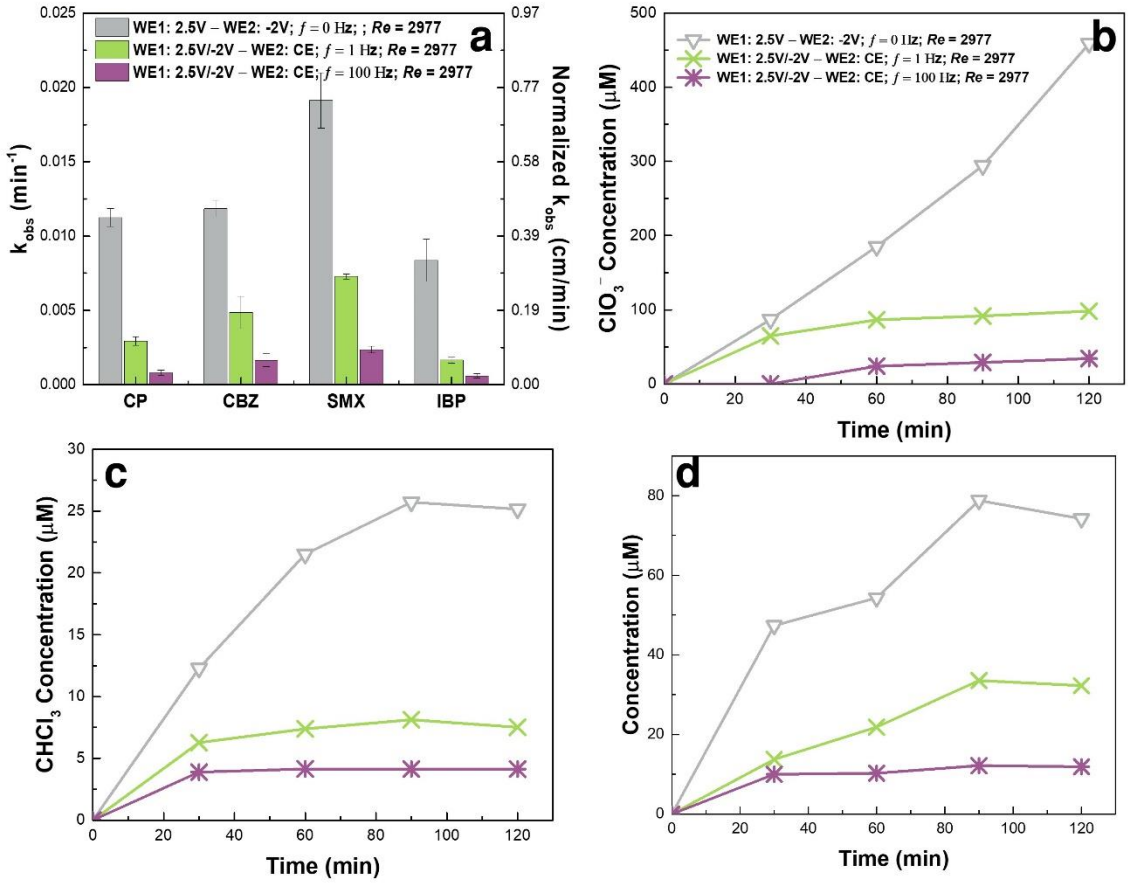

Figure 5.8 **The electrolysis of pharmaceutical in FUM was conducted at a stirring rate of 600 rpm (*Re* = 2977)**. (a) The electrolysis rates of pharmaceuticals, and the generation of (b) ClO_3^-, (c) TCM ($CHCl_3$), and (d) total chlorine in chlorinated acetic acids for the alternating scheme and AC electrolysis with alternating frequencies of 1 and 100 Hz at the amplitude of 2.5V and -2V (Figure 5.7).

5.6.2 *Generation of Chlorinated Byproducts*

As shown in Figure 5.8b, c & d, the generation of ClO_3^-, $CHCl_3$ and Cl_{CAAs} was increasingly suppressed with the increasing f. It is likely due to the suppression of $HOCl/OCl^-$ formation by the instant reduction of chemisorbed chlorine (IrO_3-Cl) when the electrolysis undergoes the cycle of cathodic reduction. Additionally, the direct reduction of ClO_3^-, $CHCl_3$ and CAAs and/or the intermediates for their formation may contribute to the suppression of CBPs formation when

negative potential is applied during AC electrolysis. Although the formation of CBPs is significantly suppressed by AC electrolysis, the degradation rates of pharmaceuticals are compromised due to the less generation of oxidants (Figure 5.8a). Therefore, it is important to determine the normalized yield of CBPs to evaluate the practicability of AC electrolysis. As shown in Table 5.3, the normalized yield of CBPs after 2hr AC electrolysis was lower than that by alternating scheme. Further suppression of CBP formation was observed with increasing alternating frequency. To achieve the degradation of SMX down to 0.1% of its initial concentration in 1.3 L fresh urine (volume of urine per person per day)[68,69] within 6 hr to avoid significant urea hydrolysis, the surface area of the electrode needs to be greater than 86 cm^2 and 265 cm^2 for the AC electrolysis with the alternating frequency of 1 Hz and 100 Hz, respectively. Nonetheless, the AC electrolysis wastes energy to charge and discharge the double layer capacitance when the polarity is alternated repeatedly on the electrode. The double layer capacitance is approximately 20 $\mu F/cm^2$ of human urine.[219] Therefore, with the applied potentials of 2.5V and -2V, the energies for charge and discharge the double layer capacitance are 1.8J and 180J for the alternating frequency of 1 Hz and 100 Hz, respectively. Furthermore, the normalized yield of CBPs by the alternating scheme (i.e., WE1: 2.5V – WE2: -2V) at Re = 11050 is similar to that via the AC electrolysis at Re = 2977. Taken all together, it is advantageous to employ electrolysis in fresh human urine with an alternating scheme at high mass transfer rates for faster pharmaceutical oxidation and less generation of CBPs.

Table 5.3 The normalized yield of CBPs after 2hr AC electrolysis in FUM and electrolysis with alternating scheme.

	WE1: 2.5V – WE2: -2V ***f*** **= 0 Hz;** ***Re*** **= 2977**	**WE1: 2.5V – WE2: -2V** ***f*** **= 0 Hz;** ***Re*** **= 11050**	**WE1: 2.5V/-2V – WE2: CE** ***f*** **= 1 Hz;** ***Re*** **= 2977**	**WE1: 2.5V/-2V – WE2: CE** ***f*** **= 100 Hz;** ***Re*** **= 2977**
Y_{ClO3-} (μM)	5.10	1.51	1.68	1.39
Y_{CHCl3} (μM)	0.28	0.17	0.13	0.17
Y_{CAAs} (μM)	0.82	0.34	0.55	0.48

5.7 CONCLUSIONS

In this chapter, we demonstrate the application of alternating scheme of oxidation and reduction for the electrochemical oxidation of pharmaceutical in fresh human urine as a proof of principle. The IrO_2 electrodes are designed and fabricated in an interdigitated electrode array structure to maximize the mass transport of the chlorinated byproducts (CBPs) from anode to cathode. The effect of the cathode potentials and the mass transfer rates in the presence of alternating scheme is studied. It shows that the electrolysis rates of all pharmaceuticals are higher with the application of alternating scheme in both synthetic fresh urine matrixes (FUM). Furthermore, the generation of ClO_3^-, $CHCl_3$ and CAAs is increasingly suppressed with the increasing cathode potentials (i.e., more negative potentials). Additionally, increasing the mass transfer rates leads to a decrease in CBPs formation. It suggests the reduction of HOCl/OCl− and/or the intermediates of CBPs formation is mixed kinetically and mass-transfer controlled on the cathode in FUM. Our findings show that the electrolysis rates of pharmaceuticals are much lower in synthetic hydrolyzed aged urine matrixes (HUM) as compared to that in FUM. It results in a greater normalized yield of CBPs, although the formation of $CHCl_3$ and CAAs remains at a low level due to the lower content of total organic carbon (e.g., citrate ions) in HUM. An AC electrolysis can be implemented as a substitution for the alternating scheme. However, the electrolysis rates of pharmaceuticals are greatly decreased with increasing alternating frequency due to the immediate reduction of chemisorbed oxidants. Although the normalized yield of CBPs remains at low level for AC electrolysis at Re = 2977, the energy wasted on the charge and discharge of double layer capacitance between each cycle is unwanted. Additionally, a similar normalized yield of CBPs is achieved with the alternating scheme at Re = 11050 as compared to that in AC electrolysis at Re = 2977. Therefore, future work aimed at engineering a flow reactor

that operates at a high mass transfer rate using IWEs is promising for rapid pharmaceutical remediation in human urine at the source of generation with minimum generation of CBPs.

5.8 SUPPLEMENTARY FIGURES

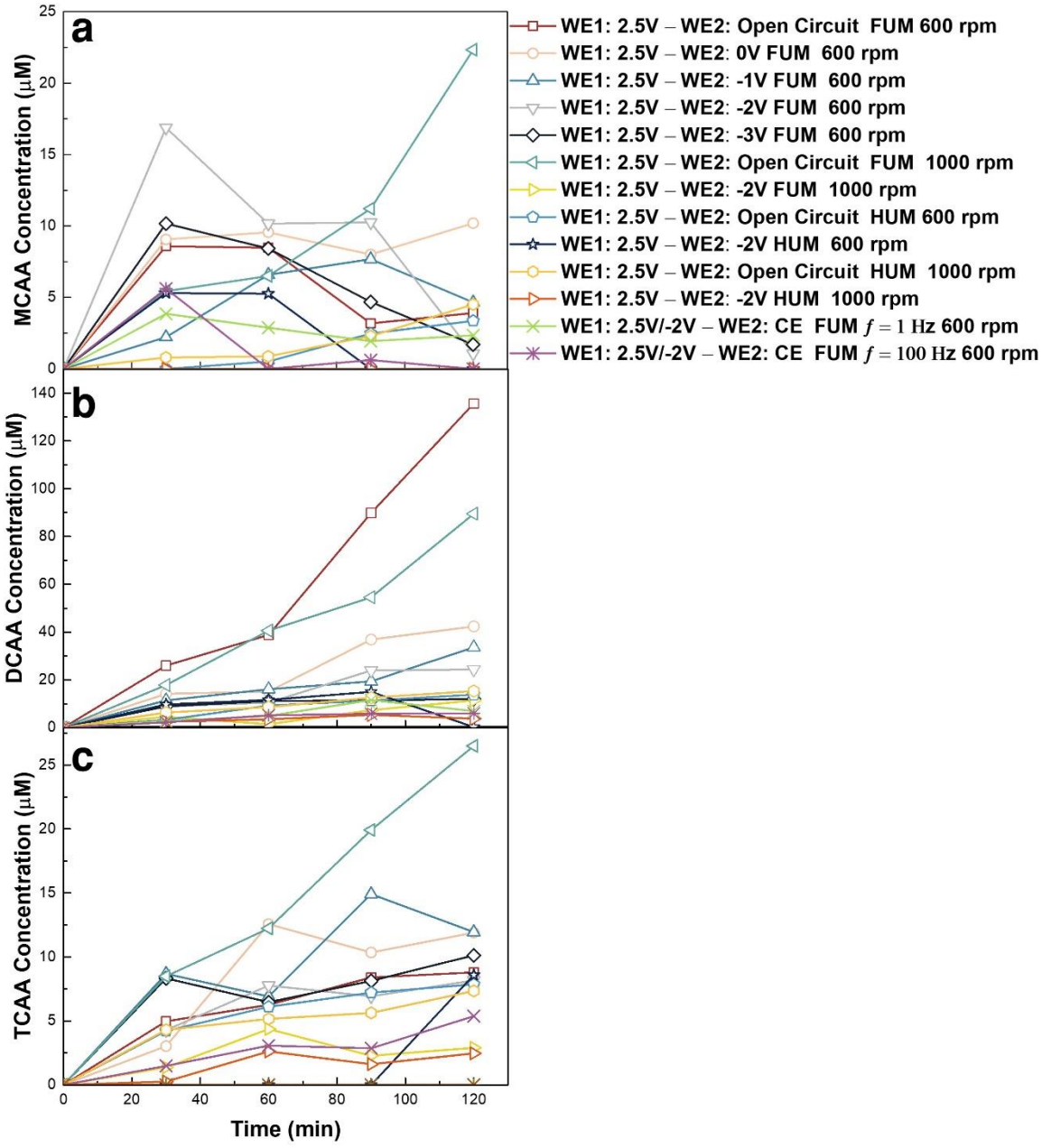

Figure 5.9. **The measured concentrations of (a) monochloroacetic acid (MCAA), (b) dichloroacetic acid (DCAA), and trichloroacetic acid (TCAA) during the electrolysis in FUM and HUM with or without the application of alternating scheme and AC electrolysis.**

Chapter 6. CONCLUSIONS AND FUTURE OUTLOOK

The above work focuses on several distinct topics within the development of electrochemical advanced oxidation processes for the mitigation of pharmaceutical contamination in human urine, from the comparison between fresh urine and hydrolyzed urine matrixes (Chapter 3), to fundamental studies of kinetics of pharmaceutical oxidation (Chapter 4), to development of proof-of-principle of alternating scheme of oxidation and reduction (Chapter 5). Several important discoveries have been made that have lasting impact on research within the electrocatalysis community and beyond:

- It is advantageous to employ the electrochemical oxidation in fresh human urine rather than hydrolyzed urine for a faster pharmaceutical degradation and less oxychloride formation (Chapter 3).
- Dissolved Cl_2 in the stagnant layer (adjacent to the anode surface) could contribute to the degradation of pharmaceuticals during electrolysis, which is overlooked by the community. The urine constituents could only scavenge the radicals leading to a slower pharmaceutical degradation in fresh human urine (Chapter 4).
- The alternating scheme of oxidation and reduction using the interdigitated working electrodes can significantly increase the rates of pharmaceutical oxidation while suppress the formation of chlorinated byproducts including ClO_3^-, chloroform and chlorinated acetic acids (Chapter 6).

During my Ph.D., the electrochemical treatment of pharmaceuticals in urine has not yet been fully studied and developed to be ready for either engineering prototype or commercialization. There are several topics to consider in determining where further scientific work can have the greatest impact.

One main objective in research dedicated toward EAOPs of the treatment of pharmaceuticals is non-selective oxidizing thousands of pharmaceuticals to nontoxic CO_2, H_2O, SO_4^{2-}, etc. without the generation of toxic byproducts. There is a huge knowledge gap between the fundamental chemistry and development of practical device. The generation of toxic byproducts is one of the major hurdles for the successful application of EAOPs in human urine. Thus, future scientific work should focus on understanding the mechanism of the formation of haloaceitc acids and trihalomethane during electrolysis of human urine. This can guide the design and development of processes or devices to further minimize the formation of oxidation byproducts. Therefore, further research could focus on the improvement of the suppression of these oxidation products.

Currently, boron-doped diamond is the most promising materials, but it is prohibitively expensive. Other electrodes materials all have respective flaws for the application, such as the use of rare-earth element (e.g., IrO_2, RuO_2, etc.), potential risk of the leakage of toxic materials (e.g., PbO_2), and short service lifetime (SnO_2, Ti_4O_7, etc.). The most important topic for continued scientific research is developing the stable and economic electrode materials. This effort has several sub-thrusts: (1) standardization of the accelerated stability test to accurately predict and calculate the real service lifetime in operational deployment, (2) materials and fabrication innovation to improve the service lifetime of electrodes and reduce the cost for large scale production, and (3) morphology engineering and surface modification to enable adequate

active sites for the generation of •OH and Cl•. If a device using stable and economic electrode materials is developed that can minimize the formation of oxidation byproducts while maintain a relative sufficient degradation rates of pharmaceuticals for the electrolysis of urine at the volume level of daily pass of a hospital urinal, then this technology will likely make it to market and succeed in mitigating the overall pharmaceutical contamination in the environment.

VITA

Yuhang Yang earned a B.S. in Materials Science and Engineering at University of Science and Technology Beijing, China. After graduation, Yuhang earned a M.S. in Materials Science and Engineering at Johns Hopkins University, Maryland, working with Dr. Howard E. Katz. Then, Yuhang started his PhD studies at University of Washington in Fall of 2017, where he has focused on developing electrochemical oxidation method for the mitigation of pharmaceutical contamination in human urine. Yuhang currently lives in Fremont, CA with his wife Sicong and his daughter Mia, and enjoys playing basketball and eating delicious Chinese food and exotic food.

BIBLIOGRAPHY

1 NationalCenterforHealthStatistics. *Health, United States, 2019 [Internet]*, 2021).

2 Escher, B. I., Bramaz, N., Richter, M. & Lienert, J. Comparative ecotoxicological hazard assessment of beta-blockers and their human metabolites using a mode-of-action-based test battery and a QSAR approach. *Environmental Science & Technology* **40**, 7402-7408 (2006). https://doi.org:10.1021/es052572v

3 Lienert, J., Burki, T. & Escher, B. I. Reducing micropollutants with source control: substance flow analysis of 212 pharmaceuticals in feces and urine. *Water Science and Technology* **56**, 87-96 (2007). https://doi.org:10.2166/wst.2007.560

4 Lienert, J., Gudel, K. & Escher, B. I. Screening method for ecotoxicological hazard assessment of 42 pharmaceuticals considering human metabolism and excretory routes. *Environmental Science & Technology* **41**, 4471-4478 (2007). https://doi.org:10.1021/es0627693

5 Luo, Y. L. *et al.* A review on the occurrence of micropollutants in the aquatic environment and their fate and removal during wastewater treatment. *Science of the Total Environment* **473**, 619-641 (2014). https://doi.org:10.1016/j.scitotenv.2013.12.065

6 Benotti, M. J. *et al.* Pharmaceuticals and endocrine disrupting compounds in US drinking water. *Environmental Science & Technology* **43**, 597-603 (2009). https://doi.org:10.1021/es801845a

7 Meador, J. P., Yeh, A., Young, G. & Gallagher, E. P. Contaminants of Emerging Concern in a Large Temperate Estuary. *Environmental Pollution* **213**, 254-267 (2016). https://doi.org:10.1016/j.envpol.2016.01.088

8 Hughes, S. R., Kay, P. & Brown, L. E. Global synthesis and critical evaluation of pharmaceutical data sets collected from river systems. *Environmental Science & Technology* **47**, 661-677 (2013). https://doi.org:10.1021/es3030148

9 Zhang, T. & Li, B. Occurrence, transformation, and fate of antibiotics in municipal wastewater treatment plants. *Critical Reviews in Environmental Science and Technology* **41**, 951-998 (2011). https://doi.org:10.1080/10643380903392692

10 DeVane, C. L. Metabolism and pharmacokinetics of selective serotonin reuptake inhibitors. *Cellular and Molecular Neurobiology* **19**, 443-466 (1999). https://doi.org:10.1023/a:1006934807375

11 Santos, L. *et al.* Ecotoxicological aspects related to the presence of pharmaceuticals in the aquatic environment. *Journal of Hazardous Materials* **175**, 45-95 (2010). https://doi.org:10.1016/j.jhazmat.2009.10.100

12 *ADVANCING HEALTH THROUGH INNOVATION NEW DRUG THERAPY APPROVALS 2019*, <https://www.fda.gov/drugs/new-drugs-fda-cders-new-molecular-entities-and-new-therapeutic-biological-products/new-drug-therapy-approvals-2019> (2020).

13 Kissler, S. M., Tedijanto, C., Goldstein, E., Grad, Y. H. & Lipsitch, M. Projecting the transmission dynamics of SARS-CoV-2 through the postpandemic period. *Science* **368**, 860-868 (2020).

14 Chaplin, B. P. The Prospect of Electrochemical Technologies Advancing Worldwide Water Treatment. *Accounts of chemical research* **52**, 596-604 (2019).

15 Miralles-Cuevas, S. *et al.* Combination of nanofiltration and ozonation for the remediation of real municipal wastewater effluents: acute and chronic toxicity assessment. *Journal of hazardous materials* **323**, 442-451 (2017).

16 Polloni-Silva, J., Valdehita, A., Fracácio, R. & Navas, J. M. Remediation efficiency of three treatments on water polluted with endocrine disruptors: Assessment by means of in vitro techniques. *Chemosphere* **173**, 267-274 (2017).

17 Wienkers, L. C. & Heath, T. G. Predicting in vivo drug interactions from in vitro drug discovery data. *Nature reviews Drug discovery* **4**, 825 (2005).

18 Daniel, W. Metabolism of psychotropic drugs: pharmacological and clinical relevance. *Polish journal of pharmacology* **47**, 367-379 (1995).

19 Shargel, L., Andrew, B. & Wu-Pong, S. *Applied biopharmaceutics and pharmacokinetics*. (Appleton & Lange Stamford, 1999).

20 Luo, Y. *et al.* A review on the occurrence of micropollutants in the aquatic environment and their fate and removal during wastewater treatment. *The Science of the total environment* **473-474**, 619-641 (2014).

21 Calero-Caceres, W. *et al.* Sludge As a Potential Important Source of Antibiotic Resistance Genes in Both the Bacterial and Bacteriophage Fractions. *Environmental Science & Technology* **48**, 7602-7611 (2014). https://doi.org:10.1021/es501851s

22 Gerrity, W. D., Benotti, J. M., Reckhow, A. D. & Snyder, A. S. in *Biophysico-Chemical Processes of Anthropogenic Organic Compounds in Environmental Systems: Xing/Anthropogenic Organic Compounds* 233-249 (John Wiley & Sons, Inc., 2011).

23 Cotillas, S., Lacasa, E., Sáez, C., Cañizares, P. & Rodrigo, M. A. Removal of pharmaceuticals from the urine of polymedicated patients: A first approach. *Chemical Engineering Journal* **331**, 606-614 (2018).

24 Schönning, C. Urine diversion–hygienic risks and microbial guidelines for reuse. *Solna, Sweden. http://www. who. int/water_sanitation_health/wastewater/urineguidelines. pdf* (2001).

25 Pradhan, S. K., Mikola, A. & Vahala, R. Nitrogen and phosphorus harvesting from human urine using a stripping, absorption, and precipitation process. *Environmental Science & Technology* **51**, 5165-5171 (2017).

26 Udert, K. & Wächter, M. Complete nutrient recovery from source-separated urine by nitrification and distillation. *Water research* **46**, 453-464 (2012).

27 Fenton, H. LXXIII.—Oxidation of tartaric acid in presence of iron. *Journal of the Chemical Society, Transactions* **65**, 899-910 (1894).

28 Mendez-Arriaga, F., Esplugas, S. & Gimenez, J. Photocatalytic degradation of non-steroidal anti-inflammatory drugs with TiO2 and simulated solar irradiation. *Water Research* **42**, 585-594 (2008). https://doi.org:10.1016/j.watres.2007.08.002

29 Keen, O. S. & Linden, K. G. Degradation of Antibiotic Activity during UV/H2O2 Advanced Oxidation and Photolysis in Wastewater Effluent. *Environmental Science & Technology* **47**, 13020-13030 (2013). https://doi.org:10.1021/es402472x

30 Zhang, R. C. *et al.* UV/H2O2 and UV/PDS Treatment of Trimethoprim and Sulfamethoxazole in Synthetic Human Urine: Transformation Products and Toxicity. *Environmental Science & Technology* **50**, 2573-2583 (2016). https://doi.org:10.1021/acs.est.5b05604

31 Sun, P. *et al.* Removal of sulfonamide antibiotics and human metabolite by biochar and biochar/H2O2 in synthetic urine. *Water research* **147**, 91-100 (2018).

32 Luo, C., Feng, M., Sharma, V. K. & Huang, C.-H. Oxidation of pharmaceuticals by ferrate (VI) in hydrolyzed urine: Effects of major inorganic constituents. *Environmental science & technology* **53**, 5272-5281 (2019).

33 Wang, N. N., Zheng, T., Zhang, G. S. & Wang, P. A review on Fenton-like processes for organic wastewater treatment. *Journal of Environmental Chemical Engineering* **4**, 762-787 (2016). https://doi.org:10.1016/j.jece.2015.12.016

34 Jung, Y. J. *et al.* Removal of amoxicillin by UV and UV/H2O2 processes. *Science of the Total Environment* **420**, 160-167 (2012). https://doi.org:10.1016/j.scitotenv.2011.12.011

35 Jojoa-Sierra, S. D., Silva-Agredo, J., Herrera-Calderon, E. & Torres-Palma, R. A. Elimination of the antibiotic norfloxacin in municipal wastewater, urine and seawater by electrochemical oxidation on IrO2 anodes. *Science of the Total Environment* **575**, 1228-1238 (2017). https://doi.org:10.1016/j.scitotenv.2016.09.201

36 Li, H., Yu, Q. N., Yang, B., Li, Z. J. & Lei, L. C. Electro-catalytic oxidation of artificial human urine by using BDD and IrO2 electrodes. *Journal of Electroanalytical Chemistry* **738**, 14-19 (2015). https://doi.org:10.1016/j.jelechem.2014.11.018

37 Tarpeh, W. A., Barazesh, J. M., Cath, T. Y. & Nelson, K. L. Electrochemical stripping to recover nitrogen from source-separated urine. *Environmental science & technology* **52**, 1453-1460 (2018).

38 Cho, K. & Hoffmann, M. R. Urea degradation by electrochemically generated reactive chlorine species: Products and reaction pathways. *Environmental science & technology* **48**, 11504-11511 (2014).

39 Zollig, H., Remmele, A., Morgenroth, E. & Udert, K. M. Removal rates and energy demand of the electrochemical oxidation of ammonia and organic substances in real stored urine. *Environmental Science-Water Research & Technology* **3**, 480-491 (2017). https://doi.org:10.1039/c7ew00014f

40 Anglada, A., Urtiaga, A. & Ortiz, I. Contributions of electrochemical oxidation to waste-water treatment: fundamentals and review of applications. *Journal of Chemical Technology & Biotechnology* **84**, 1747-1755 (2009).

41 Comninellis, C. *et al.* Advanced oxidation processes for water treatment: advances and trends for R&D. *Journal of Chemical Technology and Biotechnology* **83**, 769-776 (2008). https://doi.org:10.1002/jctb.1873

42 Girenko, D., Piletska, A., Velichenko, A. B., Mahé, E. & Devilliers, D. Novel electrode material for synthesis of low concentration sodium hypochlorite solutions. *Chemical and Materials Engineering* **1**, 53-59 (2013).

43 Waterston, K., Wang, J. W. J., Bejan, D. & Bunce, N. J. Electrochemical waste water treatment: Electrooxidation of acetaminophen. *Journal of Applied Electrochemistry* **36**, 227-232 (2006). https://doi.org:10.1007/s10800-005-9049-z

44 Beitz, T., Bechmann, W. & Mitzner, R. Investigations of reactions of selected azaarenes with radicals in water. 2. Chlorine and bromine radicals. *The Journal of Physical Chemistry A* **102**, 6766-6771 (1998).

45 Trasatti, S. Progress in the understanding of the mechanism of chlorine evolution at oxide electrodes. *Electrochimica acta* **32**, 369-382 (1987).

46 Li, F.-B., Hillman, A. R. & Lubetkin, S. D. A new approach to the mechanism of chlorine evolution: Separate examination of the kinetic steps using ac impedance on a rotating thin ring electrode. *Electrochimica acta* **37**, 2715-2723 (1992).

47 Soufan, M., Deborde, M., Delmont, A. & Legube, B. Aqueous chlorination of carbamazepine: kinetic study and transformation product identification. *Water research* **47**, 5076-5087 (2013).

48 Neta, P., Huie, R. E. & Ross, A. B. Rate constants for reactions of inorganic radicals in aqueous solution. *Journal of Physical and Chemical Reference Data* **17**, 1027-1284 (1988).

49 Jiang, P.-Y. *et al.* Pulse radiolysis study of concentrated sulfuric acid solutions. Formation mechanism, yield and reactivity of sulfate radicals. *Journal of the Chemical Society, Faraday Transactions* **88**, 1653-1658 (1992).

50 Radjenovic, J. & Sedlak, D. L. Challenges and opportunities for electrochemical processes as next-generation technologies for the treatment of contaminated water. *Environmental Science & Technology* **49**, 11292-11302 (2015). https://doi.org:10.1021/acs.est.5b02414

51 Huie, R. E., Clifton, C. L. & Neta, P. Electron transfer reaction rates and equilibria of the carbonate and sulfate radical anions. *International Journal of Radiation Applications and Instrumentation. Part C. Radiation Physics and Chemistry* **38**, 477-481 (1991).

52 Padmaja, S., Neta, P. & Huie, R. Rate constants for some reactions of inorganic radicals with inorganic ions. Temperature and solvent dependence. *International journal of chemical kinetics* **25**, 445-455 (1993).

53 Maruthamuthu, P. & Neta, P. Phosphate radicals. Spectra, acid-base equilibriums, and reactions with inorganic compounds. *The Journal of Physical Chemistry* **82**, 710-713 (1978).

54 Grabner, G., Getoff, N. & Schwörer, F. Pulsradiolyse von H3PO4, H2PO4-, HPO42− und P2O74− in wässriger lösung—II. Spektren und kinetik der Zwischenprodukte. *International Journal for Radiation Physics and Chemistry* **5**, 405-417 (1973).

55 Zepp, R. G., Faust, B. C. & Hoigne, J. Hydroxyl radical formation in aqueous reactions (pH 3-8) of iron (II) with hydrogen peroxide: the photo-Fenton reaction. *Environmental Science & Technology* **26**, 313-319 (1992).

56 Tsamba, L., Cimetière, N., Wolbert, D., Correc, O. & Le Cloirec, P. Body fluid analog chlorination: Application to the determination of disinfection byproduct formation kinetics in swimming pool water. *Journal of Environmental Sciences* **87**, 112-122 (2020).

57 Panizza, M. & Cerisola, G. Direct And Mediated Anodic Oxidation of Organic Pollutants. *Chemical Reviews* **109**, 6541-6569 (2009). https://doi.org:10.1021/cr9001319

58 Correa-Lozano, B., Comninellis, C. & De Battisti, A. Service life of Ti/SnO2–Sb2O5 anodes. *Journal of Applied Electrochemistry* **27**, 970-974 (1997).

59 Rose, C., Parker, A., Jefferson, B. & Cartmell, E. The characterization of feces and urine: a review of the literature to inform advanced treatment technology. *Critical reviews in environmental science and technology* **45**, 1827-1879 (2015).

60 Jasper, J. T., Shafaat, O. S. & Hoffmann, M. R. Electrochemical Transformation of Trace Organic Contaminants in Latrine Wastewater. *Environmental Science & Technology* **50**, 10198-10208 (2016). https://doi.org:10.1021/acs.est.6b02912

61 Udert, M. K., Larsen, A. T., Biebow, M. & Gujer, W. Urea hydrolysis and precipitation dynamics in a urine-collecting system. *Water research* **37**, 2571-2582 (2003).

62 Udert, K. M., Larsen, T. A. & Gujer, W. Estimating the precipitation potential in urine-collecting systems. *Water Research* **37**, 2667-2677 (2003).

63 Cotillas, S., Lacasa, E., Sáez, C., Canizares, P. & Rodrigo, M. A. Electrolytic and electro-irradiated technologies for the removal of chloramphenicol in synthetic urine with diamond anodes. *Water research* **128**, 383-392 (2018).

64 Jojoa-Sierra, D. S., Silva-Agredo, J., Herrera-Calderon, E. & Torres-Palma, A. R. Elimination of the antibiotic norfloxacin in municipal wastewater, urine and seawater by electrochemical oxidation on IrO anodes. *The Science of the total environment* **575**, 1228-1238 (2017).

65 Urbańczyk, E., Sowa, M. & Simka, W. Urea removal from aqueous solutions—a review. *Journal of Applied Electrochemistry* **46**, 1011-1029 (2016).

66 Zollig, H., Remmele, A., Fritzsche, C., Morgenroth, E. & Udert, K. M. Formation of chlorination byproducts and their emission pathways in chlorine mediated electro-oxidation of urine on active and nonactive type anodes. *Environmental Science & Technology* **49**, 11062-11069 (2015). https://doi.org:10.1021/acs.est.5b01675

67 Clark, J. A., Yang, Y., Ramos, N. C. & Hillhouse, H. W. Selective oxidation of pharmaceuticals and suppression of perchlorate formation during electrolysis of fresh human urine. *Water Research* **198**, 117106 (2021).

68 Larsen, T. A., Udert, K. M. & Lienert, J. *Source separation and decentralization for wastewater management*. (Iwa Publishing, 2013).

69 Putnam, D. F. Composition and concentrative properties of human urine. (1971).

70 Jasper, J. T., Yang, Y. & Hoffmann, M. R. Toxic byproduct formation during electrochemical treatment of latrine wastewater. *Environmental Science & Technology* **51**, 7111-7119 (2017).

71 Haynes, W. M. *CRC handbook of chemistry and physics*. (CRC press, 2014).

72 Cotillas, S. *et al.* The Role of the Anode Material in Selective Penicillin G Oxidation in Urine. *ChemElectroChem* **6**, 1376-1384 (2019).

73 Garcia-Segura, S., Keller, J., Brillas, E. & Radjenovic, J. Removal of organic contaminants from secondary effluent by anodic oxidation with a boron-doped diamond anode as tertiary treatment. *Journal of Hazardous Materials* **283**, 551-557 (2015).

74 Schmalz, V., Dittmar, T., Haaken, D. & Worch, E. Electrochemical disinfection of biologically treated wastewater from small treatment systems by using boron-doped diamond (BDD) electrodes–Contribution for direct reuse of domestic wastewater. *Water research* **43**, 5260-5266 (2009).

75 Huang, X. *et al.* Electrochemical disinfection of toilet wastewater using wastewater electrolysis cell. *Water research* **92**, 164-172 (2016).

76 Schaefer, C. E., Andaya, C. & Urtiaga, A. Assessment of disinfection and by-product formation during electrochemical treatment of surface water using a Ti/IrO2 anode. *Chemical Engineering Journal* **264**, 411-416 (2015).

77 Wang, F. *et al.* Revealing the mechanism of formation and transformation of chlorinated by-products during electrolyzing synthetic urine using Ti/RuOx-IrOx and BDD electrodes. *Fuel Cells* (2022).

78 Yang, Y., Ramos, N. C., Clark, J. A. & Hillhouse, H. W. Electrochemical Oxidation of Pharmaceuticals in Synthetic Fresh Human Urine: Using Selective Radical Quenchers to Reveal the Dominant Degradation Pathways and the Scavenging Effects of Individual Urine Constituents. *Water Research*, 118722 (2022).

79 Bard, A. J. & Faulkner, L. R. *Electrochemical Methods Fundamentals and Applications*. 2nd edn, (John Wiley and Sons, Inc, 2001).

80 Taama, W., Plimley, R. & Scott, K. Influence of supporting electrolyte on ferricyanide reduction at a rotating disc electrode. *Electrochimica acta* **41**, 549-551 (1996).

81 Szánto, D., Cleghorn, S., Ponce-de-León, C. & Walsh, F. The limiting current for reduction of ferricyanide ion at nickel: the importance of experimental conditions. *AIChE journal* **54**, 802-810 (2008).

82 Kolthoff, I. & Pearson, E. Stability of potassium ferrocyanide solutions. *Industrial & Engineering Chemistry Analytical Edition* **3**, 381-382 (1931).

83 Selman, J. R. & Tobias, C. W. in *Advances in chemical engineering* Vol. 10 211-318 (Elsevier, 1978).

84 Bond, A. M., Oldham, K. B. & Zoski, C. G. Steady-state voltammetry. *Analytica Chimica Acta* **216**, 177-230 (1989).

85 *BACTRIM (sulfamethoxazole and trimethoprim) injection, for intravenous use.*, <https://www.accessdata.fda.gov/drugsatfda_docs/label/2017/018374s025lbl.pdf> (

86 FDA, U. S. *CYCLOPHOSPHAMIDE injection, for intravenous use.*, <https://www.accessdata.fda.gov/drugsatfda_docs/label/2013/012141s090,012142s112lbl.pdf> (

87 FDA. *BACTRIM™ sulfamethoxazole and trimethoprim DS (double strength) tablets and tablets USP*, <https://www.accessdata.fda.gov/drugsatfda_docs/label/2010/017377s067lbl.pdf> (

88 Joqueviel, C. *et al.* Urinary excretion of cyclophosphamide in humans, determined by phosphorus-31 nuclear magnetic resonance spectroscopy. *Drug metabolism and Disposition* **26**, 418-428 (1998).

89 Yalkowsky, H. & Press, Y. H. C. (2003).

90 Burns, J. & Finlayson, B. A proposal for a standard reference artificial urine in in vitro urolithiasis experiments. *Investigative urology* **18**, 167-169 (1980).

91 FDA. *Tegretol (carbamazepine) Label*, <https://www.accessdata.fda.gov/drugsatfda_docs/label/2007/016608s098lbl.pdf> (

92 FDA. *Over-the-Counter (OTC) Ibuprofen: Cardiovascular Safety & Consumer Use*, <https://www.fda.gov/media/112979/download> (

93 Yalkowsky, S. H. & Dannenfelser, R. M. Aquasol database of aqueous solubility. *College of Pharmacy, University of Arizona, Tucson, AZ* **189** (1992).

94 Barazesh, J. M., Prasse, C. & Sedlak, D. L. Electrochemical transformation of trace organic contaminants in the presence of halide and carbonate ions. *Environmental science & technology* **50**, 10143-10152 (2016).

95 Pletcher, D., Greff, R., Peat, R., Peter, L. & Robinson, J. *Instrumental methods in electrochemistry*. (Elsevier, 2001).

96 Xie, Y. Analyzing haloacetic acids using gas chromatography/mass spectrometry. *Water research* **35**, 1599-1602 (2001).

97 Hodgeson, J., Cohen, A. & Munch, D. Determination of Chlorination Disinfection byproducts, Chlorinated Solvents, and Halogenated Pesticides/herbicides in Drinking Water by Liquid–liquid Extraction and Gas Chromatography with Electron Capture Detection. *EPA, Cincinnati USA* (1990).

98 Stumm, W. & Morgan, J. J. *Aquatic chemistry: chemical equilibria and rates in natural waters*. Vol. 126 (John Wiley & Sons, 2012).

99 Pinkernell, U., Nowack, B., Gallard, H. & Von Gunten, U. Methods for the photometric determination of reactive bromine and chlorine species with ABTS. *Water Research* **34**, 4343-4350 (2000).

100 Federation, W. E. & Association, A. P. H. Standard methods for the examination of water and wastewater. *American Public Health Association (APHA): Washington, DC, USA* (2005).

101 Parkhurst, D. L. & Appelo, C. Description of input and examples for PHREEQC version 3—a computer program for speciation, batch-reaction, one-dimensional transport, and inverse geochemical calculations. *US geological survey techniques and methods* **6**, 497 (2013).

102 Buxton, G. V., Greenstock, C. L., Helman, W. P. & Ross, A. B. Critical review of rate constants for reactions of hydrated electrons, hydrogen atoms and hydroxyl radicals (· OH/· O− in aqueous solution. *Journal of physical and chemical reference data* **17**, 513-886 (1988).

103 Garcia-Ac, A. *et al.* Oxidation kinetics of cyclophosphamide and methotrexate by ozone in drinking water. *Chemosphere* **79**, 1056-1063 (2010).

104 WHO. WHO model list of essential medicines: 17th list, March 2011. (2011).

105 Armstrong, D. A. *et al.* Standard electrode potentials involving radicals in aqueous solution: inorganic radicals (IUPAC Technical Report). *Pure and Applied Chemistry* **87**, 1139-1150 (2015).

106 Lei, Y., Cheng, S., Luo, N., Yang, X. & An, T. Rate Constants and Mechanisms of the Reactions of Cl• and Cl2•–with Trace Organic Contaminants. *Environmental science & technology* **53**, 11170-11182 (2019).

107 Grigor'ev, A., Makarov, I. & Pikaev, A. Formation of Cl 2-in the bulk of solution during radiolysis of concentrated aqueous solutions of chlorides. *Khimiya Vysokikh Ehnergij* **21**, 123-126 (1987).

108 Nagarajan, V. & Fessenden, R. W. Flash photolysis of transient radicals. 1. X2-with X= Cl, Br, I, and SCN. *The Journal of Physical Chemistry* **89**, 2330-2335 (1985).

109 Yu, X.-Y. & Barker, J. R. Hydrogen peroxide photolysis in acidic aqueous solutions containing chloride ions. II. Quantum yield of HO•(Aq) radicals. *The Journal of Physical Chemistry A* **107**, 1325-1332 (2003).

110 Wang, T. X. & Margerum, D. W. Kinetics of reversible chlorine hydrolysis: temperature dependence and general-acid/base-assisted mechanisms. *Inorganic Chemistry* **33**, 1050-1055 (1994).

111 Wagner, I., Karthäuser, J. & Strehlow, H. On the decay of the dichloride anion Cl− 2 in aqueous solution. *Berichte der Bunsengesellschaft für physikalische Chemie* **90**, 861-867 (1986).

112 Xiao, S., Qu, J., Zhao, X., Liu, H. & Wan, D. Electrochemical process combined with UV light irradiation for synergistic degradation of ammonia in chloride-containing solutions. *Water research* **43**, 1432-1440 (2009).

113 Ji, Y. *et al.* Highly selective transformation of ammonia nitrogen to N2 based on a novel solar-driven photoelectrocatalytic-chlorine radical reactions system. *Water research* **125**, 512-519 (2017).

114 Shen, Z. *et al.* Highly efficient total nitrogen and simultaneous total organic carbon removal for urine based on the photoelectrochemical cycle reaction of chlorine and hydroxyl radicals. *Electrochimica Acta* **297**, 1-9 (2019).

115 Long, L., Bu, Y., Chen, B. & Sadiq, R. Removal of urea from swimming pool water by UV/VUV: The roles of additives, mechanisms, influencing factors, and reaction products. *Water research* **161**, 89-97 (2019).

116 Qiang, Z. & Adams, C. D. Determination of monochloramine formation rate constants with stopped-flow spectrophotometry. *Environmental science & technology* **38**, 1435-1444 (2004).

117 Blatchley III, E. R. & Cheng, M. Reaction mechanism for chlorination of urea. *Environmental science & technology* **44**, 8529-8534 (2010).

118 Buxton, G. & Subhani, M. Radiation chemistry and photochemistry of oxychlorine ions. Part 1.—Radiolysis of aqueous solutions of hypochlorite and chlorite ions. *Journal of the Chemical Society, Faraday Transactions 1: Physical Chemistry in Condensed Phases* **68**, 947-957 (1972).

119 Eriksen, T. E., Lind, J. & Merényi, G. Generation of chlorine dioxide from ClO–2 by pulse radiolysis. *Journal of the Chemical Society, Faraday Transactions 1: Physical Chemistry in Condensed Phases* **77**, 2115-2123 (1981).

120 MENKIN, V., Makarov, I. & Pikaev, A. MECHANISM FOR FORMATION OF NITRITE IN RADIOLYSIS OF AQUEOUS-SOLUTIONS OF AMMONIA IN THE PRESENCE OF OXYGEN. *High Energy Chemistry* **25**, 48-52 (1991).

121 Buxton, G. V., Wood, N. D. & Dyster, S. Ionisation constants of˙ OH and HO˙ 2 in aqueous solution up to 200° C. A pulse radiolysis study. *Journal of the Chemical Society, Faraday Transactions 1: Physical Chemistry in Condensed Phases* **84**, 1113-1121 (1988).

122 Neta, P., Maruthamuthu, P., Carton, P. & Fessenden, R. Formation and reactivity of the amino radical. *The Journal of Physical Chemistry* **82**, 1875-1878 (1978).

123 Mazellier, P., Leroy, É., De Laat, J. & Legube, B. Transformation of carbendazim induced by the H 2 O 2/UV system in the presence of hydrogenocarbonate ions: involvement of the carbonate radical. *New journal of chemistry* **26**, 1784-1790 (2002).

124 Clifton, C. L. & Huie, R. E. Rate constants for some hydrogen abstraction reactions of the carbonate radical. *International journal of chemical kinetics* **25**, 199-203 (1993).

125 Canonica, S. *et al.* Photosensitizer method to determine rate constants for the reaction of carbonate radical with organic compounds. *Environmental science & technology* **39**, 9182-9188 (2005).

126 Hubler, D., Baygents, J. C., Chaplin, B. & Farrell, J. Understanding chlorite and chlorate formation associated with hypochlorite generation at boron doped diamond film anodes. *Journal of The Electrochemical Society* **161**, E182-E189 (2014).

127 Buxton, G. V., Bydder, M. & Salmon, G. A. Reactivity of chlorine atoms in aqueous solution Part 1The equilibrium Cl MNsbd+ Cl-Cl 2. *Journal of the Chemical Society, Faraday Transactions* **94**, 653-657 (1998).

128 Kapałka, A., Baltruschat, H. & Comninellis, C. Electrochemical Oxidation of Organic Compounds Induced by Electro-Generated Free Hydroxyl Radicals on BDD Electrodes. *Synthetic Diamond Films: Preparation, Electrochemistry, Characterization, and Applications*, 237-260 (2011).

129 Comninellis, C. Electrocatalysis in the electrochemical conversion/combustion of organic pollutants for waste water treatment. *Electrochimica Acta* **39**, 1857-1862 (1994).

130 Rodrigo, M. A. *et al.* Oxidation of 4-chlorophenol at boron-doped diamond electrode for wastewater treatment. *Journal of the Electrochemical Society* **148**, D60-D64 (2001). https://doi.org:10.1149/1.1362545

131 Iniesta, J. *et al.* Electrochemical oxidation of phenol at boron-doped diamond electrode. *Electrochimica Acta* **46**, 3573-3578 (2001). https://doi.org:10.1016/s0013-4686(01)00630-2

132 Halász, G., Gyüre, B., Jánosi, I. M., Szabó, K. G. & Tél, T. Vortex flow generated by a magnetic stirrer. *American Journal of Physics* **75**, 1092-1098 (2007).

133 Prentice, G. *Electrochemical engineering principles*. (Prentice Hall, 1991).

134 Dodd, M. C. & Huang, C.-H. Transformation of the antibacterial agent sulfamethoxazole in reactions with chlorine: kinetics, mechanisms, and pathways. *Environmental science & technology* **38**, 5607-5615 (2004).

135 Sivey, J. D. & Roberts, A. L. Assessing the reactivity of free chlorine constituents Cl2, Cl2O, and HOCl toward aromatic ethers. *Environmental science & technology* **46**, 2141-2147 (2012).

136 Sivey, J. D., McCullough, C. E. & Roberts, A. L. Chlorine monoxide (Cl2O) and molecular chlorine (Cl2) as active chlorinating agents in reaction of dimethenamid with aqueous free chlorine. *Environmental science & technology* **44**, 3357-3362 (2010).

137 Trellu, C. *et al.* Electro-oxidation of organic pollutants by reactive electrochemical membranes. *Chemosphere* **208**, 159-175 (2018).

138 Donaghue, A. & Chaplin, B. P. Effect of select organic compounds on perchlorate formation at boron-doped diamond film anodes. *Environmental science & technology* **47**, 12391-12399 (2013).

139 Clarke, K. *et al.* The carbonate radical: its reactivity with oxygen, ammonia, amino acids, and melanins. *The Journal of Physical Chemistry A* **112**, 10147-10151 (2008).

140 Hora, P. I., Novak, P. J. & Arnold, W. A. Photodegradation of pharmaceutical compounds in partially nitritated wastewater during UV irradiation. *Environmental Science: Water Research & Technology* **5**, 897-909 (2019).

141 Scholes, R. C., Prasse, C. & Sedlak, D. L. The Role of Reactive Nitrogen Species in Sensitized Photolysis of Wastewater-Derived Trace Organic Contaminants. *Environmental science & technology* (2019).

142 WHO. Guidelines for Drinking-Water Quality: Incorporating the First Addendum. Geneva, Switzerland. *World Health Organization* (2017).

143 Jung, Y. J., Baek, K. W., Oh, B. S. & Kang, J.-W. An investigation of the formation of chlorate and perchlorate during electrolysis using Pt/Ti electrodes: The effects of pH and reactive oxygen species and the results of kinetic studies. *Water research* **44**, 5345-5355 (2010).

144 Azizi, O., Hubler, D., Schrader, G., Farrell, J. & Chaplin, B. P. Mechanism of perchlorate formation on boron-doped diamond film anodes. *Environmental science & technology* **45**, 10582-10590 (2011).

145 Pagsberg, P. B. Investigation of the NH2 radical produced by pulse radiolysis of ammonia in aqueous solution. *Aspects of Research at Risø* **5**, 209 (1972).

146 Draganić, Z. D. *et al.* Radiolysis of aqueous solutions of ammonium bicarbonate over a large dose range. *International Journal of Radiation Applications and Instrumentation. Part C. Radiation Physics and Chemistry* **38**, 317-321 (1991).

147 Chaplin, B. P. Critical review of electrochemical advanced oxidation processes for water treatment applications. *Environmental Science: Processes & Impacts* **16**, 1182-1203 (2014).

148 Watts, M. J. & Linden, K. G. Chlorine photolysis and subsequent OH radical production during UV treatment of chlorinated water. *Water Research* **41**, 2871-2878 (2007).

149 Nowell, L. H. & Hoigné, J. Photolysis of aqueous chlorine at sunlight and ultraviolet wavelengths—II. Hydroxyl radical production. *Water Research* **26**, 599-605 (1992).

150 Fang, J., Fu, Y. & Shang, C. The roles of reactive species in micropollutant degradation in the UV/free chlorine system. *Environmental science & technology* **48**, 1859-1868 (2014).

151 Remucal, C. & Manley, D. Emerging investigators series: the efficacy of chlorine photolysis as an advanced oxidation process for drinking water treatment. *Environmental Science: Water Research & Technology* **2**, 565-579 (2016).

152 Alfassi, Z., Mosseri, S. & Neta, P. Reactivities of chlorine atoms and peroxyl radicals formed in the radiolysis of dichloromethane. *The Journal of Physical Chemistry* **93**, 1380-1385 (1989).

153 O'Neill, P., Steenken, S. & Schulte-Frohlinde, D. Formation of radical cations of methoxylated benzenes by reaction with OH radicals, Ti 2+, Ag 2+, and SO 4.-in aqueous solution. An optical and conductometric pulse radiolysis and in situ radiolysis electron spin resonance study. *Journal of Physical Chemistry* **79**, 2773-2779 (1975).

154 Hess, E. *Boron-doped Diamond Sensors for the Determination of Organic Compounds in Aqueous Media*, University of the Western Cape, (2010).

155 Montilla, F., Michaud, P., Morallon, E., Vazquez, J. & Comninellis, C. Electrochemical oxidation of benzoic acid at boron-doped diamond electrodes. *Electrochimica Acta* **47**, 3509-3513 (2002).

156 Weinberg, N., Marr, D. & Wu, C. Sensitive probe for double layer structure. Potential dependent competitive cyanation and methoxylation of 1, 4-dimethoxybenzene. *Journal of the American Chemical Society* **97**, 1499-1504 (1975).

157 de Martinez, M. C. *et al.* In situ spectroscopic investigation of the anodic oxidation of 1, 4-dimethoxybenzene at platinum electrodes. *Synthetic metals* **88**, 187-196 (1997).

158 Jing, Y. & Chaplin, B. P. Mechanistic study of the validity of using hydroxyl radical probes to characterize electrochemical advanced oxidation processes. *Environmental science & technology* **51**, 2355-2365 (2017).

159 Celdran, R. & Gonzalez-Velasco, J. Oxidation mechanism of allyl alcohol on an Au-electrode in basic solutions. *Electrochimica Acta* **26**, 525-533 (1981).

160 Maruthamuthu, P. Absolute rate constants for the reactions of sulfate, phosphate and hydroxyl radicals with monomers. *Die Makromolekulare Chemie, Rapid Communications* **1**, 23-25 (1980).

161 Brainard, R. L. & Madix, R. J. Enhanced stability of t-butanol reaction intermediates on oxygen covered Cu (110): Cleavage of unactivated C□ H bonds on metal surfaces. *Surface Science* **214**, 396-406 (1989).

162 Mertens, R. & von Sonntag, C. Photolysis (λ= 354 nm of tetrachloroethene in aqueous solutions. *Journal of Photochemistry and Photobiology A: Chemistry* **85**, 1-9 (1995).

163 Motohashi, N. & Saito, Y. Competitive measurement of rate constants for hydroxyl radical reactions using radiolytic hydroxylation of benzoate. *Chemical and pharmaceutical bulletin* **41**, 1842-1845 (1993).

164 Comninellis, C. ELECTROCATALYSIS IN THE ELECTROCHEMICAL CONVERSION/COMBUSTION OF ORGANIC POLLUTANTS FOR WASTE-WATER TREATMENT. *Electrochimica Acta* **39**, 1857-1862 (1994). https://doi.org:10.1016/0013-4686(94)85175-1

165 Weng, S. *et al.* The presence of pharmaceuticals and personal care products in swimming pools. *Environmental Science & Technology Letters* **1**, 495-498 (2014).

166 Gligorovski, S., Strekowski, R., Barbati, S. & Vione, D. Environmental implications of hydroxyl radicals (• OH). *Chemical Reviews* **115**, 13051-13092 (2015).

167 Yang, Y., Shin, J., Jasper, T. J. & Hoffmann, R. M. Multilayer Heterojunction Anodes for Saline Wastewater Treatment: Design Strategies and Reactive Species Generation Mechanisms. *Environmental science & technology* **50**, 8780-8787 (2016).

168 James A., C., Yuhang, Y., Nathanael C., R., Michael C., D. & Hugh W., H. *Oxidant Scavenging Properties of Urea Enable Selective Oxidation of Pharmaceuticals and Suppression of Oxyhalide Formation during Electrolysis of Fresh Human Urine*. (2020).

169 Eslamian, S. *Urban water reuse handbook*. (CRC Press, 2016).

170 Minakata, D., Li, K., Westerhoff, P. & Crittenden, J. Development of a Group Contribution Method To Predict Aqueous Phase Hydroxyl Radical (HO center dot) Reaction Rate Constants. *Environmental Science & Technology* **43**, 6220-6227 (2009). https://doi.org:10.1021/es900956c

171 Jafvert, C. T. & Valentine, R. L. Reaction scheme for the chlorination of ammoniacal water. *Environmental science & technology* **26**, 577-586 (1992).

172 Li, J., Jiang, J., Manasfi, T. & von Gunten, U. Chlorination and bromination of olefins: Kinetic and mechanistic aspects. *Water Research* **187**, 116424 (2020).

173 Swain, C. G. & Crist, D. R. Mechanisms of chlorination by hypochlorous acid. The last of chlorinium ion, Cl+. *Journal of the American Chemical Society* **94**, 3195-3200 (1972).

174 Pattison, D. I. & Davies, M. J. Absolute rate constants for the reaction of hypochlorous acid with protein side chains and peptide bonds. *Chemical research in toxicology* **14**, 1453-1464 (2001).

175 Prütz, W. A. Hypochlorous acid interactions with thiols, nucleotides, DNA, and other biological substrates. *Archives of biochemistry and biophysics* **332**, 110-120 (1996).

176 Fan, Z.-y. *et al.* Kinetics of aniline oxidation with chlorine dioxide. *Journal of Environmental Sciences* **16**, 238-241 (2004).

177 Zhou, Z., Jaaskelainen, A. & Vuorinen, T. Oxidation of cellulose and carboxylic acids by hypochlorous acid: kinetics and mechanisms. *Journal of Pulp and Paper Science* **34**, 212 (2008).

178 Voudrias, E. A. & Reinhard, M. Reactivities of hypochlorous and hypobromous acid, chlorine monoxide, hypobromous acidium ion, chlorine, bromine, and bromine chloride in electrophilic aromatic substitution reactions with p-xylene in water. *Environmental science & technology* **22**, 1049-1056 (1988).

179 Taraszka, A. J. *Chemical Kinetic Studies of the Reaction Between Hypochlorous Acid and Secondary and Tertiary Amines*. (The University of Wisconsin-Madison, 1962).

180 Squadrito, G. L., Postlethwait, E. M. & Matalon, S. Elucidating mechanisms of chlorine toxicity: reaction kinetics, thermodynamics, and physiological implications. *American Journal of Physiology-Lung Cellular and Molecular Physiology* **299**, L289-L300 (2010).

181 Nicovich, J. M. *et al.* An experimental and theoretical study of the gas phase kinetics of atomic chlorine reactions with CH 3 NH 2,(CH 3) 2 NH, and (CH 3) 3 N. *Physical Chemistry Chemical Physics* **17**, 911-917 (2015).

182 Andrews, L. & Keefer, R. The chlorination of aromatic hydrocarbons in carbon tetrachloride and in trifluoroacetic acid. *Journal of the American Chemical Society* **79**, 5169-5174 (1957).

183 Thomm, E. W. C. W. & Wayman, M. N-chlorination of secondary amides. II. Effects of substituents on rates of N-chlorination. *Canadian Journal of Chemistry* **47**, 3289-3297 (1969).

184 Kumar, S. & Gehlawat, J. K. Kinetics of absorption of chlorine in acetic acid in the presence of homogeneous catalysts. *Journal of Chemical Technology and Biotechnology* **29**, 353-360 (1979).

185 Ueki, H., Chapman, G. & Ashby, M. T. Reactive sulfur species: Kinetics and mechanism of the oxidation of aryl sulfinates with hypochlorous acid. *The Journal of Physical Chemistry A* **114**, 1670-1676 (2010).

186 Deborde, M. & Von Gunten, U. Reactions of chlorine with inorganic and organic compounds during water treatment—kinetics and mechanisms: a critical review. *Water research* **42**, 13-51 (2008).

187 Zwiener, C. & Frimmel, F. Oxidative treatment of pharmaceuticals in water. *Water Research* **34**, 1881-1885 (2000).

188 Tachikawa, M., Aburada, T., Tezuka, M. & Sawamura, R. Occurrence and production of chloramines in the chlorination of creatinine in aqueous solution. *Water research* **39**, 371-379 (2005).

189 Masuda, T., Shinohara, H. & Kondo, M. Reactions of hydroxyl radicals with nucleic acid bases and the related compounds in gamma-irradiated aqueous solution. *Journal of radiation research* **16**, 153-161 (1975).

190 Costa, C. R., Montilla, F., Morallón, E. & Olivi, P. Electrochemical oxidation of acid black 210 dye on the boron-doped diamond electrode in the presence of phosphate ions: Effect of current density, pH, and chloride ions. *Electrochimica Acta* **54**, 7048-7055 (2009).

191 Murugananthan, M., Latha, S., Raju, G. B. & Yoshihara, S. Role of electrolyte on anodic mineralization of atenolol at boron doped diamond and Pt electrodes. *Separation and purification technology* **79**, 56-62 (2011).

192 Bagastyo, A. Y., Batstone, D. J., Rabaey, K. & Radjenovic, J. Electrochemical oxidation of electrodialysed reverse osmosis concentrate on Ti/Pt–IrO2, Ti/SnO2–Sb and boron-doped diamond electrodes. *Water research* **47**, 242-250 (2013).

193 Song, H. *et al.* Electrochemical activation of persulfates at BDD anode: radical or nonradical oxidation? *Water research* **128**, 393-401 (2018).

194 Davies, M. J., Gilbert, B. C. & Norman, R. O. Electron spin resonance. Part 67. Oxidation of aliphatic sulphides and sulphoxides by the sulphate radical anion (SO 4–˙) and of aliphatic radicals by the peroxydisulphate anion (S 2 O 8 2–). *Journal of the Chemical Society, Perkin Transactions 2*, 503-509 (1984).

195 Merga, G., Aravindakumar, C., Rao, B., Mohan, H. & Mittal, J. Pulse radiolysis study of the reactions of SO˙–4 with some substituted benzenes in aqueous solution. *Journal of the Chemical Society, Faraday Transactions* **90**, 597-604 (1994).

196 Padmaja, S., Neta, P. & Huie, R. Rate constants and temperature effects for reactions of chlorine (1-) radical with unsaturated alcohols and hydrocarbons in aqueous and acetonitrile/water solutions. *The Journal of Physical Chemistry* **96**, 3354-3359 (1992).

197 McAskill, N. A. & Sangster, D. A Pulse Radiolysis Study of the Reaction of the Sulfate Radical Ion in Aqueous Solutions of Styrene. *Australian Journal of Chemistry* **32**, 2611-2615 (1979).

198 Zhang, R. C., Sun, P. Z., Boyer, T. H., Zhao, L. & Huang, C. H. Degradation of Pharmaceuticals and Metabolite in Synthetic Human Urine by UV, UV/H2O2, and UV/PDS. *Environmental Science & Technology* **49**, 3056-3066 (2015). https://doi.org:10.1021/es504799n

199 Van Hoonacker, A. & Englebienne, P. Revisiting silver nanoparticle chemical synthesis and stability by optical spectroscopy. *Current Nanoscience* **2**, 359-371 (2006).

200 Armstrong, D. A. *et al.* Standard electrode potentials involving radicals in aqueous solution: Inorganic radicals. *BioInorganic Reaction Mechanisms* **9**, 59-61 (2013).

201 Buxton, G. V., Bydder, M., Salmon, G. A. & Williams, J. E. The reactivity of chlorine atoms in aqueous solution. Part III. The reactions of Cl• with solutes. *Physical Chemistry Chemical Physics* **2**, 237-245 (2000).

202 Moreira, F. C., Boaventura, R. A. R., Brillas, E. & Vilar, V. J. P. Electrochemical advanced oxidation processes: A review on their application to synthetic and real wastewaters. *Applied Catalysis B-Environmental* **202**, 217-261 (2017). https://doi.org:10.1016/j.apcatb.2016.08.037

203 Zöllig, H. *Electrolysis for the treatment of stored source-separated urine*, ETH Zurich, (2015).

204 Shoaf, D. R. & Singer, P. C. An analysis of monitoring data for the stage 1 disinfectants/disinfection byproducts rule. *Journal-American Water Works Association* **99**, 69-80 (2007).

205 Seidel, C. J., Samson, C. C., Bartrand, T., Ergul, A. & Summers, R. S. Disinfection byproduct occurrence at large water systems after stage 2 DBPR. *Journal-American Water Works Association* **109**, 17-30 (2017).

206 Hozalski, R. M., Zhang, L. & Arnold, W. A. Reduction of haloacetic acids by Fe0: implications for treatment and fate. *Environmental science & technology* **35**, 2258-2263 (2001).

207 Zhou, J. *et al.* Reductive removal of chloroacetic acids by catalytic hydrodechlorination over Pd/ZrO2 catalysts. *Applied Catalysis B: Environmental* **134**, 222-230 (2013).

208 Croue, J. P. & Reckhow, D. A. Destruction of chlorination byproducts with sulfite. *Environmental science & technology* **23**, 1412-1419 (1989).

209 Mao, R. *et al.* Dechlorination of trichloroacetic acid using a noble metal-free graphene–Cu Foam electrode via direct cathodic reduction and atomic H. *Environmental science & technology* **50**, 3829-3837 (2016).

210 Hori, Y., Murata, K. & Oku, T. Electrochemical dechlorination of chlorinated hydrocarbons–electrochemical reduction of chloroform in acetonitrile/water mixtures at high current density. *Chemistry letters* **32**, 230-231 (2003).

211 Korshin, G. V. & Jensen, M. D. Electrochemical reduction of haloacetic acids and exploration of their removal by electrochemical treatment. *Electrochimica acta* **47**, 747-751 (2001).

212 Yan, M. *et al.* Electrochemical reductive dehalogenation of iodine-containing contrast agent pharmaceuticals: Examination of reactions of diatrizoate and iopamidol using the method of rotating ring-disc electrode (RRDE). *Water research* **136**, 104-111 (2018).

213 Li, Y.-P., Cao, H.-B. & Zhang, Y. Reductive dehalogenation of haloacetic acids by hemoglobin-loaded carbon nanotube electrode. *Water research* **41**, 197-205 (2007).

214 Bagastyo, A. Y. *et al.* Electrochemical treatment of reverse osmosis concentrate on boron-doped electrodes in undivided and divided cell configurations. *Journal of hazardous materials* **279**, 111-116 (2014).

215 Suh, D. H. & Abdel-Rahman, M. S. Mechanism of chloroform formation by chlorine and its inhibition by chlorine dioxide. *Fundamental and Applied Toxicology* **5**, 305-313 (1985).

216 Atkins, S. *et al.* Electrochemical reduction of carbamazepine in ethanol and water solutions using a glassy carbon electrode. *International Journal of Electrochemical Science* **8**, 2056-2068 (2013).

217 Misal, S. N., Lin, M.-H., Mehraeen, S. & Chaplin, B. P. Modeling electrochemical oxidation and reduction of sulfamethoxazole using electrocatalytic reactive electrochemical membranes. *Journal of hazardous materials* **384**, 121420 (2020).

218 Scialdone, O. *et al.* Electrochemical conversion of dichloroacetic acid to chloroacetic acid in conventional cell and in two microfluidic reactors. *ChemElectroChem* **1**, 116-124 (2014).

219 Filanovsky, B. Electrochemical response of new carbon electrodes bulk modified with cobalt phthalocyanine to some thiols in the presence of heptane or human urine. *Analytica chimica acta* **394**, 91-100 (1999).